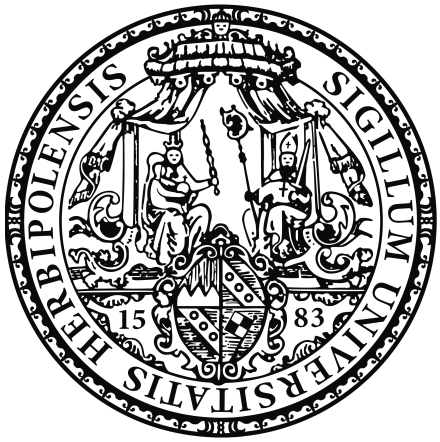

The human CCHC-type Zinc Finger Nucleic Acid Binding Protein (CNBP) binds to the G-rich elements in target mRNA coding sequences and promotes translation

Das humane CCHC-Typ-Zinkfinger-Nukleinsäure-Binde-Protein (CNBP) bindet an G-reiche Elemente in der kodierenden Sequenz seiner Ziel-mRNAs und fördert deren Translation

Doctoral thesis for a doctoral degree
at the Graduate School of Life Sciences,
Julius-Maximilians-Universität Würzburg,
Section: Biomedicine

submitted by

Sanjay Kumar Gupta

from

Varanasi, India

Würzburg, 2016

Submitted on: ……..……..

Office stamp

Members of the *Promotionskomitee*:

Chairperson: Prof. Dr. Alexander Buchberger

Primary Supervisor: Dr. Stefan Juranek

Supervisor (Second): Prof. Dr. Utz Fischer

Supervisor (Third): Dr. Markus Landthaler

Date of Public Defence: ……..……

Date of Receipt of Certificates: ……

Summary

The genetic information encoded with in the genes are transcribed and translated to give rise to the functional proteins, which are building block of a cell. At first, it was thought that the regulation of gene expression particularly occurs at the level of transcription by various transcription factors. Recent discoveries have shown the vital role of gene regulation at the level of RNA also known as post-transcriptional gene regulation (PTGR). Apart from non-coding RNAs e.g. micro RNAs, various RNA binding proteins (RBPs) play essential role in PTGR. RBPs have been implicated in different stages of mRNA life cycle ranging from splicing, processing, transport, localization and decay. In last 20 years studies have shown the presence of hundreds of RBPs across eukaryotic systems many of which are widely conserved. Given the rising number of RBPs and their link to human diseases it is quite evident that RBPs have major role in cellular processes and their regulation. The current study is aimed to describe the so far unknown molecular mechanism of CCHC-type Zinc Finger Nucleic Acid Binding Protein (CNBP/ZNF9) function *in vivo*.

CNBP is ubiquitously expressed across various human tissues and is a highly conserved RBP in eukaryotes. It is required for embryonic development in mammals and has been implicated in transcriptional as well as post-transcriptional gene regulation; however, its molecular function and direct target genes remain elusive. Here, we use multiple systems-wide approaches to identify CNBP targets and document the consequences of CNBP binding. We established CNBP as a cytoplasmic RNA-binding-protein and used Photoactivatable Ribonucleoside Enhanced Crosslinking and Immunoprecipitation (PAR-CLIP) to identify direct interactions of CNBP with 4178 mRNAs. CNBP preferentially bound a G-rich motif in the target mRNA coding sequences. Functional analyses, including ribosome profiling, RNA sequencing, and luciferase assays revealed the CNBP mode of action on target transcripts. CNBP binding was found to increase the translational efficiency of its target genes. We hypothesize that this is consistent with an RNA chaperone function of CNBP helping to resolve secondary structures, thus promoting translation. Altogether this study provides a novel mechanism of CNBP function *in vivo* and acts as a step-stone to study the individual CNBP targets that will bring us closer to understand the disease onset.

Zusammenfassung

Die in der DNA kodierte genetische Information wird transkribiert und translatiert, um funktionelle Proteine zu bilden, welche die Bausteine von Zellen sind. Lange Zeit wurde vermutet, dass die Regulation der Genexpression insbesondere auf dem Level der Transkription erfolgt. Kürzlich gemachte Entdeckungen haben jedoch die zentrale Rolle der Genregulation auf dem Level der RNA, auch bekannt als posttranskriptionelle Genregulation (PTGR), gezeigt. Neben nicht-kodierenden RNAs wie microRNAs, besitzen verschiedene RNA-Binde-Proteine (RBP) eine Schlüsselrolle in der PTGR. RBPs wurden mit diversen Ebenen des mRNA-Lebenszyklus, wie Speißen, Prozessieren, Transport, Lokalisation und Abbau in Verbindung gebracht. In den letzten 20 Jahren haben Studien die Existenz von Hunderten von RBPs in unterschiedlichen eukaryotischen Systemen gezeigt, von denen viele weithin konserviert sind. Bedenkt man die steigende Anzahl entdeckter und charakterisierter RBPs und ihren Bezug zu Krankheiten des Menschen, so ist es offensichtlich, dass RBPs eine große Rolle in der Regulation zellulärer Prozesse besitzen. Das Ziel der hier vorliegenden Studie bestand darin, die bis jetzt unbekannten molekularen Mechanismen der Funktion des CCHC-Typ-Zinkfinger-Nukleinsäure-Binde-Proteins (CNBP/ZNF9) *in vivo* zu beschreiben.

CNBP ist in verschiedenen humanen Geweben ubiquitär exprimiert und ein hoch konserviertes RBP in Eukaryoten. Es ist für die embryonale Entwicklung in Säugetieren notwendig und wurde mit der transkriptionellen und posttranskriptionellen Genregulation in Verbindung gebracht. Seine molekulare Funktion sowie die unmittelbaren Zielgene blieben jedoch unklar. In dieser Studie verwendeten wir systemweit analysierende Methoden um CNPB-Zieltranskripte zu identifizieren und dokumentierten die Folgen der Bindung von CNBP an diese. Wir haben CNBP als ein zytoplasmatisches RNA-Binde-Protein charakterisiert und Quervernetzung und Immunpräzipitation mit photoaktivierbaren Ribonukleotiden (PAR-CLIP) angewendet. Dabei wurden direkte Interaktionen von CNBP mit 4178 mRNAs identifiziert. CNBP bindet bevorzugt an ein G-reiches Motiv in der kodierenden Sequenz der Ziel-mRNA. Funktionale Analysen, unter anderem Ribosom-Profil-Untersuchungen, RNA Sequenzierung und Luciferaseproben, zeigten die Art und Weise, wie CNBP auf die Zieltranskripte wirkt. Die Bindung von CNBP an seine Zieltranskripte erhöht deren Translationseffizienz. Wir vermuten, dass dies eine RNA-Chaperon-Funktion von CNBP darstellt, die hilft Sekundärstrukturen aufzulösen und die Translation zu fördern. Zusammengefasst liefert diese Studie einen neuen Mechanismus der Funktion von CNBP *in vivo* und kann als Startpunkt dienen um einzelne CNBP Ziele zu untersuchen. Dies wird uns helfen dem Verständnis der Krankheitsentstehung näher zu kommen.

Table of contents

1 Introduction

1.1 Regulation of gene expression in eukaryotes (overview)

The genomes of multicellular organims are essentially idenatical amongst different cell types. The biological variances between cells arise due to differences in gene expression. Eukaryotic cells establish different pattern of gene expression during different phases of growth, development and differentiation (Rockman and Kruglyak 2006). The genetic material inside a cell encodes functional protein that dictates cellular function. A tempo spatial regulation of gene expression and translation governs repertoire of proteins expressed inside a cell, which in turn determines cellular characteristics. The amount of a particular protein inside a cell at a given time reflects the balance between protein synthetic and degradative pathways. Tight control of gene expression is thus a pre-requisite to govern the complex regulatory networks associated with a particular protein (Rockman and Kruglyak 2006, Keene 2007).

The beginning of a gene expression comprises of the formation of RNA from its template DNA by RNA polymerase (RNAP). RNAP recognizes the promoter region of the gene to be transcribed and position itself at the transcription start site (TSS) sequence followed by elongation. During elongation the gene is transcribed into a complementary RNA sequence. Once the polymerase reaches the termination signal, the RNA molecule is cleaved and is removed from the transcriptional machinery. After transcription, the products of RNAP II transcription (mainly protein coding RNAs) undergo heavy round of modification and is transported out of the nucleus where it is translated into the encoded protein by ribosomes. Along with the 40S and 60S ribosomal subunits there are approximately 79 other ribosomal proteins that form a huge 3.2 MDa complex and execute translation process (Graifer and Karpova 2015).

Gene expression is mainly controlled at three levels; first and foremost is the transcriptional regulation at the level of DNA, which limits the amount of mRNA that is produced from a particular gene. The second level of control is through post-transcriptional events that regulate mRNA stability and the translation of mRNA into proteins. Post-translational regulation can also affect the activity and hence fate of the translated protein (Skelly, Frungillo et al. 2016). Here in this thesis we will discuss posttranscriptional gene regulation in detail with an overview of gene regulation at transcriptional and post-translational level.

Most of the research in last couple of decades has focused on first level of gene expression, namely transcriptional regulation. Transcriptional regulation is mediated at the level of DNA by transcription factors (TFs) binding in a sequence specific manner to the promoter elements. TFs

have defined DNA binding domains with up to 10^6-fold higher affinity for the target sequence than any other DNA strand (Remenyi, Scholer et al. 2004). In eukaryotes there are more than 1300 sequence specific DNA binding TFs, which in one way or the other, regulate expression of genes at various level (Vaquerizas, Kummerfeld et al. 2009). A breakdown of this regulatory system leads to changes in the cellular system and is responsible for diverse set of diseases including cancer. One third of the human developmental disorders have been attributed to dysfunctional TFs (Boyadjiev and Jabs 2000) wherein many of these TFs regulating oncogenes have been found to be overexpressed (Furney, Higgins et al. 2006).

Once the protein is synthesized it undergoes post-translational modifications (PTMs), which profoundly affects the properties of the protein and hence its function (Skelly, Frungillo et al. 2016). Proteins can display broad range of PTMs ranging from acetylation, acylation, amidation, carboxylation, glycosylation, phosphorylation, proteolytic processing etc (Walsh and Jefferis 2006). Many of these modifications regulates critical intracellular processes, including gene expression, signal transduction and endosomal vesicle trafficking (Walsh and Jefferis 2006). Approximately 50% of human proteins are thought to be glycosylated (Wong 2005) where several oligosaccharides at N- and O- glycosylation sites are added.

The other stage in regulation of gene expression is at the level of RNA and is termed as posttranscriptional gene regulation (PTGR). PTGR is much more intricate than previously thought. In PTGR processes RNA binding proteins and ribonucleoprotein complexes have been reported to play a central role in mRNA expression ranging from metabolism, coordination maturation, transport, stability and degradation of all classes of RNAs (Gerstberger, Hafner et al. 2014) (Fig 1.1).

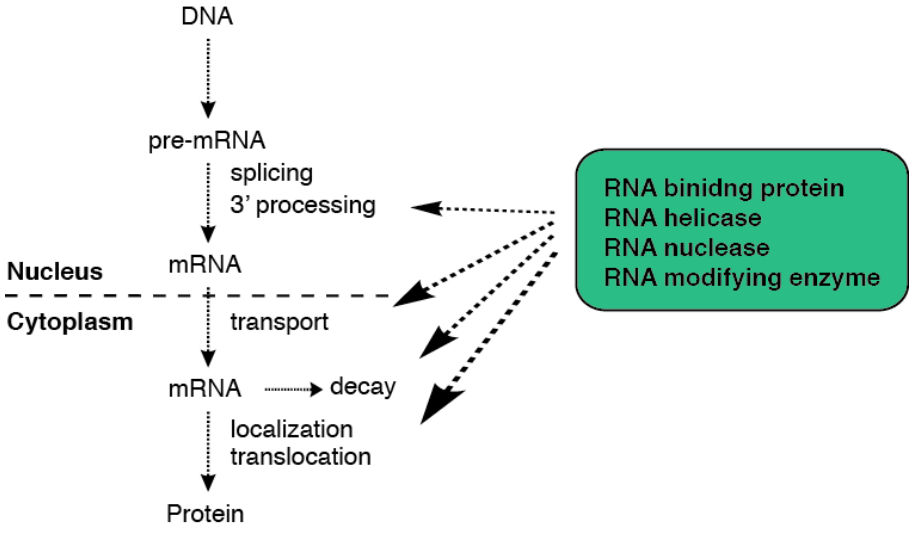

Fig 1.1: Role of different RNA binding factors in mRNA expression (modified from Keene et al,. 2007)

1.2 Post-transcriptional gene regulation (PTGR)

An mRNA is never alone inside the cell; as soon as it is transcribed ribonucleoproteins (RNPs) form co-transcriptionally on the nascent transcript and contribute to its stabilization, processing, nuclear export, transport and localization. The protein content of an mRNA-RNP is dynamic and changes constantly at every step. Recent studies involving oligo dT pull down of total cellular mRNA followed by mass-spectrometry analysis revealed more than 800 bound proteins (Baltz, Munschauer et al. 2012, Castello, Fischer et al. 2012), emphasizing on the crucial role of RBPs in determining the fate of bound mRNAs.

In eukaryotes, the pre-mRNA undergoes heavy rounds of modifications inside the nucleus before being exported to the cytoplasm for effective translation. The nuclear modifications can be broadly classified into three major steps; 5' capping, joining of exons by splicing, and poly-adenylation of 3' end. One of the first modifications encountered by nascent mRNA is when it reaches a length of 25-30 nucleotides; its 5' end is added with 7-methylguanosine by dimeric capping enzyme. The addition of m7G- is crucial for the stability of mRNA and for further downstream events.

The vast majority of protein coding genes in eukaryotes carries coding exons and non-coding introns. The removal of non-coding introns to generate an open reading frame is performed by macromolecular splicesomal machinery consisting of uridine rich small nuclear ribonucleoprotein particles (UsnRNPs). Two consecutive transesterification reactions, first on 5'ss to cleave the 5' end of the intron followed by 3' ss by the 3' OH of 5' exon, removes the intron and ligates 5' and 3' exons (Wachtel and Manley 2009). After intron removal spliceosome recruits exon junction complex (EJC) 20-25 nucleotide upstream of the exon junctions that enhances nuclear export (Le Hir, Gatfield et al. 2001), cytoplasmic localization (Hachet and Ephrussi 2004), and translation of mRNAs (Nott, Le Hir et al. 2004). EJC is composed of four proteins; Y14, MAGOH, eIF4A3, and Barentz and has also been shown to play a role in mRNA quality control and non-sense mediated decay of aberrant mRNAs (Le Hir, Gatfield et al. 2001).

Finally, the mature 3' end of mRNA is generated by polyadenylation using macromolecular polyadenylation machinery. Polyadenylation of mRNA is a two step process which begins with removal of AAUAAA from the 3'end followed by addition of 200-300 adenosine with the help of poly (A) polymerase. After the maturation of mRNA is complete it is exported out of the nucleus for protein synthesis.

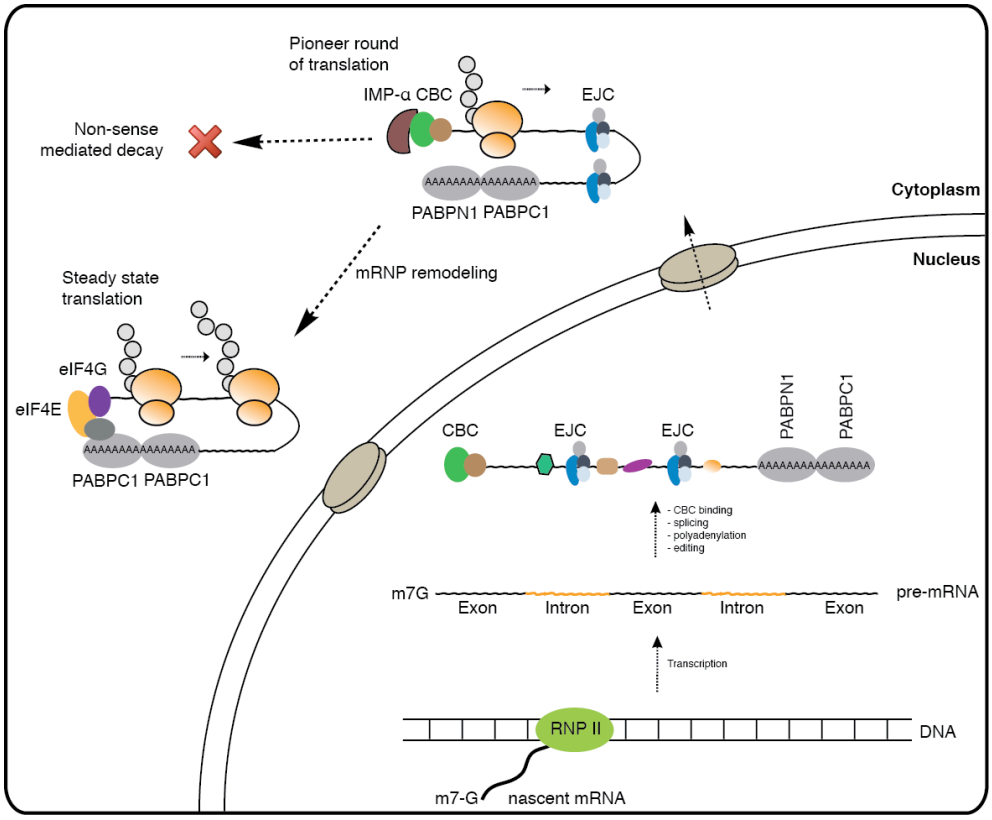

Figure 1.2: Life of a eukaryotic mRNA inside the cell.

Upon entering the cytoplasm the 5' cap-binding complex (CBC) is accompanied with importin α (IMPα). Other elongation factors bind the mRNA and marks the pioneer round of translation. After first round of translation, the CBC is replaced by eIF4E and other factors while translating ribosome displaces the EJC. At the 3' end PABPN1 is replaced by PABC1 and marks the steady-state translation. In case the message is not correctly edited the mRNA undergoes nonsense mediated decay after pioneer round of translation (Maquat, Tarn et al. 2010).

Another important factor that plays a crucial role in post-transcriptional gene regulation is small RNAs. Small RNAs are usually 20-30 nts in length and are associated with AGO protein family (Pais, Moxon et al. 2011). MicroRNAs (miRNAs), small interfearing RNAs (siRNAs) and PIWI interacting RNAs (piRNAs) constitute three major classes of small RNAs. MiRNAs are dominant type of small noncoding RNAs and are usually 22 nts long. They function as guide molecule in RNA induced silencing complex (RISC) (Eis-Hubinger, Kleim et al. 1991) and regulates the expression of target genes by binding to complementary sequence in target transcript (usually 3' UTR) causing translational repression or transcript degradation (Eis-Hubinger, Kleim et al. 1991). MiRNAs are produced by RNA Pol II proteins Dicer and Drosha. Following transcription by RNA Pol II, primary miRNA (pri-miRNA) undergoes rounds of modification to give rise to mature miRNA. miRNAs are widely distributed across animals, plants, protists and viruses

(Griffiths-Jones, Saini et al. 2008). Approximately 30% of miRNAs are present in introns of protein coding genes, where as rest are mostly present in dedicated miRNA gene loci (Lin and Gregory 2015).

1.3 RNA binding protein mediated regulation of gene expression

As discussed in the section above, RNA binding proteins play fundamental role in a variety of cellular processes. Characterization of first RNA binding proteins using biochemical method dates back around 30 years where gel electrophoresis of UV crosslinked nuclear extracts or RNA affinity purification and mass spectrometry was used (Dreyfuss, Choi et al. 1984, Pinol-Roma, Choi et al. 1988). Since then there have been hundreds of RBPs discovered playing diverse role in living systems. Recent studies have marked an astounding >10% & ~7.5% of the total yeast and human proteome respectively as RBPs (Gerstberger, Hafner et al. 2014, Beckmann, Horos et al. 2015).

Unlike DNA binding proteins, which rely on sequence specificity of their target for interaction, RBPs recognize both sequence and secondary structure of their binding site. This difference is because of the different helical configurations adapted by DNA and RNA. In many cases the RBPs recognize the single stranded regions or the opening of the double stranded regions resulting into bulges or hairpins (Draper 1999). RBPs typically contain domains known as RNA binding domains (RBDs) that can bind to RNA independently. The human RBPs are reported to contain ~600 structurally distinct RBDs of which 20 are most commonly occurring (Table 1.1). Based on presence of domains known to directly interact with RNA or reside within well characterized RNPs there are >1500 RBPs present in human genome(Gerstberger, Hafner et al. 2014). The binding of RBD to its target RNA is usually via few nucleotides (4-8 nts) and is often weak. To provide higher specificity and affinity towards their targets, these domains are usually occurring in multiple copies in a protein.

One of the most commonly occurring RBD in humans is RNA recognition motif (RRM) that is present in wide range of proteins including hnRNPs, PABPs, U2AF etc. A typical RRM is 90 amino acids long and contains four anti-parallel beta strands and two alpha helices arranged in β- α -β- β- α -β pattern. The RNA recognition is mediated by canonical β -sheet surface possessing aromatic amino acids (Phenylalanine, Tyrosine, Tryptophan) (Muto and Yokoyama 2012). RRMs bind nucleotides ranging from a minimum of two (eg: CBP20 that contains one RRM and recognizes 2 nucleotides (Clery, 2008 #21) (Mazza, Segref et al. 2002) to a maximum of eight for U2B00 RRM1 (Price, Evans et al. 1998).

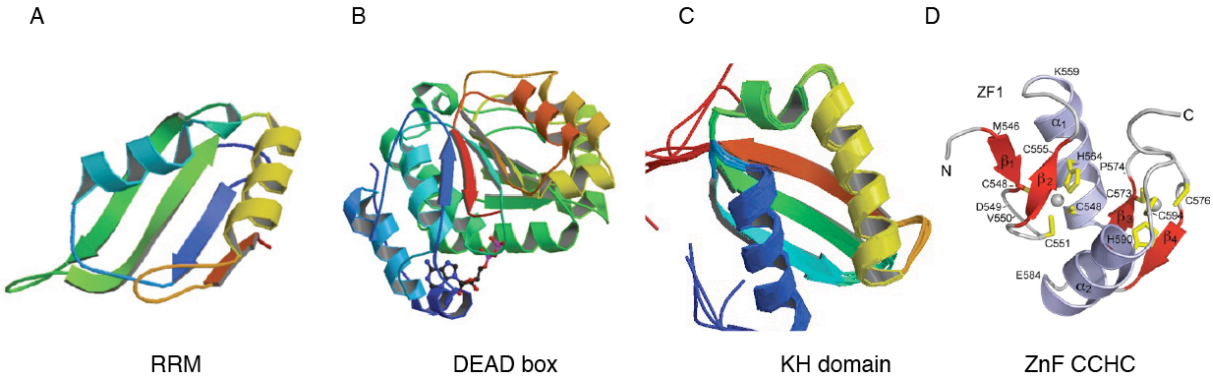

FIG 1.3: *(A)* A crystal structure of RRM of human ELAV type RBP (PDB: 4TLQ). *(B)* DEAD-box helicase DDX3X (PDB: 4PX9). *(C)* KH domain of human ribosomal protein S3 (PDB: 1WH9). *(D)* NMR structure of CCHC type zinc finger protein (PDB: 2K9H)

DEAD box helicase are the largest among the helicase family (Fairman-Williams, Guenther et al. 2010) and are another commonly occurring RBPs in human. The proteins of this family are highly conserved amongst bacteria, archaea and eukaryotes and play roles in RNA metabolism (Linder 2006, Linder and Jankowsky 2011). DEAD-box proteins are characterized by presence of an Asp-Glu-Ala-Asp (DEAD) motif and belong to helicase superfamily 2 with two virtually identical domains similar to bacterial RecA protein (Fairman-Williams, Guenther et al. 2010). The two-helicase domains form a cleft and contain the ATP-binding site required to unwind the short duplex RNA.

KH-domain is highly abundant in eukaryotes and is characterized by the presence of (I/L/V)-I-G-X-X-G-X-X-(I/L/V). It is usually ~70 amino acids long and contain three β-stranded sheets packed against three α helices. Based on the topology KH-domains can be type I, folded in a βααββα or type II, αββααβ (Beuth, Pennell et al. 2005). The crystal structure of KH-domain shows a cleft formed by GXXG loop where ssDNA or RNA binds (Braddock, Baber et al. 2002, Backe, Messias et al. 2005). Each KH-domain binds to at least 4 nucleotides although additional flanking nucleotides can make non-specific contacts as well (Valverde, Edwards et al. 2008).

Table 1.1 Overview of frequently encountered RNA binding domains

Domain	Number of proteins	Description	Example
RRM	1090	RNA recognition motif, ssRNA	hnRNP proteins

		binding.	
RG/RGG	1029	RGG sequences are substrate recognition sites for PRMTs. Involved in many physiological processes e.g. splicing, translation etc.	CNBP
DEAD	318	Belongs to helicase family. Involved in RNA metabolism.	DDX39A
KH-type 1/type 2	220/11	Type 1 contains beta-alpha-alpha-beta-beta-alpha structure. Type 2 contains alpha-beta-beta-alpha-alpha-beta.	HNRNPK
zf-CCCH	183	Involved in cycle or growth phase related regulation. Interacts with 3' UTR of target mRNA.	U2AF
zf-CCHC	164	Zinc finger, C-x2-C-x4-H-x4-C, ssRNA binding.	CNBP
dsrm	149	Double-stranded RNA binding domain. Involved in posttranscriptional gene regulation.	STAU1
TUDOR	115	Interacts with the C-terminal dimethylated Arg and Gly-rich tails of the spliceosomal Sm D1 and D3 protein.	SMN1
SAP	108	Found in a variety of nuclear proteins involved in transcription, DNA repair, and RNA processing or apoptotic chromatin degradation.	HNRNPU
G-patch	99	Contains 7 highly conserved glycine. Found in RBPs.	RBM5
MIF4G	86	Important for mRNA nuclear maturation steps and for nonsense-mediated decay.	EIF4G
GTP_EFTU_D2	83	Elongation factor Tu domain 2 bind to charged tRNAs.	EIF5B
IBN_N	75	Binds Ran GTPase protein.	Importin-5

LSM	60	Present in Sm proteins. Binds A/U rich region.	LSm1/8
OB_NTP_Bind	60	Oligonucleotide binding folds are found in C-terminus of DEAD box helicases. Regulates helicase activity through RNA binding.	DHX15
HA2	59	Helicase associated domain 2 found in RNA helicases.	DHX15/16
GTP_EFTU_D3	51	Involved in protein synthesis.	GSPT1
RnaseA	45	Pyrimidine specific endonucleases involved in endonucleolytic cleavage.	EDDM3B
zf-C2H2-jaz	45	Binds dsRNA and are required for nucleolar localization.	ZNF804B
Rnase_T	45	Responsible for the end-turnover of tRNA.	PAN2
S1	44	Found in RNA associated proteins.	EIF2S1
HGTP_anticodon	43	Found in histidyl, glycyl, threonyl and prolyl tRNA synthetases.	Tarsl2
NTF2	41	Stimulates efficient nuclear import of a cargo protein.	NXF2
R3H	40	Contains an invariant arginine and a highly conserved histidine, that are separated by three residues.	NKRF
Ribosomal_L7Ae	38	It includes 40S ribosomal protein S12 from eukaryotes, ribosomal protein L30 from eukaryotes and archaebacteria.	RPS12
KOW	34	Found in ribosomal proteins.	SUPT5H
Anticodon_1	32	This domain is found methionyl, valyl, leucyl and isoleucyl tRNA synthetases. It binds to the anticodon of the tRNA.	VARS
PAZ	29	Found members of the Argonaute protein family. Implicated in the development and maintenance of stem cells through the RNA-mediated	EIF2C1-4

		gene-quelling mechanisms associated with the protein DICER.	
PAM2	29	Located towards the C terminus of eukaryotic ataxin-2.	TOB2
Piwi	23	Found in piwi proteins and a large number of related nucleic acid-binding proteins, especially those that bind and cleave RNA.	EIF2C1-4
Xpo1	21	Interacts with RanGTP and importin-alpha, the latter binding with the nuclear localisation signal (NLS) sequences in proteins to be transported.	Exportin-1
RNase_Zc3h12a	15	Found in Zc3h12a protein that has shown to be a ribonuclease that controls the stability of a set of inflammatory genes.	ZC3H12D

1.4 RNA binding proteins in diseases

Given the diverse function of RBPs in determining the fate of the RNAs bound to it, it is not surprising that an alteration or deletion in RBPs causes malfunctions in cellular processes and hence various diseases. Interestingly there are many neurodegenerative disorders linked to the clinical manifestations of RBP defects, because of prevalence of alternative splicing in brain, a major function fulfilled by RBPs. Aberrant RBPs has also been implicated in various muscular atrophies and different types of cancer (Lukong, Chang et al. 2008) (Table 1.2).

A mutation in RBP can result in its loss-of-function or gain of function. For example a genetic change in 5' UTR of fragile X mental retardation gene (CGG trinucleotide extension) results in loss of function of FMRP protein and hence causes fragile X syndrome (FXS) (Chelly and Mandel 2001). FMRP contains two KH domains and one RGG- type RNA binding domains. A point mutation in the second KH-domain of FMRP1 from isoleucine 367 to asparagine has been associated with severe FXS (De Boulle, Verkerk et al. 1993).

The toxic mRNA gain-of-function is observed when microsatellite expansion repeats are transcribed into mRNA and results in entrapment of RBPs that associate with the repeats and interfere with the normal function of RBPs. For example CUG expansion at the 3' UTR of DMPK

mRNA results in the entrapment of RBPs MBNL1 and CUGBP1 respectively (Wang and Cooper 2007).

Many RBPs have also been implicated in cancer. Cancer is a heterogeneous disease caused by gene mutations, amplifications, and chromosomal rearrangements that often results in altered activity of oncogenes and tumor suppressors. Chromosomal rearrangements in the gene containing RGG/RRM RBDs (for e.g. TET) are the prominent cause of sarcomas (Riggi, Cironi et al. 2007).

Table 1.2 RNA binding proteins in human diseases

Type	**Disease**	**Protein involved**
Neurological disorders	Fragile X syndrome (FXS)	FMRP1
	Fragile-X associated tremor/ataxia syndrome (FXTAS)	FMRP1 Sam68
	Ataxis	ATXN1 ATXN2,
	Paraneoplastic opsoclonusm-myoclonus-ataxia (POMA)	NOVA-1,2
	Parkinson's disease (PD)	ELAV/HuB,C,D eIF4G
	Amyotrophic lateral sclerosis (ALS)	hnRNPA1 hnRNPA2 TLS/FUS C9orf72
	Myelin disorder	QKI (predicted role) PTBP1
	Schizophrenia	QKI (predicted role)
Muscular atrophies	Spinal muscular atrophy (Ingolia, Ghaemmaghami et al.)	SmD1 SmD3 SMN
	Oculopharyngeal muscular dystrophy (OPMD)	PABPN1
	Myotonic dystrophy type 1 (DM1)	MBNL1/CUGBP1/Staufen1
	Myotonic dystrophy type 2 (DM2)	CNBP
Cancer		eIF4E SF2/ASF Sam68

	QKI
	HuR

1.5 Zinc finger proteins

Zinc finger containing protein consists of the most abundant protein superfamily in mammalian genome (Klug 2010). Forty-six different conserved zinc finger domains are listed on InterPro (http://www.ebi.ac.uk/InterPro), which have different binding specificity for DNA, RNA and proteins. Based on the residues that are used to coordinate zinc there are typically Cys2His2 (CCHH), Cys3His (CCCH) or Cys2HisCys (CCHC) zinc finger domains.

Zinc finger proteins are classically DNA binding and were identified for the first time in *Xenopus laevis* in basal transcription factor TFIIIA (Miller, McLachlan et al. 1985). TFIIIA contains 9 CCHH type zinc finger where finger 1-3, 5 and 7-9 interact with DNA (Searles, Lu et al. 2000). One of the first NMR structures of the TFIIIA like zinc finger showed presence of an antiparallel β ribbon and an α helix coordinating with a central zinc ion to form a compact globular domain (Parraga, Horvath et al. 1988). Later, Pavletich et al. discovered the crystal structure of bound DNA with the zinc finger at a 2.1 A˚ resolution showing arrangement of zinc finger in a semi circular structure into the major groove of B-DNA (Pavletich and Pabo 1991). The specificity of the binding is determined by side chain base interaction involving a direct set of residues located at the fingertip or the surface of helix. Additionally, interaction between the phosphate backbone and adjacent zinc finger contributes to the binding specificity (Wolfe, Nekludova et al. 2000).

Although the most noted roles of zinc fingers are DNA binding, TFIIIA was also shown to be the protein component that associates with 5S rRNA with in the 7S particle of *Xenopus* oocytes and is essential for ribosome assembly and nuclear export (Picard and Wegnez 1979). The RNA binding property of CCHH domains 4-6 of TFIIIA is associated with the recognition helices of fingers with the two RNA loops. Tis11D, a CCCH type zinc finger protein, binds to AU-rich elements at the 3' UTR of tumor nacrosis factor α and granulocyte-macrophage colony stimulating factor mRNA and regulates their levels inside the cell (Carballo, Lai et al. 1998).

CCCH- and CCHC-Znfs are most commonly found in eukaryotes (Klug and Rhodes 1987). Increasing evidence suggests that zinc fingers are more widely used to recognize RNA and play crucial roles in posttranscriptional regulation (Nagai, Muto et al. 2001) (Finerty and Bass 1997, Nam, Chen et al. 2011). One of the common features of these RBPs in general and zinc finger proteins in particular is their occurrence in homotypic or heterotypic arrays of multiple nucleic acid binding domains. For example, human ZFP100 contains up to 18 ZnF-domains of four

different types (Gerstberger, Hafner et al. 2014). Given that most nucleic acid binding domains recognize short and degenerate 4-6 nucleotide long segments, it is thought that such a modular design can increase affinity and sequence specificity of the protein-nucleic acid interaction (Ascano, Hafner et al. 2012).

1.6 CNBP as RNA binding protein

CCHC-Type Zinc Finger, nucleic acid binding protein (CNBP) is among the proteins with the highest number of repeats of the same nucleic acid binding domain. It is evolutionary conserved in eukaryotes and harbors seven CCHC-type ZnF domains. Additionally it contains one arginine-glycine (RG/RGG)-rich motif (Fig. 1.5). This high level of conservation of CNBP from yeast to humans, specially all the 7 CCHC domains, indicates towards its role in fundamental cellular processes. *CNBP* is ubiquitously expressed at high levels in adult tissues (Gerstberger et al. 2014), and gene knockout in mice is embryonically lethal, presumably due to impaired embryonic forebrain development (Chen et al. 2003; Shimizu et al. 2003). In humans, a CCTG expansion in intron 1 of CNBP causes myotonic dystrophy type 2 (Liquori et al. 2001), nevertheless, little is known about the function of CNBP, and its targets remain largely elusive.

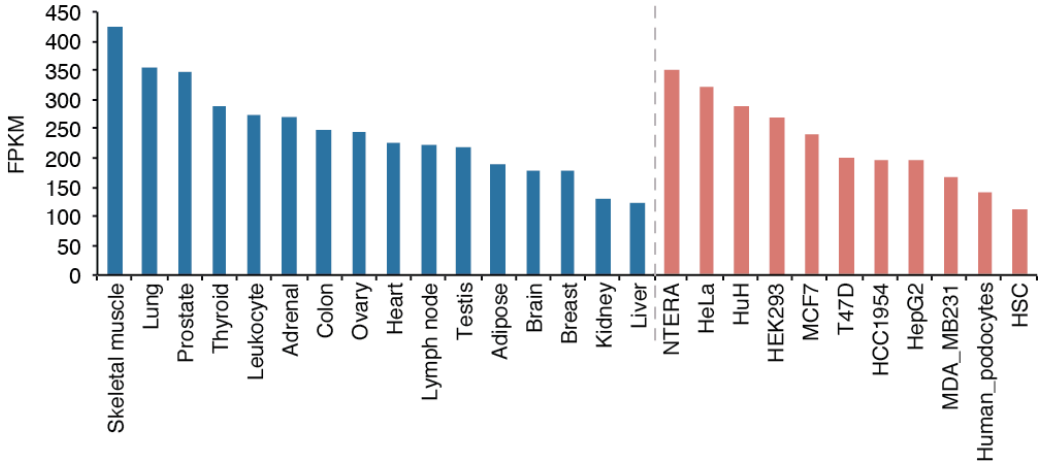

Fig 1.4: CNBP expression levels in human tissues and cell lines. CNBP mRNA expression levels. Blue bars indicate FPKM values of CNBP across different human tissues (from the Ilumina body map). Red bars show the expression levels of CNBP in different cell lines.

CNBP was first described as a DNA-binding protein and potential regulator for the sterol regulatory element (SRE). It scored high in an *in vitro* screen for binders of single-stranded DNA (ssDNA) with the defined sequence GTGCGGTG (Rajavashisth et al. 1989). A role for CNBP in transcriptional regulation was further suggested by its ability to bind the CT element of the *c-myc* gene *in vitro,* and by overexpression experiments in cultured mouse cells (P19) resulting in

strong *c-myc* promoter activity (Michelotti et al. 1995; Shimizu et al. 2003). In contrast, pulldown of polyadenylated RNA after *in vivo* UV crosslinking identified CNBP as an RNA-binding protein (RBP) in amphibian oocytes (Pellizzoni et al. 1997; Calcaterra et al. 1999). Other studies suggested that human CNBP interacts with G-rich ssRNA *in vitro* (Armas et al. 2008) and associates with the terminal 5' oligopyrimidine (TOP) sequence of specific mRNAs (Iadevaia et al. 2008) to promote their translation (Huichalaf et al. 2009). Its yeast homolog Gis2, associates with PABPC1 & translational machinery, and localizes to stress-induced cytoplasmic granules, which further support its potential function in translational regulation (Rojas et al. 2012).

Figure 1.5 ClustalW multiple sequence alignment of CNBP from various eukaryotes, from yeast to human,.

Box 1 | High throughput techniques for characterizing RBPs

The advent of recent, affordable high-throughput techniques combined with crosslinking and immunoprecipitation (CLIP) technologies has not only made the characterization of RBPs feasible but has also provided us with the detailed information about protein-RNA interaction sites (Ascano, Hafner et al. 2012).

All Crosslinking and Immunoprecipitations techniques uses a common approach, where upon UV-exposure RNA is covalently crosslinked to the interacting protein. The protein of interest is IPed along with bound RNA using antibody specific for the protein or tag-associated with the protein. After further downstream processing, the bound RNA is isolated, deep-sequenced and mapped on the genome for identification.

Three major CLIP techniques; PAR-CLIP, HiTS-CLIP and iCLIP are widely used to characterize RBPs. HiTS-CLIP and iCLIP utilizes UV of 254 nm to crosslink uridine in the RNA with aromatic amino acids of protein/peptide in direct contact. In iCLIP the cross linking site serves as a barrier for reverse-transcription and causes a truncation in RNA that gives us the exact interaction site. On the other hand PAR-CLIP utilizes photoactivatable ribonucleoside analogs 4SU or 6SG which upon 365 nm exposure causes a covalent bond with aromatic amino acids. In this case the cross-linked site serve as a bump and causes nucleotide exchange upon reverse transcription (Figure 1.5).

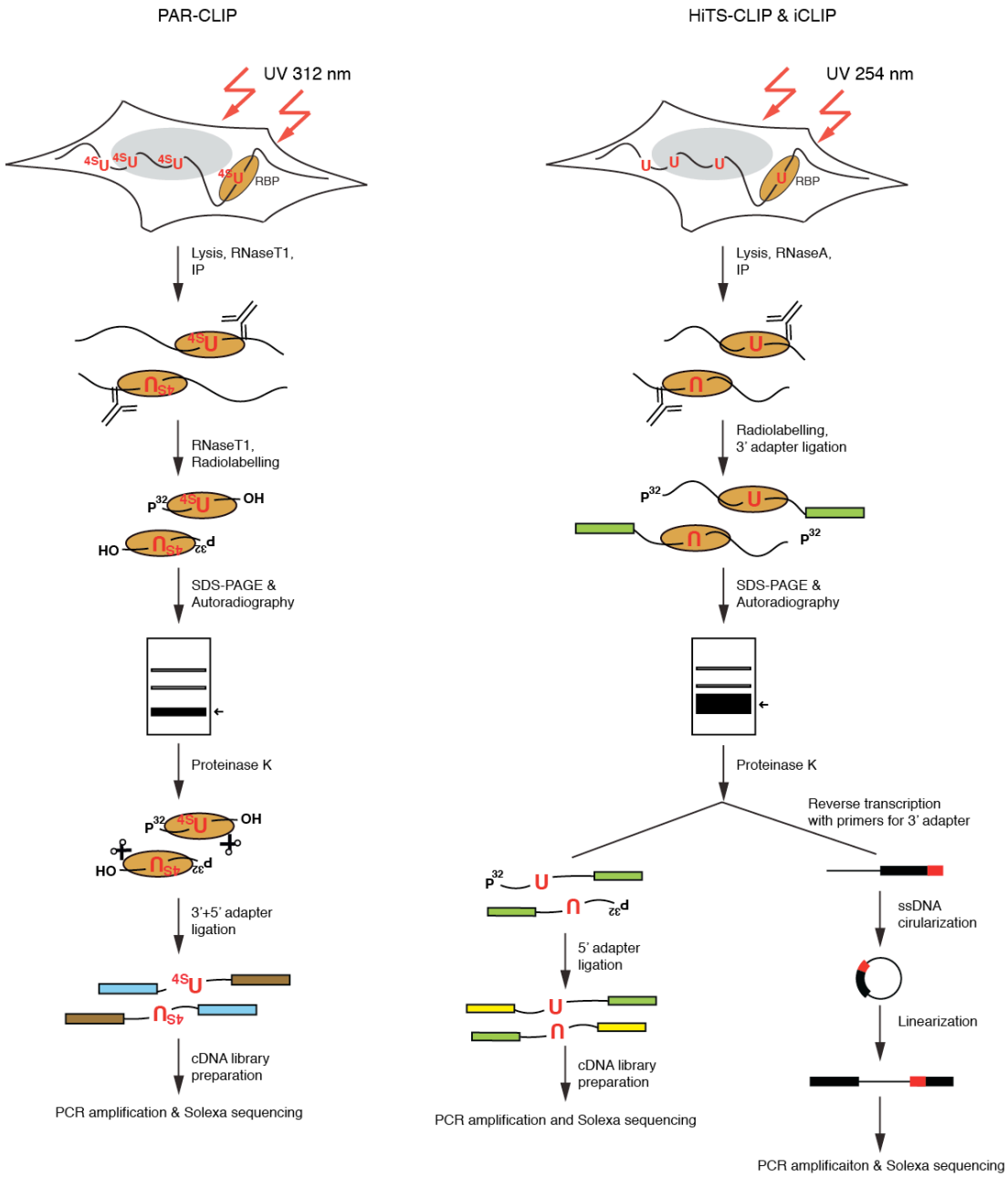

Fig 1.5 Flowchart of different CLIP techniques (from left to right, PAR-CLIP, HiTS CLIP and iCLIP).

1.7 Aim of the study

It is now very clear that RBPs play vital roles in deciding the fate of a transcript and in turn the cellular processes linked to it. Every RBP has a distinct role to play inside the cell. As mentioned above, based on presence of RBDs, there are more than 1500 RBPs documented in human system but the functions and *in vivo* binding specificities of most of them are not well understood and only a small number have been validated for RNA binding *in vivo*. The

characterization of proteins transiently or stably interacting with RNAs is a prerequisite for the dissection of RNA regulatory processes.

Various *in vitro*, *in vivo* and *in silico* approaches, such as electrophoretic mobility shift assays (EMSA) or UV crosslinking of protein to their target RNAs or SELEX, have been used to study RNA-protein interaction over past three decades (Marchese, de Groot et al. 2016). Recent developments in the high-throughput technologies for e.g. CLIP, RIP-ChIP, RNAcompete assay have not only eased the characterization of RBPs on genome wide scale but also has provided us with the detailed information about protein-RNA interaction sites (Hafner, Landthaler et al. 2010). These methods work on a similar concept where the RBP complex together with its target RNAs is first extracted and then the target RNA is identified using microarray or sequencing analysis. Computational approaches such as RBPmap, RNAcontext, MEME and HOMER have been developed to accurately predict the transcriptome wide RNA binding sites and consensus motifs.

Here, we aimed to consolidate disparate hypotheses about CNBP's regulatory function using biochemical and systems-wide approaches. We found that CNBP is a cytoplasmic mRNA-binding protein and support a function in translational regulation. We identified CNBP-binding sites on target RNAs on a transcriptome-wide scale at nucleotide level resolution using Photoactivatable Ribonucleoside Enhanced Crosslinking and Immunoprecipitation (PAR-CLIP) (Hafner et al. 2010b). CNBP bound 4178 mRNAs at 7545 distinct sites, distributing mainly to G-rich regions in the first 50 nucleotides (nt) downstream of the AUG start codon. Using RNA-sequencing (RNAseq), ribosome profiling and Stable Isotope Labeling by Amino Acids in Cell Culture (SILAC)-based proteomics to quantify cellular mRNA and protein levels respectively we concluded that CNBP promoted translation of its targets. Our data are consistent with a possible role for CNBP as nucleic acid chaperone resolving structured mRNA sequence stretches proximal to the start codon.

2 Results

2.1 HEK293 has simultaneously expressed isoforms of CNBP

Human *CNBP* is predicted to encode multiple splice isoforms that change the composition of its nucleic acid binding domains and potentially modify target specificity (Chen et al. 2013). Till date there are six splice variants of CNBP documented in human system but nothing is known about their expression pattern. CNBP isoform1 is the largest isoform, while isoform 2 & 3 lacks few amino acids in their third CCHC domain. Isoform 4-6 has shorter RGG domain, with isoform 5 & 6 additionally missing few amino acids in their third CCHC domain (Figure 2.1A). I used HEK293 cells as our model cell line, extracted total RNA and performed reverse transcription using oligo dT primer. The CNBP cDNA was amplified using universal primers for all the isoforms and cloned into pETM-11. The sequencing of 22 cloned plasmids could detect presence of all the 6 CNBP isoforms in HEK293 cells (Figure 2.1B). CNBP isoform 3, which harbors a deletion in the third CCHC domain, and isoform 6, which contains deletions in the third CCHC domain and the RG-rich region, were the most abundant, representing more than 60% of the sequenced CNBP clones (Figure 2.1A,B).

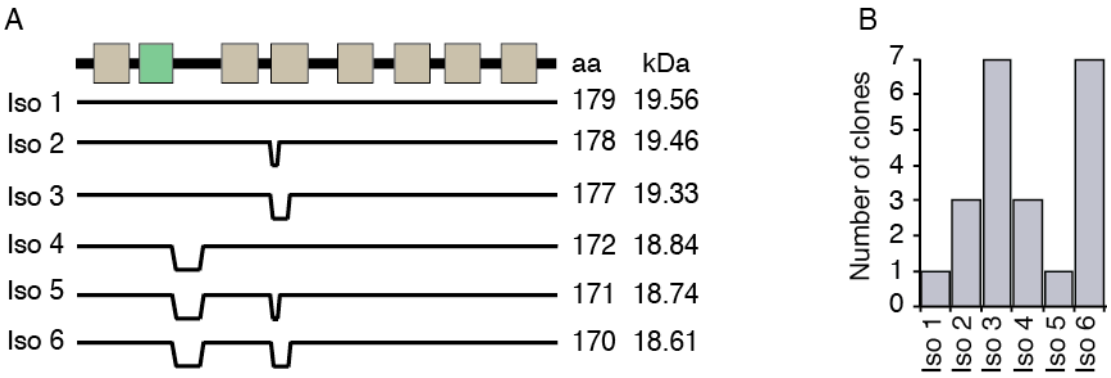

Figure 2.1. Overview of the human CNBP mRNA. (*A*) Sequence domain comparison of all six isoforms of human CNBP. Grey boxes represent the seven CCHC-zinc finger domains of CNBP while the green box represent the RG/RGG domain. The figure shows various splice variants of *CNBP*. Isoforms 1 (iso1) is the full length protein with 179 amino acids while the different splice variants are missing few amino acids either in CCHC or RGG domain (*B*) Clone count distribution across six CNBP isoforms from 22 sequenced full-length clones from HEK293 cDNA.

2.2 CNBP interacts with PRMT1 *in vivo* and is exclusively cytosolic

Methylation at arginine residues in RG-rich domains could influence protein function in two

ways: methylated arginine residues can be recognized by adapter proteins shuttling between cytoplasm and nucleus, resulting in changes of subcellular localization (Lee et al. 2012). Alternatively arginine methylation could influence the nucleic acid binding properties of adjacent domains (Wei et al. 2014).

Similar to CNBP, SERBP1 (a protein implicated in tumor progression) also contains a RG/RGG domain. A recent study has shown the methylation of SERBP1 RG/RGG domain by PRMT1 influences its cellular localization and nucleic acid binding property (Lee et al. 2012). In an attempt to identify, if similar to SERBP1, CNBP also interacts with PRMT1 protein we performed FLAG immunoprecipitation of CNBP using HEK293 CNBP isoform 3 overexpressing cell line followed by mass-spectrometry. The SDS-PAGE followed by silver staining of CNBP co-IP revealed a prominent band at around 40 kDa (band in red box) (Figure 2.2A). The band was cut out and sent for mass spectrometry analysis to AG Schlosser. After processing the band was indeed revealed as PRMT1.

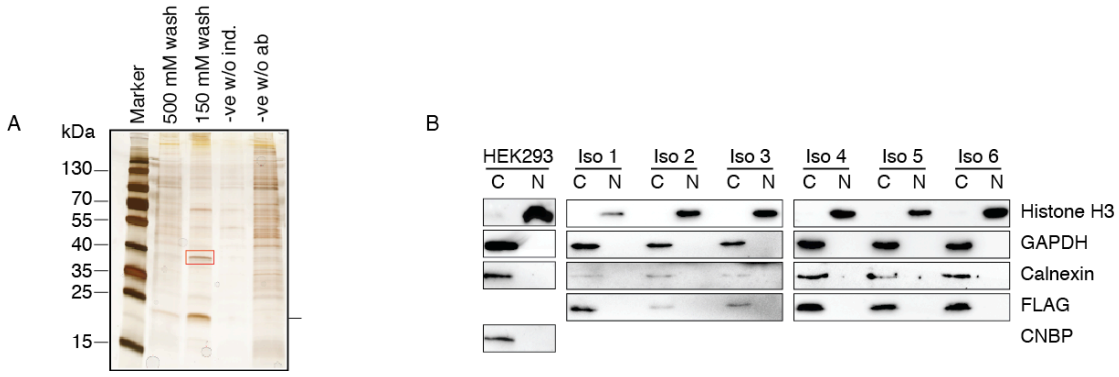

Figure 2.2. CNBP interacts with protein arginine methyl transferase-1 *in vivo* and is exclusively cytosolic. (*A*) SDS-PAGE showing CNBP co-immunoprecipitation. The HEK293 cells over expressing FH-CNBP iso 3 under the control of inducible promoter were used. Various salt washes were tested to optimally IP the CNBP and its binding partners (lane2-3). As a negative control cells without tetracycline induction or IP without antibody was used (lane 4-5). The small arrow shows the IPed CNBP and the red box shows the band used for mass spectrometry (*B*) Analysis of nucleocytoplasmic distribution of FH-CNBP isoforms 1-6 in HEK293 cell lines, as indicated. Cytoplasmic (C) and nuclear (N) fractions were probed with anti-CNBP, anti-FLAG (FH-CNBP), anti-Histone H3 (nuclear marker), anti-GAPDH (cytoplasmic marker), and anti-Calnexin (endoplasmic reticulum marker) antibodies

Next, to investigate if the association of CNBP with PRMT1 affects its cellular localization and also because previous reports suggested nuclear as well as cytoplasmic functions for CNBP, I investigated whether differential inclusion of the RG-rich domain could influence subcellular localization. I generated stable HEK293 cell lines expressing FLAG/HA-tagged CNBP iso1-6

under the control of tetracycline-inducible promoter (Spitzer et al. 2013). Subcellular fractionation from these six cell lines revealed that all CNBP isoforms mainly localize to the cytoplasm (Figure 2.2B). To confirm if the endogenous CNBP behaves similarly as the over-expressed isoforms, I performed cellular fractionation with the wild type HEK293 cells and blotted the fractions with CNBP antibody. As expected we could see the presence of CNBP only in cytoplasmic fraction. This result favors a predominantly posttranscriptional, rather than transcriptional function for CNBP, with RNA presumably being its major nucleic acid binding partner.

2.3 CNBP PAR-CLIP revealed its preference for CDS binding

To investigate the RNA binding property of all the six isoforms of CNBP *in vivo*, 4-thiouridine (4SU) PAR-CLIP was performed. 4SU irreversibly crosslink the RNA and interacting protein upon 365 nm UV exposure (Hafner et al. 2010b). Stable cell lines overexpressing various isoforms of CNBP under tetracycline inducible promoter were used. 14 hours after induction cells were exposed to 1 J/cm^2 of UV light of 365 nm wavelength. Autoradiography of the crosslinked, ribonuclease-treated, immunoprecipitated, and radiolabeled FH-CNBP isoforms 1-6 ribonucleoprotein (RNP) complexes revealed one major band at the expected size of ~20 kDa molecular mass. As a negative control the CNBP isoform 1 cells were used which was not exposed to UV (Figure 2.3A). This indicated that isoform-specific differences in the RG-rich region did not influence the ability of CNBP to interact with RNA ligands *in vivo*.

To identify the RNA population bound to CNBP, I chose one of the two most abundant CNBP isoform in HEK293, isoform 3. I recovered the interacting RNA from the crosslinked RNP by proteinase K digestion, performed adapter ligations and generated complementary DNA (cDNA) libraries for next generation sequencing. The recovered RNA was deep sequenced using Illumina Hi-seq2500 sequencer in the lab of Markus Hafner (NIH). Markus performed further downstream bioinformatics analysis of the sequenced library. The PARalyzer (Corcoran et al. 2011) software identified 8420 high confidence clusters (binding sites), of which 7545 distributed over 4178 mRNAs (appendix 4)(Fig. 2.3B). Consistent with its cytoplasmic localization, CNBP preferentially interacted with mature mRNAs, with 54% of the clusters in coding sequences (CDS) and 27% in the 3' untranslated regions (UTR) (Fig. 2.3B,C). In order to show the enrichment of CNBP binding sites for CDS over other regions, we performed further analysis and compared the distribution of crosslinked sites to the overall distribution of nucleotides in mRNA. Our analysis revealed a clear-cut enrichment in CDS binding sites number when compared expected over observed. On the other hand the 3' UTR binding site number had depletion in binding site number (Fig. 2.3D), showing CDS binding preference for CNBP.

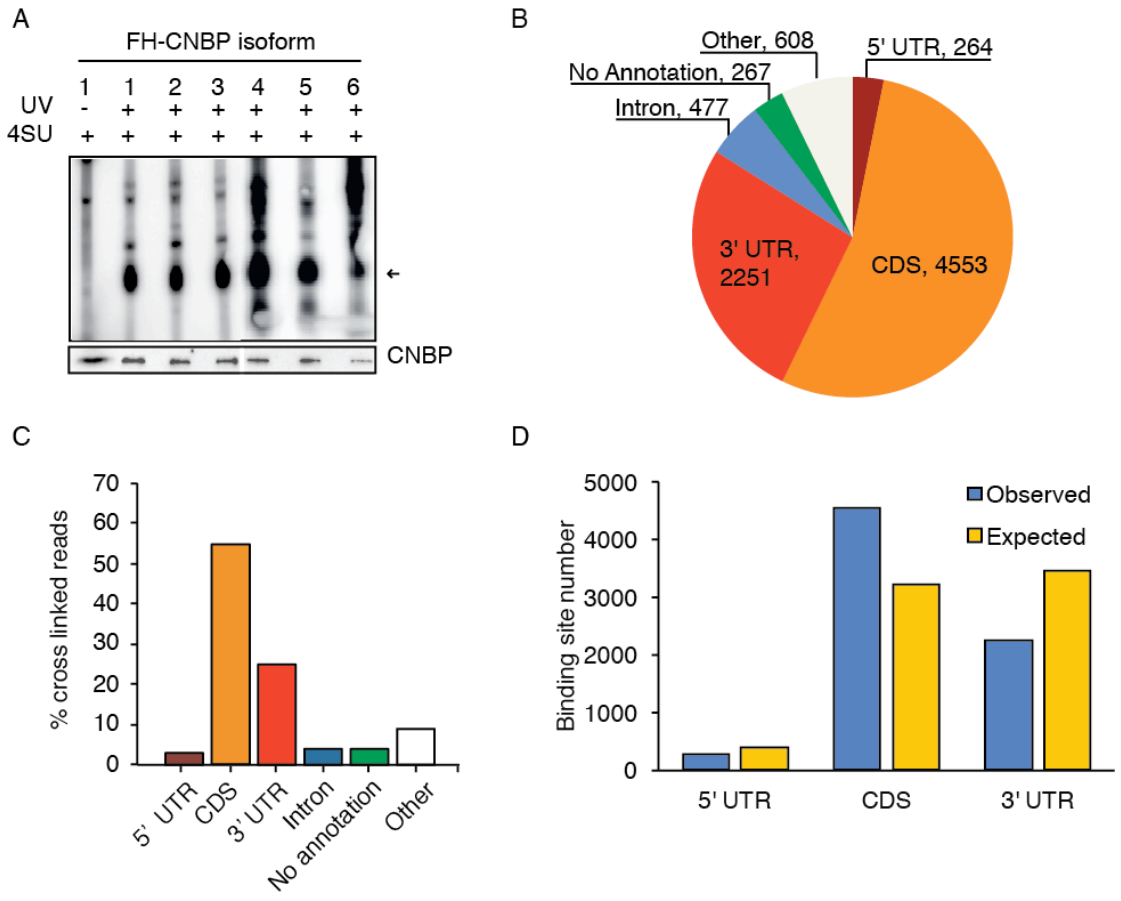

Figure 2.3. CNBP binds to RNA *in vivo* with a preference for CDS binding. *(A)* Autoradiograph of CNBP PAR-CLIP samples showing RNA-protein complex (indicated by the arrow). The *in vivo* UV cross-linked RNA bound to the CNBP was radiolabelled and ran on 4-12% SDS-PAGE**.** 1-6 represents the six different isoforms of CNBP derived from HEK293 cells stably expressing different isoforms upon induction. All the samples were fed with 4SU and cross-linked with UV 365 before harvesting. As a negative control the full length CNBP (iso1) was not exposed to the UV. The blot below shows the IPed protein by western blot. FLAG antibody was used as primary antibody to detect CNBP. *(B)* Distribution of CNBP isoform 3 bound clusters from PAR-CLIP analysis across different annotation categories. Stringent filtering conditions were used to generate high confidence clusters. Others include ncRNAs, lincRNAs, and other RNAs *(C)* Distribution of percentage of cross-linked reads across different annotation categories. Out of total cross-linked read counts (807392), more than 50% belongs to the CDS indicating the high preference of CNBP towards CDS binding. *(D)* Analysis of target transcript regional preferences for CNBP. The number of exonic binding sites annotated as derived from the 5' UTR, CDS or 3' UTR of a target transcript is shown (blue bars). Yellow bars show the expected location distribution of clusters if CNBP bound without regional preference to the set of target transcripts.

2.4 CNBP interacts with mature mRNAs in G-rich regions

RNA binding proteins often recognize their target RNAs in a sequence specific manner usually 4-6 nucleotide long, to carry out the assigned function (Stefl, Skrisovska et al. 2005). In order to define the preferred RNA recognition element (RRE) for CNBP, I used HOMER (Heinz et al. 2010) for computational sequence analysis on the complete set of PAR-CLIP-defined binding sites. HOMER uses zero or one occurrence per sequence coupled with hypergeomatric enrichment calculations to determine motif enrichment. This approach identified UGGAGNW as the most common RRE (>40% of all binding sites), with other G-rich motifs containing a GGA or GGG core also showing strong enrichment in the computational analysis and often occurring multiple times in CNBP binding sites (Figure 2.4A,B).

A

B

Gene	PAR-CLIP cluster sequence	Total reads	XL- reads
STAG2	AACAGAATGGAGTGGAAAACATGATGTTGTTT	3668	1983
PDCD4	GAGCTGTTGGAGATGGAATTTATG-------	3499	1564
HNRNPDL	TAACTATGGGAACTATGGATATGGACAGGGAT	3385	1728
SON	GTGGCGCTGGAGATCTCTGTTCAGTCTGTGGT	3175	1820
PMAIP1	GGAGATTTTGGAGACAAACTGAACTTCCGGCAG	2503	1300
NUP155	--TTATATGGATTTACTCTGGCGGTATTACGA	2353	1167
ADAMTS1	TTCCTTTGGGAGTGGGCCTGCGGTGGAATGGA	2346	1300
HNRNPH3	TAGTGATGGGACAGTACGACTTCGTGGACTAC	1998	1059
IRS4	TGCTGTATGGATATTTCTCTCTCCCCCAG---	1994	987
NCL	GCCTCAGAGGATGAGGACGATGAGGATGACGA	1860	965
IVNS1ABP	-----AATGGAAAGTTATACATCGTTGGTGGC	1719	902
LUC7L3	CAGTTGTTGGATGAGTTAATGGGCCGGGAC--	1397	818
GRSF1	GTTTGAGAGGACTTCCTTATAGTTGCAATG--	1309	608
SNRPD3	AGTTCATTGGAGTGGGTGCTTGTGCATATATG	1087	442
TMEM123	--ATACTGGGAGCTTTGTTGGTGGTATTGTATT	1064	456
GALNT2	GTGTGGTTGGAGTTTATGAATGTCACAATGCT	1026	549
CDCA2	TTACTTTTGGAGAGGACTTAAGCCCGGAAG--	1021	604
DDX42	TTGGCTTTGGAGGTTTTGCCATCAGTGCTGGG	858	619
TMPO	------CCGGAGTTCCTGGAAGACCCCTCGGT	826	420

Figure 2.4 CNBP binds to G-rich sequences at the start of its target mRNAs. *(A)* Weblogo of representative RRE from CNBP PAR-CLIP binding sites generated by HOMER (Heinz et al. 2010). Top 3

motifs above showing a G-rich binding motif for CNBP. GGAG or GGGG or GGA comprised more than 80% of the total clusters. *(B)* Top PAR-CLIP clusters showing presence of one or more predicted RREs (in red). The number of total and crosslinked reads for the clusters are shown.

2.5 CNBP binds to G-rich sequences *in vitro*

In order to evaluate the impact of putative GGAG containing RRE on CNBP binding electrophoretic mobility shift assays (EMSA) with purified recombinant CNBP isoform 3 was used. I designed synthetic, 20 nt long single-stranded RNAs (ssRNAs) either consisting of (1) four uridines flanked by 8 adenosines, (2) one GGAG group flanked by 8 adenosines, (Yoon, De et al.) or two GGAG groups, each flanked by 4 adenosines on either side (Figure 2.5.2A). While the oligoribonucleotide without GGAG did not show any appreciable interaction with the CNBP at concentrations of up to 5 μM protein, the addition of GGAG caused slight shift at CNBP concentration of 3 and 5 μM, and the addition of a second GGAG resulted in an almost complete shift of the oligoribonucleotide at CNBP concentrations >0.5 μM (Figure 2.5.1A). The EMSA proved difficult to quantitate and we switched to filter binding assays to derive precise binding constants. The synthetic oligoribonucleotides with zero, one, or two GGAG groups showed dissociation constants (K_d) of >10 μM, 0.33 μM, or 0.12 μM, respectively, confirming that the presence of the G-rich motif confers binding to CNBP (Fig. 2.5.2A).

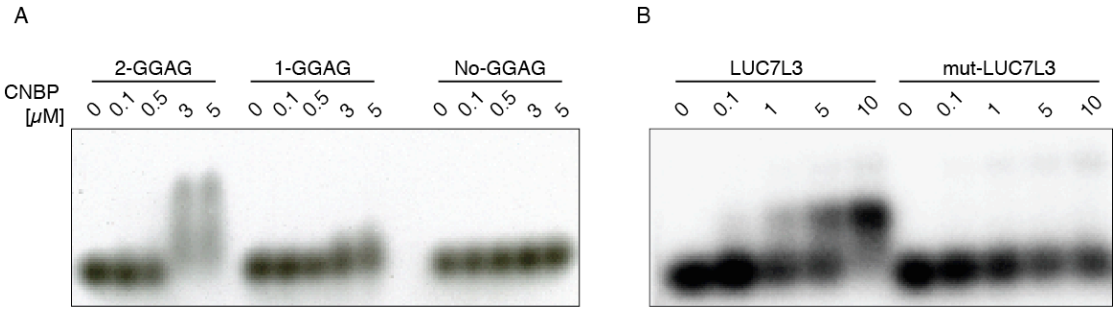

Figure 2.5.1 CNBP interacts with G-rich sequence elements *in vitro*. *(A)* EMSA showing interaction of CNBP with synthetic RNA targets. The RNA fragments were 20-mers with 2-GGAG, 1-GGAG and No-GGAG in them. The binding of CNBP drastically reduces in RNA with one GGAG and the binding is completely lost in RNA without any GGAG. *(B)* EMSA as above performed for one of the top PAR-CLIP target cluster. Upon mutation of GGAG motifs from the target sequence the binding is completely lost.

Next, I validated the binding of CNBP to PAR-CLIP derived binding sites *in vitro*. I generated ssRNA representing four different binding sites by *in vitro* transcription (Figure 2.5.2B) and quantified their affinity to CNBP by filter binding. I quantified the bound and unbound

radioactivity signal using Prism software and calculated the dissociation constants. The obtained K_d varied between the range of 0.06 and 1.4 μM. The K_ds for different tested targets were LUC7L3: 0.06, TMPO: 0.08, DDX42 & HNRNPH3: 1.4 μM respectively. Mutations in the core G-rich binding motif resulted in loss of CNBP binding (Figure 2.5.2B,C). Finally, in an attempt to define the role of RG-rich domain and individual CCHC-domains I used three recombinantly expressed CNBP constructs either lacking the RG-domain, the N-terminal CCHC domain or the two C-terminal CCHC domains (Figure 2.5.2D). All of the above mentioned three constructs had severely reduced binding affinities compared to the full length CNBP which led to conclude that in addition to the ZnF domains, CNBP also requires RG-domain for high affinity RNA binding (Figure 2.5.2E). In summary, the *in vitro* studies confirmed PAR-CLIP-derived CNBP binding sites and emphasized the requirement of G-rich sequences for high-affinity binding.

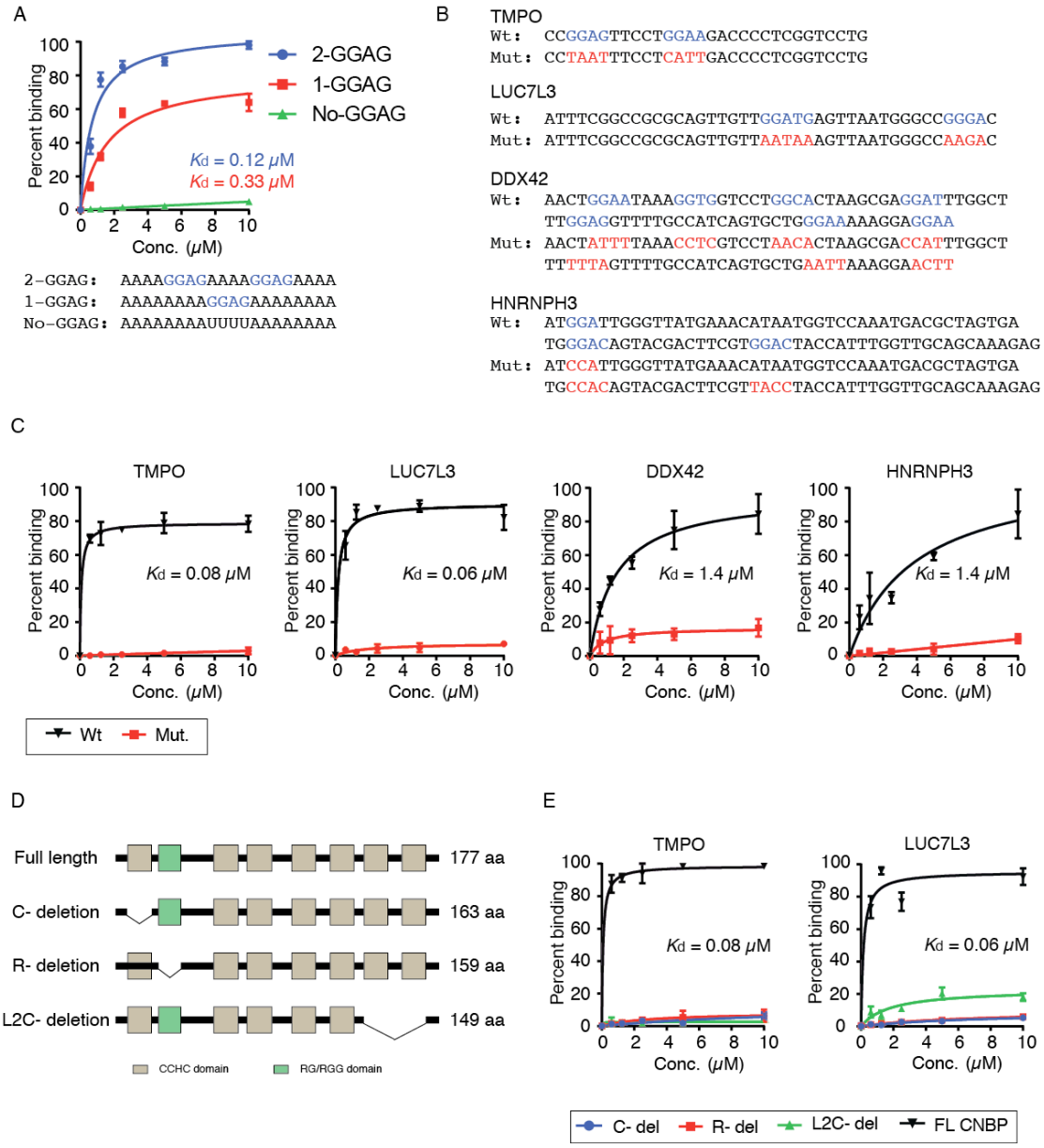

Figure 2.5.2 CNBP interacts with G-rich sequence elements *in vitro*. *(A)* Filter binding assay using recombinant CNBP with synthetic RNA targets containing 2-GGAG, 1-GGAG, and No-GGAG. Sequences shown below *(B)* Sequence of representative PAR-CLIP binding sites used to perform filter-binding assays. Nucleotides highlighted in blue correspond to the predicted CNBP binding motif and were mutated (red). *(C)* Quantification and K_d calculation of target and mutant sequence shown in (B). *(D)* Pictorial representation of different mutant constructs of CNBP generated and used to perform filter-binding assay. *(E)* Quantification and K_d calculation of 2 PAR-CLIP binding sites using different mutant constructs shown in (D).

2.6 CNBP binding slightly reduces target mRNA abundance

We next wanted to establish whether CNBP is involved in cytoplasmic posttranscriptional gene

regulatory processes, and investigated its influence on target mRNA stability. Charles Danan from Markus Hafner's lab (with my input) generated CNBP knockout (KO) HEK293 cell lines with CRISPR-Cas9 mediated gene knockout (Figure 2.6A,B). Together we generated the RNA library using rRNA depletion kit followed by NEB library preparation kit (Figure 2.6C). The generated library was sequenced and Markus Hafner and I performed further downstream processing. Our analysis revealed that loss of CNBP led to a marginal albeit statistically significant increase of target mRNA levels (Figure 2.6D). CNBP PAR-CLIP top targets, determined either by binning according to number of binding sites or by number of crosslinked reads, increased in abundance by only 2% (Figure 2.6D,E) (appendix 4).

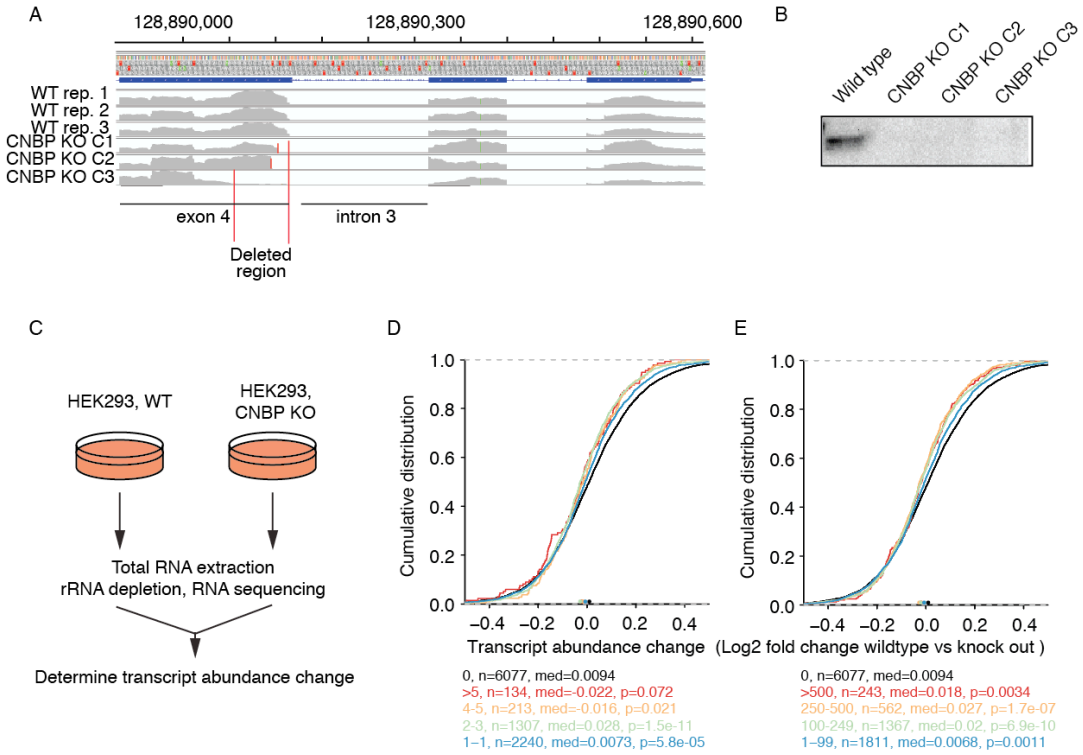

Figure 2.6 CNBP target mRNAs are accumulate in the cell upon CNBP knockdown. (A) IGV screen shot showing deleted regions in exon 4 of CNBP compared to the wildtype after CRISPR/Cas9 mediated CNBP knockout. *(B)* Anti-CNBP immunoblot of HEK293 cell lysate after CRISPR/Cas9-mediated CNBP knockout. Three CNBP KO clones are shown compared to the parental HEK293 cell lines. *(C)* Scheme of CNBP knockout and RNA-seq experiment**.** *(D,E)* Cumulative distribution analysis of change in average mRNAs expression comparing the three CNBP KO cell lines from (B) with parental HEK293 cells (n=3). Target mRNAs are binned based on number of binding sites (D) and crosslinked reads (E). Significance (p-value) was determined using two-sided KS (Kolmogorov–Smirnov) test. Bin size is indicated in the legend.

2.7 CNBP preferentially binds to start of the target mRNAs

Given the rather small magnitude of the effect on mRNA abundance, I next wanted to investigate whether CNBP influences other cytoplasmic posttranscriptional regulatory (PTGR) processes beyond mRNA stability. An analysis of the distribution of CNBP PAR-CLIP binding sites on all mRNA targets revealed no particular enrichment of binding sites at recognizable mRNA features with the exception of a striking enrichment of CNBP binding sites close to the mRNA start site, within the first 50 nt of the CDS (Figure 2.7A). At the same time, I performed polysome profiling of HEK293 cells and could see co-sedimentation of CNBP with the 40S, 80S, and the polysomal fraction (Figure 2.7B). Taken together, these data pointed to a role for CNBP in translational regulation and we hypothesized that CNBP might influence translational elongation across G-rich regions at mRNAs.

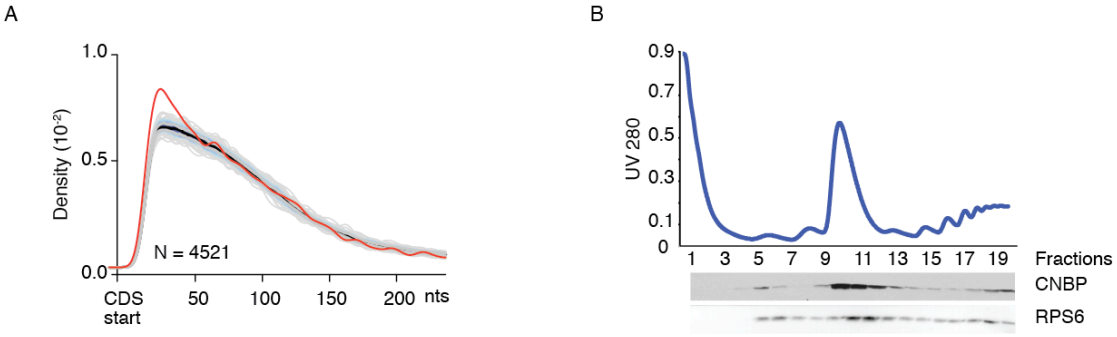

Figure 2.7 CNBP preferentially binds to the start of the target mRNAs and co-sediments with 40S, 80S and polysomal fraction. *(A)* Distribution of CNBP binding region across the length of target mRNAs. Spatial, a part of PARpipe package (Ohler lab) was used to generate the output. X-axis represents the distance from start codon in nucleotides and Y-axis represents the density, i.e. normalized cluster count. Top 4521 clusters were taken into consideration. The software creates a background set of the same number of sequences from the same region as cluster set is matching and plots the distribution (after repeating it approx. 10,000 times). *(B)* Western blot of HEK293 cellular extracts separated via sucrose density gradient centrifugation (5-45%) shows the co-sedimentation of CNBP with 40S, 80S and polysomal fractions. RPS6 blot is used as control.

2.8 Ribosome profiling shows stalling of translating ribosome on target mRNAs upon CNBP knockdown

Ribosome profiling is a quantitative genome wide analysis of *in vivo* translation by deep sequencing. A translating ribosome roughly covers 30 nts portion of the template mRNA and protects it from nuclease digestion. This nuclease protected mRNA fragments are used to map the exact position of ribosome across the transcript. Deep sequencing of the ribosome positions

along with the quantitative expression profile of the transcripts enables to measure the translation (Ingolia, Ghaemmaghami et al. 2009).

Despite previous studies claiming the role of CNBP in translation, the exact mode of CNBP function on its target mRNAs translation was pretty unclear. In order to shed light on CNBP mechanistic function and directly measure the impact of CNBP on translational efficiency Daniel Ben Halevy performed ribosome foot printing or ribosome profiling with CNBP knock out and parental HEK293 cells. CNBP loss resulted in a robust decrease in ribosome occupancy on target mRNAs and its effect correlated with the number of CNBP binding sites (Figure 2.8.1A). Ribosome occupancy decreased by ~30% for the 134 CNBP targets (p=0) with more than 5 binding sites. Even for the 2214 targets with only a single CNBP site, ribosome occupancy decreased by ~9% ($p=13x10^{-10}$) (appendix 4). Previous studies have shown that the number of crosslinked sequence reads in a cluster frequently correlates with the occupancy of the RNA-binding protein on the RNA (Hafner et al. 2010b; Ascano et al. 2012b). Therefore, we binned the CNBP target transcripts by the number of crosslinked sequence reads found in their cognate clusters. As before, we found an ~30% decrease (p=0) in ribosome occupancy on the 243 target mRNAs with more than 500 crosslinked reads compared to mRNAs showing no interaction with CNBP. In the next 3 bins containing 558, 1355, and 1791 CNBP target genes ribosome occupancy changed by 18%, 12% and 8% respectively compared to non target genes (Figure2.8.1B).

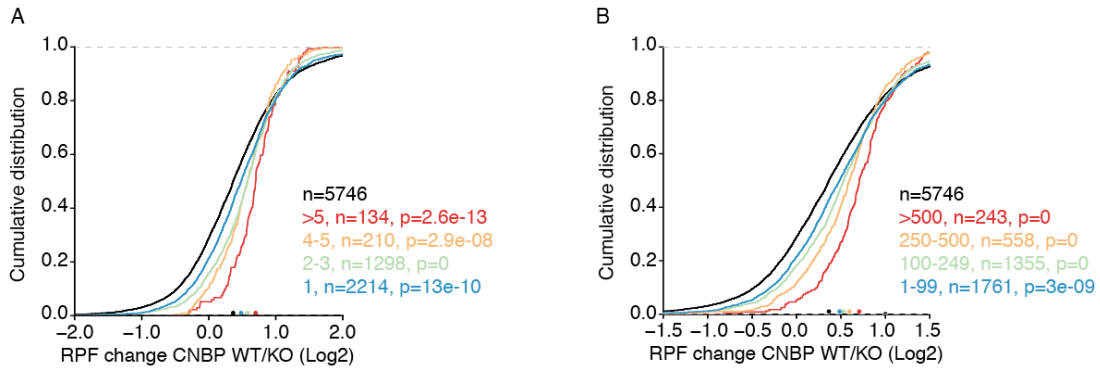

Figure 2.8.1 CNBP knockdown causes reduction in abundance of translating ribosome on target transcripts. *(A)* Cumulative distribution of change in ribosome protected fragments (RPF) upon CNBP knockout determined by ribosome profiling. CNBP PAR-CLIP target transcripts were binned based of number of clusters and their RPF were compared in wild type (WT) and knockout (KO) cells. The positive value on X-axis shows decrease in ribosome occupancy upon CNBP knockout. The black line (n=5746) with no CNBP binding sites was used as control to compare the RPF. *(B)* Same as in (A) except the targets were binned based on number of crosslinking sites.

While protein level changes often mirror the changes in mRNA expression profiles (Baek et al. 2008; Selbach et al. 2008), our observed decrease in ribosome occupancy and, by extension, protein expression levels of CNBP targets upon CNBP loss contrasted with our finding of a minor accumulation of target mRNAs. This pointed towards a role for CNBP in promoting translation, possibly by lowering the energy necessary for translation across structured mRNA regions. Thus, we calculated translational efficiency for each gene by normalizing the changes in ribosome occupancy with the changes in mRNA levels upon CNBP loss (Ingolia et al. 2009; Guo et al. 2010; Bazzini et al. 2012). Indeed, we found that CNBP loss correlated with increased translational efficiency on CNBP targets (~33% increase for the 243 top CNBP targets binned by intensity of crosslinking, Figure 2.8.2A,B, p=0). Similar to want we observed for the RPF change, the effect on translational efficiency change was directly correlated with the number of crosslinking sites.

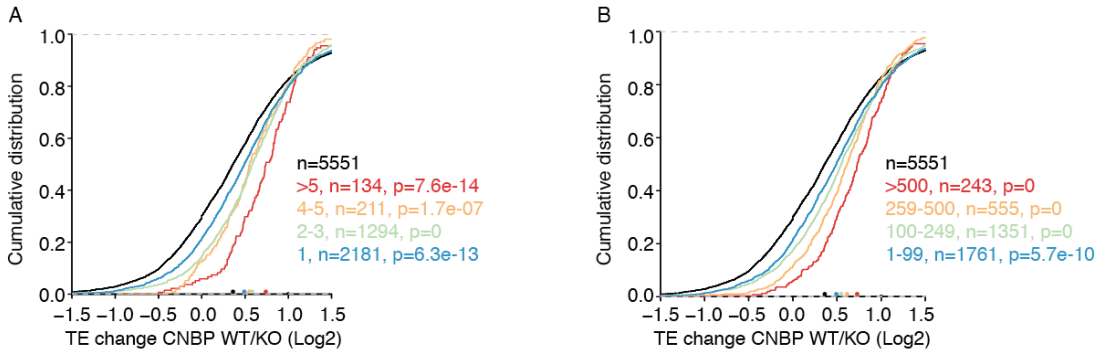

Figure 2.8.2 CNBP promotes translation of target mRNAs. *(A)* Cumulative distribution of translational efficiency (TE) change. The efficiency matrix was calculated (as described in text) and the change for target transcripts was plotted. The transcripts were binned based on number of clusters. *(B)* Same as in (A) except the targets were binned based on number of crosslinked reads.

2.9 CNBP preferentially affects the translation of CDS targets without any site preference within CDS

We also asked whether the location of the CNBP binding sites had an impact on gene regulation. Even though we did find ~30% of the binding sites in target mRNA 3'UTR, we did not find evidence of changes in transcript abundance or ribosome occupancy in RNA-seq or Ribo-seq experiments upon CNBP loss (Figures 2.9A,B). The RPF change and translational efficiency change for 617 tested CDS was ~30% & 33% whereas 3' UTRs (n=104) gave a mere 7% & 7.5% change when compared with the control (Figure 2.9B,C).

To analyze the positional preference of CNBP binding across the CDS, we compared the

translational efficiency change of the targets with in first 50 nts of start codon or more than 50 nt downstream of start codon. As shown in Fig 2.9D binding of CNBP anywhere in the CDS was sufficient to increase target mRNA translational efficiency, with no preference detectable for sites close to the translational start, despite their enrichment in that region (Figure 2.9D).

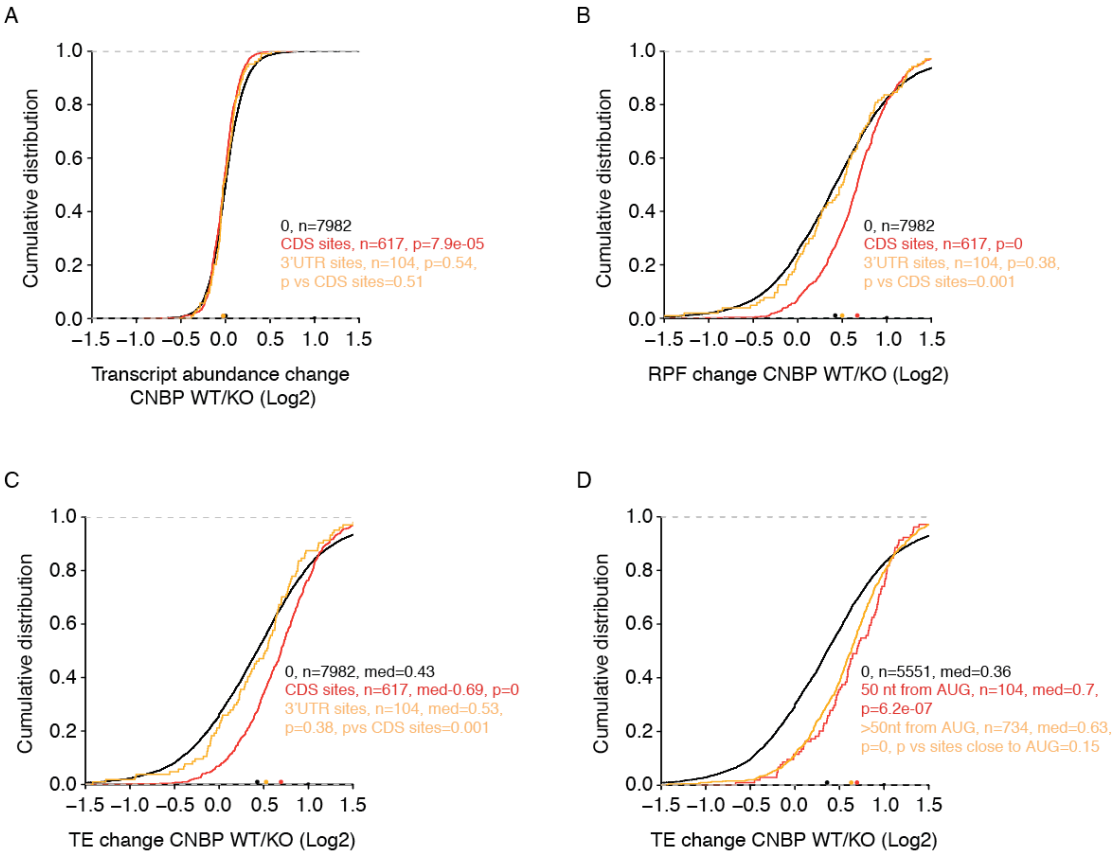

Figure 2.9 CNBP affects CDS target transcript translation. *(A)* Cumulative distribution analysis of change in transcript abundance obtained from RNAseq (WT vs KO). *(B)* Cumulative distribution of RPF change obtained from ribosome profiling data comparing CDS (in red) and 3' UTR sites (in yellow). *(C)* Cumulative distribution analysis of change in translational efficiency of targets in CDS (red line) and 3' UTR (yellow line). *(D)* Cumulative distribution analysis of change in translational efficiency oftargets with binding sites in the CDS within 50 nt of the start codon (red line) or more than 50 nt downstream of the start codon (yellow line). Only targets containing more than 200 crosslinked reads are plotted. p-value of KS-test against non targets (black line), as well as between the two target bins is indicated.

2.10 CNBP knockdown reduces the target protein levels

To directly measure the impact of CNBP on protein levels we use Pulsed Stable Isotope Labeling by Amino Acids in Cell Culture (pSILAC) coupled with quantitative proteomics. I performed siRNA-mediated knockdown of CNBP and compared the protein expression profile of CNBP

targets in WT/Knockdown cells. siRNA mediated CNBP knockdown lead to a reduction in CNBP levels upto 20%. The WT cells were labeled with heavy media (heavy lysine and heavy arginine) and the knockdown cells were labeled with medium heavy amino acids. After a pulse of 24 hours cells were lysed and the lysates were sent to AG Schlosser for mass spectrometry analysis. Jens Venslow in RVZ, performed the analysis of the mass spec samples and was able to reliably quantify 4887 proteins. We compared the expression levels of PAR-CLIP target mRNAs. The knockdown of CNBP resulted in a small but significant decrease in abundance of proteins encoded by mRNAs with more than 25 CNBP binding sites (Figure 2.10A) compared to products of mRNAs showing no CNBP binding.

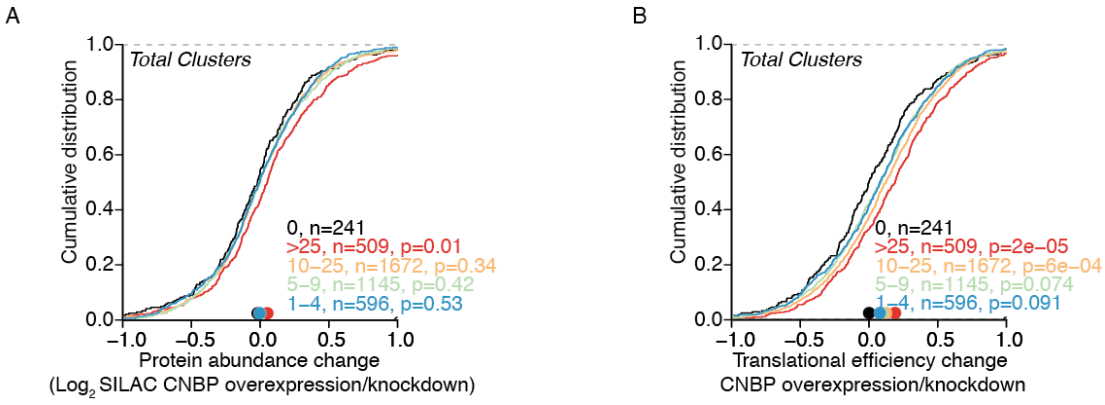

Figure 2.10 CNBP knockdown reduces the target protein levels. *(A)* Cumulative distribution of protein level change upon CNBP knock down determined by pSILAC. Significance was determined using two-sided KS (Kolmogorov–Smirnov) test. Bin size is indicated in the legend. *(B)* Same as in (A), except the cumulative distribution of a translational efficiency metric (Dprotein - DRNA) is plotted.

Similar to ribosome profiling, we generated a translational efficiency metric by subtracting the change in mRNA levels for each gene from the observed changes in protein levels upon CNBP knockdown and overexpression. Indeed, we found that increased levels of CNBP were correlated with increased translational efficiency on CNBP targets (14% increase for CNBP targets with more than 25 PAR-CLIP binding sites, Figure 2.10B).

2.11 CNBP enhances the translation rate of target mRNAs by resolving the G-rich secondary structure

To further test the observation that CNBP binding leads to increased translational output I designed the reporter assays using representative PAR-CLIP binding sites from the TMPO, LUC7L3, and DDX42 mRNAs. Each of these binding sites is previously documented to bind CNBP

in vitro, and is located within the CDS, less than 50 nt from the start codon (Figure 2.5.2B,C). The sequences were cloned in-frame with the firefly luciferase mRNA directly downstream of the AUG codon in the psiCHECK-2 dual luciferase reporter assay system (Figure 2.10.1A). Upon knockdown of CNBP I observed a highly significant (20-40%) decrease in firefly luciferase-reporter levels (Figure 2.10.1B). This decrease could be rescued by mutations within the G-rich CNBP binding sites, which were previously shown to abrogate CNBP binding *in vitro* (Figure 2.5.2B,C). In summary, our data are consistent with a function of CNBP as an RNA chaperone enhancing translation across G-rich elements at the 5' end of target mRNAs, which have the potential to form stable secondary RNA structures.

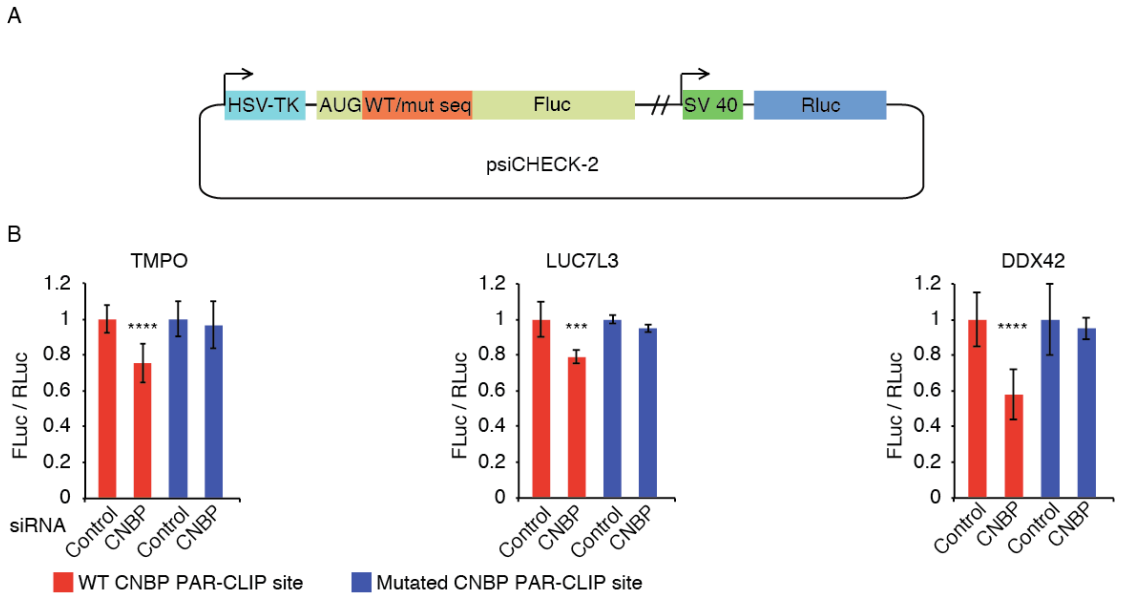

Figure 2.11.1 CNBP resolves the G-rich secondary structure and promotes translation. *(A)* Schematic representation of reporter system. The wild type (WT) and mutant sequences (mut) are cloned behind the firefly luciferase start codon in dual luciferase vector. *(B)* Effect of CNBP knockdown on luciferase reporter expression. Firefly luciferase expression is normalized to Renilla luciferase expression and set to 1 for the control knockdown. Paired t-test was performed using Prism software to determine the p-value (****, <0.0001; ***, <0.0006).

In order to check if the G-rich target motifs used in this study (to perform *in vitro* and luciferase assays) forms secondary structure we used selective 2'-hydroxyl acylation analyzed by primer extension (SHAPE). SHAPE chemistry uses the nucleophilic property of the ribose 2'-position, which is exquisitely sensitive to the electronic influence of the adjacent 3' phosphodiester group (Wilkinson, Merino et al. 2006). The 2' hydroxyl group is more sensitive to modification when unconstrained. Whereas upon base pairing, the 2' hydroxyl group is scantly available for

modifications. An electrophile (e.g. NMIA) is used to modify the 2'hydroxyl end and hence to determine the position of base pairing upon reverse transcription.

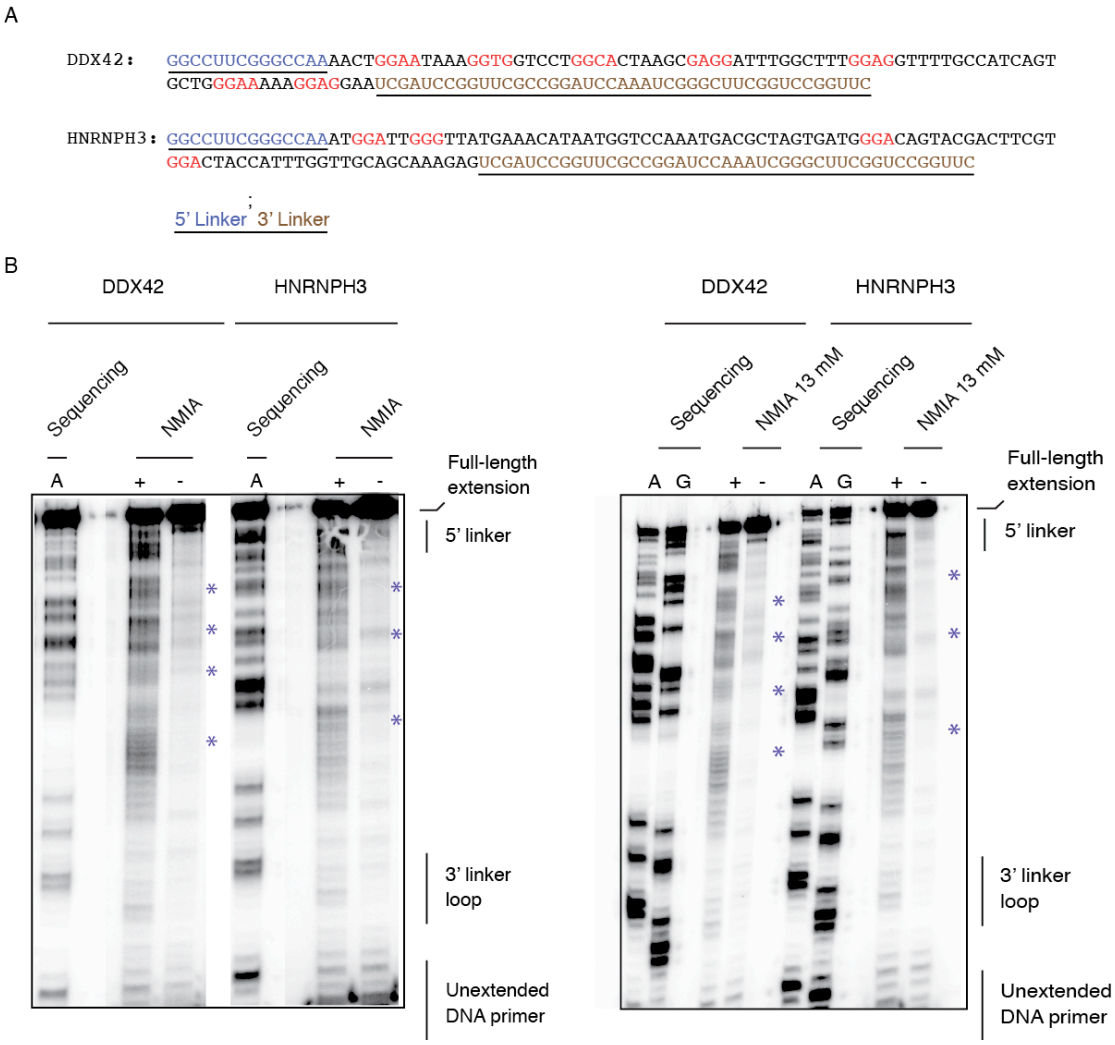

Figure 2.11.2 CNBP resolves the G-rich secondary structure and promotes translation. *(A)* Sequence of the target RNAs used for SHAPE experiments. CNBP RREs and 5' and 3' linker sequences are indicated. *(B)* Autoradiograph of 12% denaturing polyacrylamide gel after fractionation of NMIA treated and untreated sequences from (A). For the sequencing reactions, primer extension spiked with ddATP or ddGTP was performed on the substrate RNA. Black bars indicate potentially structured regions.

For two different binding sites (obtained from PAR-CLIP, DDX42 & HNRNPH3) I performed folding followed by NMIA/mock treatment. Upon treatment with NMIA, I could detect the secondary structure formation at the 3' and the 5' linker region as described in Wilkinson et al 2006 (Wilkinson, Merino et al. 2006). Except that, I could also detect some potential secondary structures (marked with stars) for both the sequences that were absent in sample treated with only mock (DMSO) (Figure 2.10.2A,B).

3 Discussion

Gene expression inside a eukaryotic cell plays a major role in determining the cellular fate. Out of approximately 20,000 protein coding genes in human cells only a fraction is expressed at a time during particular phase of growth and development. At any given time the amount of a particular protein in cell reflects the balance between that protein's synthetic and degradative biochemical pathways (Rothman 2010). To ensure the adequate spatiotemporal expression of different proteins various regulatory networks are required. One of the key regulations at the level of RNA is mediated by variety of transcript-associated proteins. Ranging from lower prokaryotes to most developed eukaryotic system, RBPs have been discovered to play crucial role in cellular processes (Gerstberger, Hafner et al. 2014).

Recent genome wide high-throughput studies in 2 different labs have identified more than 800 RBPs bound to mRNAs in 2 different human cell lines (Baltz, Munschauer et al. 2012, Castello, Fischer et al. 2012). Out of ~800 identified RBPs only a handful has been characterized and we still don't know the target RNAs and the mode of action for most of them. Many of these RBPs have been implicated in various human diseases ranging from Fragile-X-syndrome to cancer (Table 1.2). To fully understand molecular mechanism and the root cause of underlying disease related to these RBP, their characterization is highly warranted.

A RBP that have been linked to myotonic dystrophy type2 (DM2) in humans and embryonic lethality in mouse and zebra fish is the topic of interest in this work. DM2 share many clinical features with myotonic dystrophy type 1(Meola 2000) and have been linked with muscle weakness and myotonia with cardiac conduction effect and smooth muscle involvement (Schneider, Ziegler et al. 2000). Similar to DM1 (which is caused by CTG repeats in the 3' UTR of DMPK mRNA), a CCTG extension in the intron 1 of CNBP pre-mRNA gives rise to non-translated mRNA and hence causes the disease onset.

In this thesis we have focused on the molecular characterization of CNBP. CNBP was identified as an mRNA binding protein in both of the above mentioned studies. We present the first comprehensive characterization of the poorly studied CNBP. We have introduced a number of genome wide studies that improves the current knowledge of CNBP molecular function *in vivo*. In addition to the previously known RNA binding property of CNBP, we have provided a genome wide picture of CNBP binding to target mRNAs. Using recently developed genome wide advanced CLIP technique (PAR-CLIP) we show for the first time the RNA binding property of all isoforms of CNBP present in human system. Using combinations of genome wide RNA-seq and ribosome profiling studies we show how the binding of CNBP affects the translation of target

mRNAs. Our work shows the possible and most likely chaperone activity of CNBP on its target mRNAs and provides a platform for studying individual target RNAs regulated by CNBP.

3.1 Cytoplasmic localization of CNBP

In humans, CNBP encodes at least six protein isoforms. These isoforms contain differences in the third CCHC domain, as well as in the RG-rich region conceivably involved in nucleo-cytoplasmic shuttling. Previous studies have shown various roles of RG/RGG domain (Thandapani, O'Connor et al. 2013) including nucleic acid binding, protein-protein interaction and protein localization. RG/RGG domains are also preferred sites for certain PRMTs for methylation (Thandapani, O'Connor et al. 2013). A recent study on SERBP1, an RGG domain containing protein, showed its association with PRMT1 which methylates the arginine residues and plays key role in its cytoplasmic distribution. On the similar line CNBP was also found in association with PRMT1 *in vivo* (this study). The association of PRMT1 led to methylated RG/RGG domain of CNBP but did not affect its localization (Wei, Hu et al. 2014).

Previous immunofluorescence studies on CNBP indicated its cytoplasmic and nuclear localization (Calcaterra, Armas et al. 2010) and were shown to play role as transcriptional activator (Borgognone, Armas et al. 2010). Before this work, nothing was known about the localization pattern of different isoforms of CNBP. Given the fact that the shorter isoforms 4-6 lacks few amino acids in RG/RGG domain, we asked ourselves the question if different isoforms have different localization pattern inside the cell. Our subcellular fractionation with HEK293 cell lines expressing each isoform under tetracycline inducible promoter showed that all the isoforms of CNBP could only be detected in the cytoplasm, similar to its homolog in mouse (Warden, Krisans et al. 1994) and *Xenopus laevis* (Calcaterra et al. 1999).

3.2 All CNBP human isoforms binds to RNA

Zinc finger proteins are classically characterized as transcription factor that bind to DNA sequences and acts as transcriptional regulators. Many studies have also shown the RNA binding properties of zinc finger proteins (Laity, Lee et al. 2001). Like many ZnF-containing proteins (Pace and Weerapana 2014; Hall 2005) CNBP was described as multifunctional and suggested to interact with both DNA and RNA. In an *in vitro* screen for the binders of ssDNA, CNBP was first described as DNA binding protein (Rajavashisth, Taylor et al. 1989). While later studies showed the association of CNBP with c-Myc promoter (Shimizu, Chen et al. 2003). At the same time studies involving polyA pulldown with amphibian oocyte lysates and *in vitro* assays showed RNA binding properties of CNBP (De Dominicis, Lotti et al. 2000). Together these studies lead to conflicting reports claiming its function as a transcriptional as well as post-transcriptional gene

regulator (Borgognone et al. 2010; Calcaterra et al. 1999; Sammons et al. 2011; Shimizu et al. 2003).

The predominant localization of CNBP in cytoplasm (Figure 2.2B, Calcaterra et al. 1999 and(Warden, 1994 #8)) and its strong preference for single strand nucleic acid binding (Rajavashisth et al, 1989) support its preferential RNA binding property. Our interest to discover for the differences amongst the various CNBP isoforms led us to check for their RNA binding property. Given the fact that various splice isoforms provide the protein with functional diversity and hence different role in cellular processes (Brett, Pospisil et al. 2002), we were interested to know if different isoforms of CNBP in human have differences in RNA binding property. Our PAR-CLIP autoradiograph with the various isoforms (under the control of CMV promoter) showed no differences in RNA binding properties of CNBP (Figure 2.3A). In line with the presence of all isoforms predominantly in the cytoplasm all six CNBP isoforms bound to RNA *in vivo* where as the control without UV-exposure showed no corresponding signal, proving all the isoforms of CNBP specifically bound RNA (Figure 2.3A).

3.3 CNBP exclusively binds to CDS of the target transcripts

The *in vivo* association of all CNBP isoforms with cellular RNA raised the question of molecular role of CNBP on its bound RNAs. Given the high degree of conservation of CNBP in different eukaryotes (Figure 1.4), its role in binding to the target RNA *in vivo* was very inquisitive.

The cDNA generated from one of the most abundant isoforms (isoform 3) in HEK293 cells was sequenced using Illumina Hi-seq-2500 and aligned to the human genome (HG19). The characteristic property of 4SU, to covalently crosslink the aromatic amino acid in direct contact upon UV 365 nm exposure, allowed us to pinpoint the sites of interaction between CNBP and its target RNAs.

Previous studies have claimed the binding of CNBP at 5' UTRs of the mRNAs in TOP-dependent manner and in turn acting as translational enhancer (Huichalaf, Schoser et al. 2009). Other studies have showed binding of CNBP to PABP1, eEIF1A, RPS6, β-actin and GAPDH mRNAs in TOP independent manner and acting as translational enhancer (Datu and Bag 2013). These data however gave a conflicting image of CNBP binding preference in target mRNAs. The distribution of the number of clusters from CNBP PAR-CLIP data showed a very high and well defined preference for CDS binding (Figure 2.3B). More than 50% of the clusters were CDS while 27% fell into 3'UTRs. The confidence of obtained clusters in PAR-CLIP data is a direct reflection of the number of crosslinked reads (Gerstberger, Hafner et al. 2013). As expected we could notice more than 55% of the total crosslinked reads in CDS region that confirms its preference for CDS binding in target transcripts (Figure 2.3C). The further line of evidence supporting CDS

preference of CNBP came from the analysis of distribution of crosslinked sites to the overall distribution of mRNAs (Figure 2.3D).

3.4 CNBP preferred targets contain GGAG rich stretches and all the CCHC domains and RGG domain contributes toward target binding

Out of hundreds of RBPs in eukaryotes only a handful have been studied in detail. One of the preliminary characterizations of RBPs is to define their preferred binding motif. In humans 15% of RBD containing proteins have known RNA binding motifs (Ray, Kazan et al. 2013). ZnF proteins show diverse binding sequence specificity; e.g. recent structural work for CCCH-type ZnF of the yeast Nab2 and the fly Unkempt proteins showed their strong preference for adenine and uridine bases, respectively (Kuhlmann et al. 2014; Murn et al. 2015).

The HOMER analysis of the PAR-CLIP clusters revealed GGA or GGG rich sequence motif for CNBP (Figure 2.3A, B). The preferential binding to the GGA rich motif is in consistent with the previous reports of CNBP binding to G-rich RNA stretches (Armas, Nasif et al. 2008). Recent studies on Lin28 protein family, which has 2 ZnFs homologous to CNBP seven CCHC ZnFs (Fig below), interact *in vitro* and *in vivo* with a GGAG motif (Nam, Chen et al. 2011). With the help of crystal structure, both CCHC ZnFs of Lin28 was shown to interact with GGAG via hydrogen bonding. This motif mirrors the CNBP RRE characterized in this study. RNA-protein crosslinking in 4SU-PAR-CLIP, HiTS-CLIP, and other CLIP-seq procedures occurs predominantly at uridines (Kramer et al. 2014; Sharma et al. 2015) and therefore requires the presence of uridine bases within a few nucleotides of the binding site. Nevertheless, our unbiased motif enrichment analysis revealed CNBP's G-rich RRE mitigating concerns that results from UV-crosslinking based protocols are disproportionately skewed towards U-rich RREs.

```
CNBP-1     CFKCGRSGHWAREC
CNBP-2     CYRCGESGHLAKDC
CNBP-3     CYNCGRGGHIAKDC
CNBP-4     CYNCGKPGHLARDC
CNBP-5     CYSCGEFGHIQKDC
CNBP-6     CYRCGETGHVAINC
CNBP-7     CYRCGESGHLARDC
Lin28-1    CYNCGGLDHHAKEC
Lin28-2    CHFCQSISHMVASC
```

Fig 3.1 Comparison of various CNBP ZnF (CCHC) domains with Lin28 ZnF domains.

Presence of more than one copy of nucleic acid binding domains in a RBP or DBP provides higher affinity and sequence specificity to the targets (Gerstberger, Hafner et al. 2014). Using

different domain truncations of CNBP we discovered that all the CCHC domains and the RGG domain contributes towards the binding. The N-terminal CCHC mutant and the C terminal 2 CCHC mutant showed no appreciable binding with the RNA. The binding affinities for the mutant proteins with RNA constructs containing CNBP binding motifs were in the similar range as with the full length protein with constructs missing the binding motifs. Our data provides convincing evidence of the requirement of CCHC domains for RNA binding. RG/RGG domains are canonical RNA binding motifs and have been reported for nucleic acid chaperone activity for various proteins (Nam, Chen et al. 2011). Previous reports have shown the inability of CNBP RGG mutants to bind to RNA. Coherence with previous reports our data also confirms the requirement of RGG motif for nucleic acid binding activity of CNBP.

3.5 Function of CNBP binding to its target RNAs

The detection of 4178-bound mRNA to CNBP raised the question of its role on these transcripts. Being a predominantly cytoplasmic protein, it is conceivable that CNBP effects either stability or the translation of target mRNAs. Cytoplasmic RBPs have been known to preferably interact with sequences or structural elements present in 3' UTR and in turn affects their stability (Iadevaia and Gerber 2015). For eg: AUF1 is a 3' UTR binder that stabilizes the target mRNAs and its knockdown causes more than 2 fold reduction (Yoon, De et al. 2014). On the other hand RBPs binding to the CDS have been know to confer functionality for e.g. forming post-transcriptional operons or RNA regulons enabling coordinated control of mRNA expression (Imig, Kanitz et al. 2012) (Tenenbaum, Carson et al. 2000, Keene 2007, Cook, Hughes et al. 2015). The loss of CNBP in HEK293 cells leads to a very marginal accumulation of target mRNAs (Figure 2.6) indicating that binding of CNBP on its target transcripts has very mild effect on their stability. In this work we show the binding of CNBP to the CDS of its target mRNAs. The co-sedimentation of CNBP with 40S, 80S, and polysomal fraction (Figure 2.7) along with association of Gis2 (a yeast homologue of CNBP) with translational machinery (Rojas, Farr et al. 2012), indicates towards the possible conservatory role of CNBP in translation. In line with the proposed role of CNBP in translation, a stress assays followed by immunofluorescence showed accumulation of CNBP into stress granules (Rojas, Farr et al. 2012). Stress granules are formed to protect translating mRNAs upon external stress. Apart from scaffolding proteins e.g. TIA1, stress granules are rich in translation initiation factors and other mRNPs involved in translation regulation (Buchan and Parker 2009).

The ribosome occupancy on a given transcript directly mirrors the degree of its translation (Ingolia, Ghaemmaghami et al. 2009). To calculate the effect of CNBP on the translation of target mRNAs we used a novel genome wide ribosome profiling approach, combined with high

throughput sequencing. Using CNBP KO and parental HEK293 cell lines we compared the ribosome occupancy on target transcripts. Our ribosome profiling study from CNBP KO cells showed a strongly reduced translation of target transcripts (Figure 2.8.1). Reduced ribosome occupancy in CNBP KO cells at the target transcript site containing GGAG/GGA motif is an indicative of the role of CNBP in facilitating their translation. In accordance with our data, previous studies on Gis2 and CNBP using various reporter systems have also shown the effect of CNBP as translational enhancer (Sammons, Antons et al. 2010) (Sammons, Samir et al. 2011) (Gerbasi and Link 2007).

Next, we were interested to check the effect of CNBP KO on the rate of target translation. We generated translation efficiency matrix by comparing the change in ribosome occupancy and mRNA levels for a particular mRNA. The translational efficiency of top targets with more than >500 crosslinked was in average reduced by 30% and that of all ~4000 targets went down by 10% on average upon CNBP loss (Figure 2.8.2). Taken together this represents a massive shift in the gene regulation of the ensemble of target mRNAs, which is consistent with the embryonic lethality upon CNBP loss.

A study on myoblast cells from DM2 patients detected reduced expression of functional CNBP when compared to the normal cells. The reduction of CNBP expression in DM2 cells was the outcome of CCUG repeats present in its mRNA, which gave rise to compromised RNA binding. In agreement with our data the RNA binding property of CNBP is vital for its role *in vivo*. Upon knock down or knock out of CNBP, which mimics the condition inside DM2 cells, the translation of a plethora of target transcript is reduced which in turn leads to the pathogenicity (Huichalaf, Schoser et al. 2009).

3.6 CNBP showing chaperone like activity on target transcripts

Our luciferase based reporter assay where we cloned the GGAG rich region right next to the start codon of firefly showed an effect on CNBP knockdown. Upon siRNA mediated CNBP knockdown we could see 20-40% reduced firefly luciferase reporter levels (Figure 2.10.1). The effect on luciferase assays could be rescued when tested with mutated motifs (Figure 2.10.1) .The effect of CNBP on luciferase assay is in coherence with our ribosome profiling data where we noticed an approximate 30% reduced translational efficiency for the top targets. Taken together, our data clearly indicates the preference of CNBP to bind GGAG rich motifs and acting as translational enhancer.

Our failed attempt to repeat the luciferase assay with CNBP KO cells and an approximate three fold decrease in both renilla and firefly signals while their RNA levels remains same, indicates the role of G-rich motifs. As seen in our ribosome profiling data the location of G-rich sequence

across the CDS doesnot play much role in CNBP mode of action. The presence of multiple G-rich sequence across firefly and renilla CDS was most likely the cause of reduction in luciferase protein levels. The complete loss of CNBP makes the luciferase genes expression sensitive while the reduction in CNBP levels affects the strongest targets.

G-rich stretches tend to form secondary structures for example G-quadruplex that influences translation and play roles in gene regulation (Bochman et al 2012). Secondary structures with the potential to form G-quadruplex are important part of oncogenic gene expression program and requires cellular factors including eIF4A and Aven for efficient translation (REF Wolfe et al., 2014; Thandapani et al., 2015). From the preliminary SHAPE data we could see the potential of tested sequences to form secondary structures (Figure 2.10.2). These secondary structures could act as roadblock for the translational machinery and hence slowing down the translation. Our work on CNBP suggests its possible role as translational enhancer by reducing the secondary structure on target mRNAs formed by G-rich stretches.

3.7 Possible model for CNBP

Taken all the data together and with the current state of research on CNBP molecular function, we propose a possible and most likely model for CNBP mode of action (Figure 3.2). First CNBP binds to the CDS of target mRNAs, containing G-rich stretch, independent of the location. Upon binding, CNBP reduces possible secondary structures/roadblocks in the CDS. In absence of CNBP the secondary structure proves as a roadblock for ribosome movement and hence reducing the translation rate. In presence of CNBP the target transcripts containing one or multiple GGAG/GGA are easily translated.

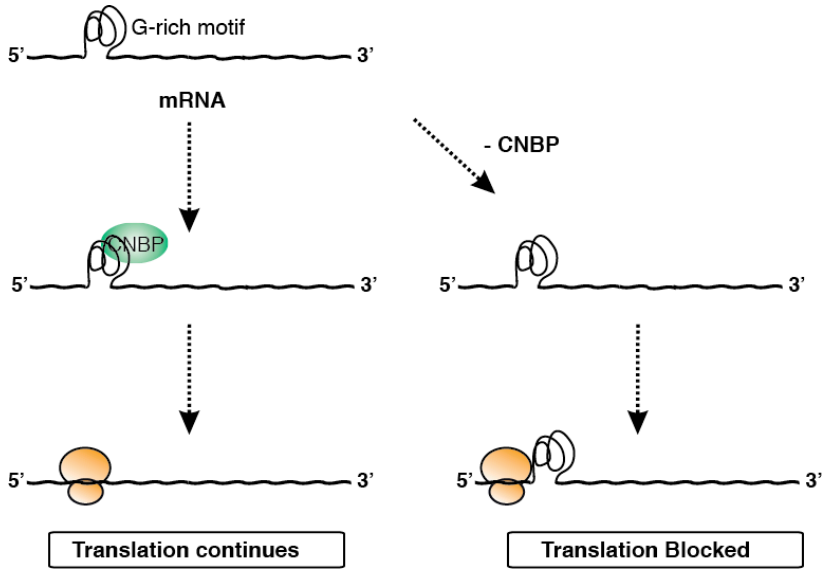

Fig 3.2 A proposed model of CNBP function *in vivo*.

This chaperone like activity of CNBP is in coherence with other protein chaperons. Proteins with chaperon like activity has been shown to act in 2 ways; either by annealing the unfolded structures or by unwinding the folded structures. Unlike helicases, protein chaperons function without requiring ATP and are usually transient (Semrad 2011). With our proposed model, CNBP binds only transiently to the target transcripts and resolves the secondary structure, which allows the ribosome to translate efficiently.

3.7 Conclusion and perspective

The present study aimed to characterize the human RBP protein CNBP and its various isoforms in HEK293 cells. Due to the high degree of conservation of CNBP from simpler eukaryotes to most complex systems, the characterization of CNBP in cellular processes was highly warranted.

Based on the findings of this thesis the most likely model for CNBP mode of action is presented where CNBP is shown to function as chaperone and facilitating the movement of ribosomes across the target transcripts upon binding. But other models still remain possible. For instance, if CNBP is recruiting other proteins to the GGAG sites across the ORF which in turn facilitates the translation of target mRNAs. A CNBP-IP followed my mass-spectrometry to determine the interacting proteins will help this study to rule-in/rule-out this hypothesis.

CNBP is shown to bind thousands of mRNAs preferably at GGAG/GGA rich regions. However the exact mechanism of CNBP binding is still unclear. From the current study it is still an open question if one or multiple zinc finger domains are involved in binding single GGAG motif. The CNBP truncation studies showed the requirement of all CCHC and RGG domains for its RNA binding property but the mode of binding is still elusive. Although the work by Y Nam et al shown the involvement of 2 CCHC domains in binding one GGAG motif in Lin28, it would be pretty interesting to see if the CNBP CCHC domains behave similarly. A crystal structure of CNBP with bound RNA will not only shed light on this question but will also prove beneficial in ZnF domain conservation and further studies.

Previous *in vivo* studies on CNBP have shown the importance of CNBP in mammalian embryonic development. Based on the finding of this study it would be interesting to characterize the different targets of CNBP and their importance in embryonic development and cellular processes. This study shows association of CNBP with 4187 mRNAs in HEK293 cells which provides a starting point to study the individual target RNAs and its regulation by CNBP.

In summary, the analyzed chaperone activity of CNBP and its role as a translational enhancer on its target mRNAs is novel. Further studies will have to observe its effect on individual targets, its possible other mode of actions and its binding mechanism to get a deeper and better understanding of CNBP across various systems.

4 Appendix

Table showing the top CNBP PAR-CLIP targets and the effect of CNBP knockout (column 3)on the expression levels of target mRNAs (by RNAseq) and ribosome occupancy (column 4).

Column 1: Gene symbols

Column2: Clusters obtained from PAR-CLIP

Column3: Log fold change on the expression of target transcripts upon CNBP knockout

Column4: Log fold change of the ribosome occupancy on target transcripts upon CNBP knockout

Gene_Symbol	Clusters	LFC	LFC_CHX_HRN
SPEN	23	-0,195	0,937
CENPF	21	-0,164	0,182
ERC1	21	0,129	0,640
MKI67	17	-0,155	0,254
NUCKS1	15	0,270	-0,289
SON	15	0,319	-0,095
ZNF711	13	0,344	0,630
PRKDC	12	-0,092	0,451
KLHL15	12	-0,220	0,377
ILF3	11	-0,183	0,723
STAG2	11	0,096	0,055
CLTC	10	-0,015	0,549
CSDE1	10	0,035	0,051
PMAIP1	10	-0,046	0,322
TSC22D3	10	-0,179	0,335
CEBPG	10	-0,357	-0,795
FASN	9	-0,087	0,898
TOMM20	9	-0,058	0,126
DDX3X	9	-0,151	0,322
SYNCRIP	9	0,030	0,363
NUP155	9	-0,032	-0,144
KIF5B	9	-0,027	-0,053
HNRNPUL1	9	-0,057	0,394
PRRC2C	9	0,049	0,000
USP22	9	-0,201	0,122
TM9SF3	9	0,108	-0,868
FAM168B	9	-0,158	-0,195
TRIM28	8	-0,251	0,473
CANX	8	0,165	0,388
PDCD4	8	0,239	-0,079
DDX17	8	-0,056	0,159
POLR2A	8	-0,333	0,326
HNRNPH3	8	0,176	0,058
MSH6	8	0,070	0,152
NUP205	8	-0,162	-0,157
DYNC1H1	8	-0,001	0,120
CCND2	8	0,012	0,574
TCERG1	8	0,152	0,568
RBM12	8	-0,164	0,268
SOX4	8	0,135	0,376
PHIP	8	-0,069	0,276
MCL1	8	-0,026	-0,221
WAPAL	8	-0,225	0,270
PTPN11	8	0,066	-0,765
SMAD5	8	-0,012	-0,754
FAT1	8	0,289	-0,249
NR1D2	8	-0,013	-0,544
UBA2	7	-0,493	0,038
EIF3A	7	0,183	0,446
SFPQ	7	0,105	0,270
HSPA4	7	-0,036	0,123
SLC16A1	7	-0,031	0,330
PFKP	7	0,096	0,572
RFC3	7	-0,145	-0,090
NOP14	7	-0,058	0,511
PNN	7	0,221	0,340
ADAMTS1	7	0,218	0,419
RBM39	7	-0,162	0,015
DSP	7	-0,009	0,220
PUM1	7	-0,185	-0,077
CHD1	7	-0,085	0,569
TMED2	7	0,023	-0,422
ANKRD17	7	-0,174	0,093
RLIM	7	0,056	-0,278
UBE3C	7	-0,006	0,555
VCAN	7	0,138	-0,345
SLC38A1	7	-0,278	0,042
IVNS1ABP	7	-0,148	0,237
IBTK	7	0,129	-0,348
MPZL1	7	0,133	0,353
CREBZF	7	0,003	1,343
PHF3	7	-0,050	0,015
PDZD8	7	-0,366	0,236
ETNK1	7	0,092	-0,302
DCP2	7	0,193	0,119
AMD1	7	0,011	-0,585
NONO	6	-0,058	0,466
HSP90B1	6	0,042	-0,023
IRS4	6	0,069	1,172
DDX21	6	-0,159	0,468
EIF4G1	6	-0,150	0,954
SERBP1	6	0,070	0,477
CNBP	6	-0,085	0,501
LMNB1	6	-0,033	0,043
NOLC1	6	0,012	0,404
PRPF8	6	-0,022	0,573
VCP	6	-0,075	0,385
PDIA6	6	0,214	0,421
LBR	6	-0,200	0,140
IARS2	6	0,107	0,308
KHSRP	6	-0,121	0,401
SF3B3	6	0,047	-0,066
CCDC47	6	0,124	0,028
G3BP1	6	-0,043	0,173
CTNNA1	6	-0,011	0,214
ATP2A2	6	-0,079	0,339
CHD4	6	0,251	-0,072
XPO5	6	0,144	0,616
SMARCC1	6	-0,016	0,416
LMNB2	6	0,082	0,456
SUPT5H	6	0,052	0,323
BCOR	6	-0,447	0,327
NUP62	6	-0,165	0,715
ACSL3	6	0,119	0,649
LUC7L3	6	0,081	0,554
CAND1	6	-0,076	-0,159
DDIT4	6	-0,720	-0,812
NFE2L1	6	-0,059	0,025
TNPO1	6	-0,359	-0,552
MFN2	6	0,019	0,347
TIMM17A	6	0,001	-0,306
RBM15	6	-0,202	0,475
CUTC	6	0,111	-0,096
XPO7	6	-0,146	-0,403
WNK1	6	-0,171	0,188
HSPA14	6	-0,104	-0,494
PANK3	6	0,223	0,479
UBR4	6	-0,101	0,333
ASPM	6	-0,236	-0,024
AKAP1	6	-0,145	0,267
GTF3C4	6	-0,262	0,656
POFUT1	6	0,224	0,430
PTP4A1	6	-0,275	-0,445
SMG1	6	0,105	0,085
MLLT4	6	0,267	0,710
MLEC	6	0,089	0,047
CELF1	6	-0,022	-0,364
DYRK1A	6	-0,023	0,408
SPTBN1	6	0,215	-0,106
HIPK1	6	-0,342	-0,522
NSD1	6	0,010	0,081
LNPEP	6	-0,048	-0,039
TNRC6B	6	-0,030	0,617
INSR	6	0,049	0,019
HNRNPU	5	-0,065	0,677
CSE1L	5	-0,132	-0,187
HNRNPF	5	-0,147	0,247
MCM4	5	-0,054	0,172
GDI2	5	-0,058	-0,146
RRM1	5	0,030	-0,008
HNRNPD	5	0,262	0,180
TRAP1	5	-0,222	0,332
PRPF6	5	-0,087	0,907
SHMT2	5	-0,069	-0,193
SAE1	5	0,036	0,307
IPO5	5	-0,228	0,041
PRC1	5	-0,006	0,552
HNRNPDL	5	-0,113	0,176
GTPBP4	5	0,117	0,372
KCTD12	5	-0,131	1,529
CKAP5	5	-0,146	0,653
SRRM2	5	-0,128	0,327
TMPO	5	-0,038	0,037
SDE2	5	0,058	0,407
DHX15	5	-0,170	0,334
TPR	5	-0,083	0,483
POLR2B	5	0,048	-0,061
MAZ	5	-0,030	-0,365
LAMC1	5	0,258	0,564
HELLS	5	0,016	0,033
SRPK1	5	0,187	-0,074
TXLNA	5	-0,103	0,125
GAPVD1	5	-0,119	0,734
NUP153	5	-0,052	-0,128
TXNRD1	5	-0,006	0,009
PHF10	5	0,112	1,237
LARP1	5	-0,152	0,318
USP9X	5	-0,293	-0,029
MCMBP	5	-0,069	-0,298
TSPAN3	5	-0,060	-0,177

SQLE	5	0,246	-0,078	**PSMA4**	4	0,001	-0,357	**TMEM194A**	4	0,225	0,169
EIF4A2	5	-0,285	-0,276	**CDK1**	4	-0,175	-0,430	**IMPDH1**	4	0,126	0,407
MCM10	5	0,049	-0,042	**APLP2**	4	0,019	0,409	**VKORC1L1**	4	0,014	-0,101
MGEA5	5	-0,130	0,027	**MRFAP1**	4	0,036	0,358	**MAGEF1**	4	0,026	-0,534
IGF2BP1	5	-0,002	0,357	**SAT1**	4	0,121	0,135	**STARD7**	4	-0,053	0,308
CTNNAL1	5	-0,116	0,016	**DDX24**	4	0,008	0,277	**TMEM259**	4	-0,156	0,050
PKN1	5	-0,027	0,629	**RRM2**	4	0,143	0,101	**BAG5**	4	0,000	0,276
CDV3	5	0,088	0,770	**SAFB**	4	0,076	0,394	**SLC7A1**	4	-0,376	0,113
IRGQ	5	0,145	0,511	**NARS**	4	0,070	0,080	**PIGS**	4	0,148	0,452
SRSF11	5	-0,078	-0,265	**JUN**	4	-0,056	0,152	**IREB2**	4	-0,139	0,157
MDM2	5	0,021	-0,451	**AARS**	4	0,373	-0,298	**AKAP12**	4	0,140	0,443
BUB1	5	-0,046	0,135	**SMC4**	4	-0,466	0,248	**PRRC2B**	4	0,057	0,726
RAE1	5	-0,080	-0,694	**YTHDF2**	4	-0,195	0,293	**ACP1**	4	0,001	-0,074
DNAJB1	5	-0,312	0,136	**NSUN2**	4	0,235	-0,054	**RANBP6**	4	-0,009	0,592
ATP2B1	5	-0,046	0,035	**EIF4G2**	4	0,029	0,228	**EIF5**	4	-0,086	-0,099
ARID4B	5	-0,261	0,608	**GARS**	4	-0,132	-0,379	**ASXL1**	4	-0,081	1,073
MRPL19	5	0,089	0,011	**KIF11**	4	-0,116	-0,478	**NNT**	4	-0,195	0,206
MDN1	5	0,249	0,823	**KIF20A**	4	-0,051	-0,112	**PTGFRN**	4	0,007	0,258
LEMD3	5	-0,085	-0,055	**HDLBP**	4	-0,032	0,721	**HIATL1**	4	-0,023	0,220
SCAF11	5	-0,046	-0,071	**SERINC1**	4	-0,138	-0,360	**MTF2**	4	-0,079	-0,121
CHD8	5	0,050	-0,040	**EIF5B**	4	0,001	0,693	**TMTC3**	4	-0,014	-0,173
PNMA1	5	0,101	-0,237	**TACC3**	4	-0,095	0,447	**BAZ2A**	4	0,125	0,281
ERO1L	5	0,073	0,257	**SEC23B**	4	-0,061	-0,329	**JAGN1**	4	-0,058	-0,255
PPP1R14C	5	0,084	1,721	**HDGFRP2**	4	0,256	0,434	**STRN4**	4	-0,078	0,003
UCK2	5	0,015	0,242	**DNAJA2**	4	0,261	-0,134	**RC3H1**	4	0,235	1,633
POLE	5	-0,090	0,432	**DHCR24**	4	0,144	0,395	**CASP8AP2**	4	0,095	0,974
SIN3A	5	-0,174	0,273	**SMC2**	4	-0,134	0,321	**EEA1**	4	0,278	-0,018
PAWR	5	0,077	0,525	**ITGB1**	4	-0,026	-0,070	**LARP4B**	4	-0,081	-0,040
WDR26	5	-0,016	-0,214	**DDX23**	4	0,128	0,575	**NHLRC2**	4	-0,224	-0,069
SREBF2	5	-0,047	0,337	**RRP1B**	4	0,199	0,399	**ZNF644**	4	-0,238	-0,013
ZDBF2	5	-0,113	0,810	**WDR6**	4	-0,175	0,231	**RAB3GAP2**	4	0,018	0,272
ASPH	5	0,212	0,276	**TFAM**	4	-0,028	0,515	**KIF1B**	4	-0,065	0,396
MGA	5	-0,166	0,102	**SQSTM1**	4	-0,034	1,010	**SLC20A1**	4	-0,017	-0,152
FEM1B	5	-0,222	0,477	**METAP2**	4	0,403	-0,464	**CAPN1**	4	0,191	0,635
WHSC1	5	0,015	0,630	**SLC38A2**	4	-0,140	-0,341	**SETD3**	4	-0,031	0,279
APPL1	5	0,025	-0,824	**FUCA2**	4	0,254	-0,048	**URB1**	4	0,192	-0,158
YLPM1	5	-0,072	-0,430	**RAD21**	4	-0,171	-0,188	**AMOTL1**	4	-0,189	1,020
KMT2D	5	-0,144	-0,036	**STT3A**	4	-0,192	-0,031	**ADNP**	4	-0,266	-0,286
FLNB	5	-0,175	0,302	**CLSPN**	4	-0,047	0,456	**GGA2**	4	0,238	-0,264
MACF1	5	0,151	-0,251	**PAIP2**	4	0,267	-0,432	**PLCG1**	4	0,041	0,199
ZFP91	5	-0,255	1,524	**KIF4A**	4	-0,065	0,643	**AKT3**	4	-0,163	-0,207
MBTPS1	5	0,077	-0,085	**CCAR2**	4	-0,191	0,228	**BIRC5**	4	-0,074	-0,536
TXNDC5	5	0,127	-0,676	**ADAR**	4	0,000	0,546	**ICMT**	4	-0,029	-0,300
AES	5	-0,018	-0,505	**SRPR**	4	0,070	0,385	**ADAM10**	4	0,015	0,254
NAT8L	5	-0,004	0,601	**CCDC85C**	4	0,195	1,617	**MCPH1**	4	0,013	0,475
SOGA1	5	-0,122	-0,018	**USP1**	4	-0,153	-0,036	**SORT1**	4	-0,008	-0,111
UHRF1BP1	5	0,014	-0,086	**NAA15**	4	-0,069	0,279	**ZNF664**	4	-0,203	0,790
SERGEF	5	0,180	1,154	**RAB11A**	4	0,007	-0,134	**PLXNB2**	4	0,073	0,269
ANKRD11	5	0,203	-0,575	**EIF2S1**	4	0,130	-0,068	**NCOR1**	4	-0,159	0,377
ADIPOR2	5	-0,032	-1,322	**ACAT1**	4	0,137	-0,076	**USP48**	4	0,018	-0,103
ARHGAP35	5	0,017	-0,582	**PFKM**	4	-0,084	0,206	**CHD7**	4	0,020	1,116
HNRNPUL2	5	-0,195	-0,898	**EIF4G3**	4	0,101	0,580	**NETO2**	4	0,182	0,116
AGPAT3	5	0,257	-0,814	**HMGCR**	4	-0,033	0,179	**GALNT2**	4	0,026	-0,097
PAPD7	5	0,185	-0,823	**G3BP2**	4	-0,057	0,673	**TLE3**	4	-0,013	-0,498
AHNAK	5	0,291	-0,858	**CDC25A**	4	-0,149	0,276	**ADAM9**	4	0,109	-0,009
HSPA8	4	-0,147	0,688	**SEC24C**	4	-0,130	0,086	**PRR14L**	4	-0,016	0,348
HNRNPA2B1	4	0,155	0,455	**ATF4**	4	-0,238	-0,506	**PCF11**	4	0,017	0,314
CCT5	4	-0,036	0,326	**OCIAD1**	4	0,088	-0,444	**CD2BP2**	4	0,132	-0,591
CCT3	4	-0,196	0,178	**NAA50**	4	0,078	0,131	**DDI2**	4	-0,037	0,114
HSPA9	4	-0,127	0,299	**TCOF1**	4	-0,059	0,551	**ZNF134**	4	0,119	-0,060
HNRNPM	4	0,167	0,586	**DNAJC11**	4	0,386	0,517	**HECTD1**	4	0,082	-0,644
RPL15	4	-0,052	0,233	**NUP210**	4	0,248	0,105	**IMPAD1**	4	0,160	0,783
PSAP	4	0,339	0,607	**SEC11A**	4	-0,093	-0,033	**ZNF106**	4	-0,063	0,063
FUS	4	0,030	0,267	**MELK**	4	-0,045	-0,059	**POGK**	4	-0,069	1,020
GANAB	4	-0,045	0,400	**GRSF1**	4	0,059	0,062	**TRIO**	4	-0,236	0,318
KPNB1	4	-0,354	0,001	**SEC61A1**	4	-0,095	-0,076	**TRIM25**	4	-0,083	-0,153
USP7	4	-0,188	1,038	**SPTAN1**	4	0,009	0,289	**FBXO45**	4	-0,147	0,310
ACTN4	4	-0,059	0,562	**EMC1**	4	-0,413	0,282	**ADD1**	4	0,051	-0,048
EIF2S3	4	0,161	-0,013	**MAP1B**	4	-0,069	0,013	**LIMD1**	4	-0,089	0,720
MBD3	4	-0,106	2,582	**HDAC2**	4	-0,102	0,013	**SENP5**	4	-0,186	0,605
EPRS	4	-0,172	0,101	**SUB1**	4	0,156	-0,681	**KTN1**	4	0,075	0,078
AURKB	4	0,015	0,512	**NCBP2**	4	-0,226	0,996	**CCNT1**	4	-0,075	0,119
PPIF	4	0,077	0,636	**DDX42**	4	-0,111	0,066	**FOXK2**	4	-0,030	1,118
MCM6	4	-0,033	0,346	**URI1**	4	0,131	0,186	**LUZP1**	4	0,135	0,516
ATIC	4	0,089	0,597	**HLTF**	4	-0,032	-0,340	**E2F1**	4	0,039	0,292
TMBIM6	4	0,105	0,161	**NDC1**	4	-0,237	-0,204	**TMEM181**	4	0,036	1,021
NUP133	4	-0,100	0,468	**TAOK1**	4	-0,118	0,762	**FGFR1**	4	0,058	0,022
SCD	4	0,117	0,039	**MIDN**	4	-0,244	-0,344	**PPTC7**	4	-0,107	1,298
ALDH18A1	4	0,215	0,445	**KPNA6**	4	-0,005	-0,197	**EFNB2**	4	-0,054	0,735
FEN1	4	-0,044	0,619	**PIM3**	4	-0,279	-0,289	**EGLN1**	4	-0,118	0,268

ZBTB10	4	-0,054	0,261	**BCLAF1**	3	-0,034	0,339	**RCN2**	3	0,103	0,183
FGFR2	4	-0,146	0,501	**UTP11L**	3	-0,115	0,117	**KDM3B**	3	-0,092	0,645
COL25A1	4	0,250	0,377	**POMP**	3	-0,074	-1,101	**MZT1**	3	-0,030	0,696
MIB1	4	0,050	0,618	**SF3B1**	3	-0,231	0,273	**KIF2A**	3	-0,116	-0,216
CTBP1	4	-0,086	0,236	**SNW1**	3	0,136	0,604	**PPP1CC**	3	0,041	-0,326
CASK	4	0,065	-0,564	**KDM1A**	3	-0,133	0,416	**ATXN2L**	3	0,154	-0,433
IGF1R	4	0,037	0,900	**OS9**	3	0,396	0,477	**RTN4**	3	-0,033	0,199
BICD2	4	0,064	1,031	**SMARCB1**	3	-0,227	-0,008	**MED10**	3	-0,023	-0,751
POLQ	4	0,054	0,191	**DDX46**	3	0,001	0,335	**ZNF791**	3	0,082	0,463
SLC7A5	4	-0,239	-1,251	**SF3B2**	3	0,083	0,338	**PPP5C**	3	0,018	0,017
ZBTB18	4	-0,268	0,797	**KRI1**	3	0,216	1,023	**ZNF330**	3	0,234	-0,010
PCNX	4	-0,002	0,487	**MAPRE1**	3	-0,039	-0,476	**TRAFD1**	3	0,102	0,294
UHMK1	4	-0,018	0,989	**MTHFD1L**	3	0,096	0,092	**SAR1A**	3	-0,177	-0,302
LIFR	4	0,162	-0,277	**MYH10**	3	-0,153	0,533	**OAZ1**	3	-0,104	-0,552
NIN	4	0,059	0,076	**PAK1IP1**	3	0,029	0,295	**PCM1**	3	0,016	-0,003
SLC4A7	4	0,116	-0,336	**RBBP4**	3	-0,077	-0,224	**EML2**	3	-0,423	1,325
HECA	4	-0,037	-0,248	**SDHA**	3	-0,032	0,585	**SLC39A14**	3	0,025	0,539
DCTD	4	0,019	-0,676	**ATXN10**	3	-0,020	0,596	**KDELC2**	3	0,296	0,430
TSPAN12	4	0,012	-0,435	**TARDBP**	3	0,049	0,133	**TFDP1**	3	-0,145	0,375
PRKD3	4	-0,111	-0,174	**U2AF1**	3	0,131	-0,085	**ZNF227**	3	-0,033	-0,082
SLC25A24	4	0,132	-0,360	**HEATR1**	3	-0,141	0,347	**PRPF4B**	3	0,100	0,269
RASSF3	4	0,171	-0,121	**HN1**	3	0,199	-0,358	**PFKL**	3	0,322	0,493
CABLES1	4	-0,208	0,691	**CALM3**	3	0,242	-0,245	**TUSC3**	3	0,172	0,368
SSFA2	4	0,265	-0,776	**COPG1**	3	0,061	1,470	**EPB41**	3	-0,036	-0,088
C19orf68	4	-0,520	0,392	**TBCB**	3	-0,038	0,140	**KIAA0368**	3	-0,159	-0,038
DST	4	0,019	-0,274	**DEK**	3	0,074	0,078	**DAZAP1**	3	-0,005	0,012
IER2	4	-0,399	-0,460	**DAP3**	3	0,005	-0,089	**PUS7**	3	0,068	0,283
SPECC1L	4	-0,135	0,000	**GNAI3**	3	-0,002	0,060	**CTCF**	3	-0,011	-0,009
C14orf169	4	0,261	0,000	**CD63**	3	0,504	-0,301	**KIF20B**	3	-0,353	-0,149
SLC5A3	4	0,327	0,000	**SF1**	3	-0,070	0,042	**MOAP1**	3	0,052	0,003
HSP90AB1	3	-0,104	0,181	**CSTF2T**	3	-0,161	0,622	**VWA9**	3	0,120	0,561
HSP90AA1	3	-0,115	0,174	**KDM4A**	3	-0,257	1,294	**SEH1L**	3	-0,102	0,360
LDHB	3	0,056	0,329	**HDGF**	3	-0,012	0,420	**CCND1**	3	0,195	1,020
NCL	3	0,032	0,693	**GTF2E2**	3	0,142	0,549	**BTBD1**	3	0,085	0,280
CCT7	3	0,055	0,441	**ABL2**	3	0,063	1,353	**EPHA7**	3	0,075	0,334
H2AFX	3	-0,053	0,155	**CDC45**	3	-0,085	0,101	**MTDH**	3	0,055	0,141
CCT2	3	-0,180	0,049	**XPO1**	3	-0,046	-0,036	**RBM14**	3	-0,034	-0,036
DHX9	3	-0,048	0,478	**ZC3H15**	3	-0,065	-0,155	**ABCD3**	3	-0,236	-0,283
CCNB1	3	-0,090	-0,044	**AIMP1**	3	0,028	0,186	**CLPX**	3	-0,044	-0,044
XRCC5	3	-0,159	0,550	**SLFN11**	3	0,055	0,234	**SERINC3**	3	0,062	0,405
PA2G4	3	-0,019	0,099	**DHX30**	3	-0,174	0,621	**VHL**	3	-0,065	0,186
CCT6A	3	-0,040	0,502	**CALM2**	3	0,062	-0,653	**HN1L**	3	-0,177	-0,231
OAT	3	0,221	0,047	**COPB2**	3	0,002	-0,012	**SLC35B1**	3	-0,147	1,019
GPI	3	0,013	0,498	**GCN1L1**	3	0,041	0,278	**PYCR2**	3	0,066	0,342
ATP1A1	3	0,000	0,354	**CLSTN1**	3	-0,006	0,636	**ATAD1**	3	0,020	-0,433
HMGB2	3	-0,107	0,005	**HARS**	3	-0,143	0,159	**AFG3L2**	3	-0,283	0,056
HNRNPH1	3	0,207	0,192	**EIF3M**	3	0,003	-0,545	**RAI14**	3	0,071	0,360
CERK	3	-0,050	2,104	**NDUFV1**	3	-0,055	0,251	**SCAF8**	3	0,172	-0,289
DNAJA1	3	-0,171	-0,179	**PSIP1**	3	0,090	-0,005	**ANKLE2**	3	0,007	0,063
PCK2	3	-0,116	3,531	**CORO1C**	3	-0,069	-0,059	**SBNO1**	3	-0,202	0,079
TARS	3	0,103	0,037	**WDR3**	3	-0,080	0,405	**YIPF4**	3	0,158	0,121
BUB3	3	-0,156	0,187	**PRKAR1A**	3	0,183	0,451	**ZC3H13**	3	0,032	0,615
ADRM1	3	-0,174	0,329	**DIS3**	3	0,025	0,455	**TFCP2**	3	-0,129	0,648
SRSF3	3	0,060	-0,022	**FBN2**	3	-0,065	0,616	**PRPF38B**	3	-0,124	-0,377
TCP1	3	-0,031	0,083	**ETF1**	3	-0,093	-0,446	**YY1**	3	-0,101	0,339
HMGCS1	3	-0,004	0,571	**CDH2**	3	-0,154	0,260	**MAP4**	3	-0,214	0,347
GNL3	3	-0,093	-0,165	**CSTF1**	3	0,027	0,019	**CD164**	3	0,207	-0,125
PSMB7	3	-0,079	0,108	**GNB1**	3	-0,093	0,099	**KBTBD6**	3	-0,081	0,375
SUPT16H	3	0,096	0,206	**TSR2**	3	-0,082	0,355	**ME2**	3	0,056	-0,758
LARS	3	0,011	0,669	**CHAF1A**	3	-0,033	0,307	**CBX5**	3	0,454	0,101
NAP1L1	3	-0,023	0,124	**UBTF**	3	-0,254	0,329	**WDR82**	3	-0,217	0,123
NDUFS2	3	-0,096	0,410	**ALDH1B1**	3	-0,005	0,584	**PAK4**	3	-0,056	0,687
PSMD4	3	-0,061	0,338	**ACIN1**	3	0,014	0,589	**MIA3**	3	0,039	-0,023
EIF2S2	3	0,090	-0,270	**TTLL12**	3	-0,139	0,370	**IGF2BP2**	3	-0,152	0,532
MYBBP1A	3	-0,129	1,095	**NID1**	3	0,261	0,399	**FAM129B**	3	0,221	0,525
MATR3	3	-0,037	0,302	**ZNF460**	3	-0,115	-0,104	**PRRC1**	3	-0,072	0,293
EZR	3	0,187	0,394	**M6PR**	3	0,000	0,167	**ZNF770**	3	-0,069	-0,171
MORF4L2	3	0,077	-0,378	**EZH2**	3	-0,041	0,543	**NAA25**	3	-0,188	-0,010
CTNNB1	3	-0,074	-0,053	**NCAPG2**	3	0,136	0,922	**TOR1A**	3	-0,021	0,039
ANP32A	3	-0,044	0,592	**CNOT1**	3	0,187	-0,540	**NUDT21**	3	0,330	-0,937
PELP1	3	-0,307	0,907	**URB2**	3	-0,178	0,517	**RBM27**	3	-0,191	-0,093
SRRT	3	-0,283	0,783	**TIMMDC1**	3	0,207	0,079	**HK2**	3	-0,201	-0,091
ATP1B3	3	-0,316	-0,160	**XPOT**	3	-0,211	-0,155	**PCYOX1**	3	0,084	-0,261
RARS	3	0,037	-0,173	**CALM1**	3	0,052	-0,615	**KIAA2013**	3	-0,105	0,450
PPM1G	3	0,161	0,781	**CPSF2**	3	0,164	0,078	**ARPC5**	3	0,117	-0,299
IARS	3	-0,325	0,141	**CPSF6**	3	0,298	0,251	**ALKBH5**	3	-0,183	0,463
PSMC5	3	-0,123	0,559	**INCENP**	3	-0,206	0,507	**POLDIP3**	3	-0,133	-0,205
PLK1	3	0,007	0,038	**RAD23A**	3	-0,072	0,119	**KDM5B**	3	0,122	-0,068
GLUL	3	0,038	0,604	**MRPS27**	3	0,099	0,247	**PPP6R3**	3	-0,145	0,114
ODC1	3	-0,030	0,053	**ECT2**	3	-0,292	-0,089	**TNFRSF10B**	3	-0,091	-0,381

UBR5	3	0,151	0,318	**SSH2**	3	-0,053	0,652	**SLC30A1**	3	-0,214	-0,331
NR2F2	3	-0,341	0,093	**IRS2**	3	-0,090	0,643	**DYRK2**	3	-0,039	1,301
RAB3GAP1	3	-0,312	-0,246	**DIEXF**	3	-0,135	-0,169	**C5orf51**	3	-0,004	-1,426
PHRF1	3	-0,122	1,261	**AZIN1**	3	-0,043	-0,764	**FAT3**	3	-0,171	-0,464
BPTF	3	-0,230	0,233	**NUDCD2**	3	0,053	-0,173	**LEMD2**	3	0,025	0,105
WDR4	3	0,058	0,032	**MSI2**	3	-0,109	0,869	**MPDZ**	3	0,071	-0,700
MAP7D1	3	0,244	0,553	**FAM122B**	3	0,097	0,381	**HRK**	3	-0,315	-0,230
SP3	3	-0,227	-0,036	**TNKS**	3	0,115	0,215	**NHSL1**	3	0,224	-0,449
RAF1	3	-0,111	0,959	**FADS2**	3	0,349	-0,661	**FANCC**	3	-0,083	-1,068
PTPRF	3	-0,082	0,456	**ARHGEF12**	3	0,022	0,179	**CHSY1**	3	-0,595	-0,382
MYO1B	3	-0,013	0,221	**HLCS**	3	0,274	-0,328	**RAP2A**	3	-0,206	1,123
RMND5A	3	-0,007	0,774	**BRD1**	3	-0,086	0,002	**SEMA6A**	3	-0,261	-0,734
NUMA1	3	-0,061	0,007	**PDXK**	3	0,059	0,051	**TCFL5**	3	0,060	-0,473
POLR1A	3	-0,122	0,648	**FNBP4**	3	-0,058	0,059	**ZNF148**	3	-0,476	-0,988
NMT1	3	-0,166	0,058	**SMAD4**	3	-0,244	0,466	**BTBD3**	3	-0,029	-0,471
HOXA9	3	-0,046	-0,374	**CSNK1D**	3	-0,088	-0,243	**KCTD15**	3	-0,234	-0,882
SENP3	3	-0,209	-0,049	**PPM1B**	3	0,075	-0,073	**HS2ST1**	3	0,057	-0,966
RIF1	3	-0,031	-0,282	**MIEF1**	3	-0,108	0,039	**GRB10**	3	-0,145	-0,745
TWISTNB	3	0,085	0,687	**RNF220**	3	-0,121	0,864	**MTUS1**	3	-0,172	-1,233
EIF2AK2	3	0,044	0,010	**ZC3H7B**	3	0,046	-0,468	**SH3RF3**	3	-0,067	1,746
NSL1	3	0,215	0,365	**TBC1D22A**	3	0,005	1,062	**MTSS1L**	3	0,076	-2,286
BRI3BP	3	-0,064	-0,100	**JARID2**	3	0,101	0,614	**DCAF8**	3	-0,037	0,244
TYSND1	3	0,170	0,858	**ZNF337**	3	0,095	1,160	**TET1**	3	0,049	-0,588
TFIP11	3	-0,198	-0,187	**FAM89A**	3	0,171	0,990	**SPTB**	3	0,235	-1,579
ASNSD1	3	-0,103	-0,306	**STK3**	3	0,022	0,221	**GALNT18**	3	-0,185	-2,110
ARL5B	3	0,003	0,459	**PHF13**	3	-0,062	0,047	**HIPK2**	3	0,009	-0,744
HSDL2	3	-0,065	-0,072	**SKIL**	3	-0,287	-0,051	**ZCCHC3**	3	-0,434	0,000
FAM178A	3	0,162	0,307	**PTPRG**	3	0,121	0,018	**BCL2L2**	3	0,114	0,000
PPM1D	3	-0,066	0,124	**ZBTB21**	3	0,063	-0,749	**DCP1A**	3	0,000	0,000
CCDC43	3	0,063	0,270	**VGLL4**	3	0,095	-0,605	**HIST1H2AD**	3	-0,163	0,000
ZNF45	3	0,031	0,260	**LTBP1**	3	0,082	-0,298	**LUC7L2**	3	0,000	0,000
MED1	3	-0,206	0,371	**BRWD1**	3	0,246	0,261	**OAZ2**	2	-0,090	2,115
ADCK2	3	0,242	0,443	**SPTLC2**	3	0,017	-0,377	**EEF2**	2	-0,047	0,571
RBM26	3	-0,004	0,449	**LPGAT1**	3	0,043	0,384	**ATP5B**	2	-0,111	0,145
IQGAP1	3	-0,075	-0,143	**REST**	3	0,208	0,759	**TUBA1C**	2	-0,100	0,123
HBS1L	3	0,033	0,037	**KBTBD2**	3	-0,136	-0,669	**C1QBP**	2	-0,130	0,676
INSIG1	3	0,404	0,152	**DR1**	3	-0,166	-0,380	**TUBB4B**	2	-0,175	0,573
SOD2	3	0,029	-0,072	**ZNF652**	3	-0,079	0,559	**CALR**	2	-0,062	0,512
AGGF1	3	0,076	0,750	**CCSAP**	3	-0,038	0,317	**XRCC6**	2	-0,058	0,297
CBX6	3	-0,006	0,229	**SLC35B4**	3	0,100	0,498	**BTF3**	2	-0,179	-0,032
EDEM3	3	-0,151	0,112	**GXYLT1**	3	-0,190	-0,119	**CCT8**	2	0,132	-0,005
NOTCH2	3	0,087	0,303	**ZNF507**	3	-0,029	-0,565	**EIF3I**	2	-0,077	0,264
CSNK2A2	3	0,459	0,042	**CBR4**	3	0,183	-0,077	**CCT4**	2	-0,030	0,272
DPH2	3	-0,276	-0,349	**FBXW2**	3	-0,039	0,306	**HIST1H1D**	2	-0,209	-0,022
AEN	3	-0,058	0,563	**KDM3A**	3	-0,158	0,160	**HNRNPK**	2	-0,019	0,007
AKT2	3	-0,103	-0,048	**ZNF629**	3	0,107	-0,401	**MCM7**	2	-0,062	0,160
TOR1AIP2	3	-0,069	0,332	**LONRF2**	3	0,021	0,049	**TUBA1B**	2	-0,056	0,059
BMP7	3	-0,386	0,286	**KLC1**	3	0,125	0,103	**RPS24**	2	-0,137	-0,178
PARD3	3	0,055	0,310	**ARPC5L**	3	-0,067	-0,977	**HMGB1**	2	-0,053	0,808
CDK12	3	-0,126	0,088	**FAM105A**	3	-0,260	-0,016	**RAN**	2	-0,131	0,065
SLC7A2	3	-0,141	0,009	**AKAP9**	3	0,031	-0,367	**UQCRFS1**	2	0,041	-0,133
AP1G1	3	0,125	-0,813	**PURB**	3	-0,052	0,436	**PTGES3**	2	-0,078	-0,214
GOLGB1	3	-0,010	-0,210	**OTUD3**	3	-0,228	-0,013	**TUFM**	2	0,236	-0,002
TICRR	3	-0,107	0,221	**LRP6**	3	0,028	-0,055	**PARP1**	2	-0,144	0,403
MESDC2	3	-0,146	0,579	**STC2**	3	-0,412	-1,707	**HNRNPC**	2	0,044	0,293
DAPK3	3	0,043	-0,268	**EI24**	3	0,136	-0,641	**SLC1A5**	2	-0,187	0,158
TMEM123	3	-0,196	-0,561	**IGSF3**	3	0,174	0,594	**EIF3K**	2	0,000	0,034
TAOK2	3	0,027	0,855	**CELSR2**	3	-0,108	0,608	**RPLP0**	2	-0,212	0,356
CAMSAP2	3	-0,256	0,818	**VAPB**	3	-0,056	0,196	**FKBP4**	2	0,177	0,474
ZRANB1	3	-0,065	0,737	**CACHD1**	3	-0,058	-0,474	**GHITM**	2	-0,043	0,109
GMFB	3	0,041	1,210	**RBFOX2**	3	0,001	0,543	**SNRPD3**	2	0,011	0,251
DYNC2H1	3	0,117	-0,116	**SIPA1L3**	3	-0,007	-0,509	**PSMB4**	2	-0,137	-0,089
STRBP	3	-0,140	0,109	**EFHD2**	3	0,173	-1,267	**HNRNPA3**	2	0,397	0,543
RBM12B	3	0,048	0,312	**TMEM184C**	3	0,031	-1,236	**PRDX4**	2	-0,152	-0,298
TNKS1BP1	3	0,048	0,478	**CNOT6**	3	0,221	0,462	**LGALS3BP**	2	0,031	0,302
KDM5A	3	-0,117	-0,094	**HIF1AN**	3	0,247	-0,801	**PGRMC1**	2	-0,063	0,490
TRIM41	3	-0,024	-0,095	**LIMK2**	3	0,117	-0,110	**ATP5A1**	2	-0,132	0,078
QKI	3	0,031	0,479	**UNC119B**	3	-0,101	-1,793	**EIF3D**	2	-0,041	0,410
TBL1XR1	3	-0,201	0,611	**MAPKAP1**	3	0,035	-0,064	**DPM1**	2	0,094	0,115
SLC30A5	3	-0,018	-0,189	**MBNL1**	3	-0,031	-0,412	**PSMB5**	2	0,324	-0,100
AGPS	3	-0,122	-0,446	**ZXDC**	3	-0,028	0,288	**STIP1**	2	-0,131	0,265
DLG5	3	0,009	1,303	**ZNF609**	3	-0,107	-0,077	**SNRNP70**	2	0,117	1,111
UBE2Z	3	0,010	-0,111	**B3GALT6**	3	-0,227	-0,365	**DDOST**	2	-0,142	-0,182
CHUK	3	0,030	0,694	**TRIM35**	3	-0,054	-0,235	**RTCB**	2	0,057	0,766
WDR33	3	-0,209	-0,150	**BACH1**	3	-0,182	-1,128	**NASP**	2	0,198	0,555
CEPT1	3	-0,208	-0,626	**ANKHD1**	3	0,000	1,130	**FKBP3**	2	0,186	0,327
GNPTAB	3	0,080	0,519	**MINK1**	3	-0,059	0,713	**SLC25A3**	2	-0,013	0,078
ADCY3	3	-0,116	0,392	**CBY1**	3	0,349	-0,159	**BZW1**	2	0,027	0,468
ATP13A3	3	-0,243	-0,186	**BBX**	3	-0,070	-0,579	**RPL22**	2	0,127	0,089
SETD2	3	-0,093	0,402	**PBX1**	3	0,095	0,321	**DEGS1**	2	0,014	0,334

MYH9	2	0,047	0,950	**NOL11**	2	-0,149	-0,227	**LAMB1**	2	0,348	0,064
EIF3G	2	-0,090	0,113	**VRK1**	2	-0,017	-0,270	**RANBP2**	2	-0,163	0,171
TOP1	2	0,012	0,163	**RUVBL1**	2	0,080	0,490	**NDUFB5**	2	-0,235	0,289
P4HB	2	-0,033	-0,072	**ADSS**	2	0,006	-0,093	**SKP2**	2	-0,106	0,275
RBBP7	2	0,181	0,294	**USP11**	2	-0,178	0,129	**NGDN**	2	0,058	0,387
UNG	2	-0,101	0,106	**MMADHC**	2	-0,057	-0,310	**ME1**	2	0,378	0,229
SRSF1	2	0,167	-0,115	**PWP2**	2	0,044	0,604	**SLIT2**	2	-0,411	0,555
SNRPC	2	-0,042	-0,494	**ATP6V1G1**	2	-0,056	-0,166	**NUP85**	2	-0,222	0,209
SMC3	2	-0,011	0,258	**RNF187**	2	-0,058	0,274	**NRD1**	2	-0,086	-0,295
PSMA3	2	-0,079	-0,032	**MSH2**	2	-0,042	-0,004	**BUB1B**	2	-0,091	-0,204
HNRNPA0	2	-0,221	0,286	**ZNF703**	2	-0,247	-0,144	**DSN1**	2	-0,062	0,137
LTA4H	2	0,028	-0,638	**WDR43**	2	0,026	0,160	**GTPBP3**	2	-0,069	0,153
RRAGC	2	-0,226	3,345	**CCAR1**	2	0,046	0,002	**CMAS**	2	0,150	0,277
GMNN	2	0,023	0,258	**TFRC**	2	-0,278	0,434	**GTF3C1**	2	0,159	0,453
TPT1	2	0,018	0,296	**CCNG1**	2	0,025	0,002	**CERS2**	2	0,065	-0,181
SSRP1	2	-0,061	0,423	**CDK4**	2	-0,065	-0,427	**SRSF2**	2	0,026	0,537
EIF3B	2	-0,055	0,526	**LRPPRC**	2	0,026	0,038	**TLN1**	2	0,064	0,492
MYL12B	2	0,004	0,091	**RACGAP1**	2	0,012	0,282	**CHTOP**	2	-0,032	0,360
ATP5J	2	0,159	-0,407	**BRIX1**	2	-0,163	-0,299	**THOC2**	2	-0,160	0,106
TSPYL1	2	0,134	0,323	**DDX27**	2	-0,167	0,550	**GGCT**	2	0,060	-0,460
PSMD2	2	-0,263	0,571	**CBX3**	2	-0,025	-0,558	**RPL17**	2	-0,188	-0,719
MAT2A	2	-0,028	0,163	**ZFR**	2	-0,089	-0,184	**ELAVL1**	2	-0,081	-0,092
MARS	2	-0,087	0,405	**NUP188**	2	-0,175	0,248	**CLTA**	2	0,097	-0,991
CDC37	2	0,271	0,689	**PABPC4**	2	-0,047	0,224	**EXOSC3**	2	-0,090	0,642
NOP58	2	0,036	-0,183	**TOP2B**	2	-0,056	0,377	**CDCA7**	2	-0,057	0,578
NCAPD2	2	0,057	0,273	**PPP2R5D**	2	-0,198	1,106	**SFXN1**	2	0,149	0,088
FARSB	2	-0,077	0,451	**PUS1**	2	-0,056	0,155	**NUP160**	2	-0,056	0,510
TPX2	2	-0,095	-0,080	**ENOPH1**	2	-0,255	1,159	**MRFAP1L1**	2	-0,077	0,126
MEA1	2	0,017	0,096	**KXD1**	2	0,126	-0,071	**GINM1**	2	0,101	-0,120
UQCRC1	2	-0,070	0,450	**NOB1**	2	0,194	-0,341	**TMEM59**	2	-0,099	-0,249
RSL1D1	2	0,295	-0,016	**NGRN**	2	-0,108	0,906	**ADPRHL2**	2	-0,051	0,583
DRG1	2	-0,103	-0,314	**CNN3**	2	-0,035	-0,382	**REEP5**	2	0,265	0,233
PMPCB	2	-0,020	0,237	**GPS1**	2	-0,038	0,339	**SSR3**	2	-0,174	-0,030
DDX56	2	-0,123	0,164	**DTL**	2	-0,007	0,453	**DYNC1LI1**	2	-0,224	0,345
PHF5A	2	0,143	0,157	**FOXC1**	2	0,269	0,753	**PPP1R15B**	2	-0,207	0,741
MTPN	2	0,135	0,844	**CHAF1B**	2	0,280	0,337	**TIMM44**	2	0,003	0,585
RAB7A	2	-0,234	-0,184	**SYAP1**	2	-0,039	0,313	**NUF2**	2	-0,142	0,115
DDRGK1	2	-0,165	0,891	**ATP5G3**	2	0,003	-0,377	**CTSB**	2	0,073	0,118
TM9SF2	2	-0,108	-0,233	**ATP6V1E1**	2	0,135	0,115	**SYF2**	2	-0,018	0,033
SNRPB2	2	-0,057	-0,288	**TNPO2**	2	-0,323	-0,645	**ATP6V1B2**	2	-0,125	0,256
SND1	2	-0,301	0,180	**STAU1**	2	-0,068	0,047	**AAAS**	2	-0,130	0,133
TTC1	2	0,061	0,329	**IDI1**	2	0,202	-0,205	**NDUFS1**	2	0,082	0,259
TOMM40	2	0,007	0,278	**ZNF146**	2	-0,033	-0,428	**AHCYL1**	2	0,010	0,451
EWSR1	2	-0,079	0,455	**CKAP4**	2	0,164	0,634	**C19orf48**	2	-0,107	-0,306
YARS2	2	-0,003	0,990	**ACO2**	2	-0,167	0,626	**GBF1**	2	-0,134	0,474
AIFM1	2	0,117	-0,050	**ATP6V1A**	2	0,129	0,170	**SDCBP**	2	-0,020	0,036
PJA2	2	0,112	0,169	**PGAM5**	2	-0,352	0,626	**HSPA13**	2	0,020	0,899
RPN1	2	0,025	-0,304	**DLGAP5**	2	-0,164	0,229	**OTUB1**	2	-0,127	-0,165
RPA1	2	-0,057	0,766	**PPIH**	2	-0,100	-0,128	**GLRX5**	2	-0,084	0,759
POP7	2	-0,156	0,490	**PPP2CA**	2	-0,034	-0,279	**IVD**	2	-0,131	0,626
CDC6	2	-0,312	0,268	**PPP1R8**	2	-0,199	0,783	**TBC1D15**	2	-0,001	0,161
CTPS1	2	0,001	0,481	**TRA2A**	2	0,023	-0,262	**NUP98**	2	-0,228	0,638
LRRC47	2	-0,034	0,893	**BCAT2**	2	0,149	0,770	**ACADM**	2	0,055	0,232
FDFT1	2	0,124	0,148	**KIF2C**	2	-0,483	-0,708	**PPP2R4**	2	-0,081	0,305
TSR1	2	-0,034	0,280	**GRAMD1A**	2	0,257	1,003	**U2SURP**	2	0,058	0,177
SMARCA5	2	0,082	0,546	**HP1BP3**	2	-0,091	0,353	**TRUB1**	2	0,154	0,575
TIMM50	2	-0,165	0,199	**PPIL1**	2	0,143	0,212	**PAFAH1B2**	2	-0,021	0,057
AURKA	2	-0,133	0,066	**FKBP8**	2	0,125	0,342	**KCTD3**	2	-0,022	0,134
ACTR2	2	0,077	-0,220	**ELAC2**	2	-0,090	0,260	**NCOR2**	2	-0,101	-0,953
WDR77	2	-0,225	0,184	**ECI1**	2	-0,475	0,313	**TST**	2	0,105	0,054
DLD	2	0,075	0,018	**WLS**	2	0,116	-0,250	**TMEM9**	2	0,173	0,407
CDC5L	2	0,087	0,565	**ATAD2**	2	0,098	-0,008	**ZWINT**	2	-0,026	-0,091
PES1	2	-0,114	0,592	**DTYMK**	2	-0,076	0,202	**VAT1**	2	0,176	0,847
LAPTM4A	2	0,262	-0,137	**CAPZA1**	2	-0,032	-0,506	**TOMM70A**	2	0,007	-0,041
DCUN1D5	2	-0,006	0,534	**POMK**	2	0,075	-0,025	**CLPTM1**	2	0,014	-0,134
B2M	2	-0,076	-0,391	**NAP1L4**	2	0,025	0,158	**BAZ1A**	2	0,036	-0,428
FAF1	2	-0,163	0,414	**YWHAG**	2	-0,035	-0,420	**KRT19**	2	0,172	-1,469
CKAP2	2	-0,058	0,763	**TP53**	2	-0,383	0,144	**PAFAH1B1**	2	-0,142	-0,067
NUDT19	2	0,264	0,481	**DDX50**	2	-0,220	0,265	**NUB1**	2	0,150	0,103
CAPZB	2	0,104	0,136	**ACOT7**	2	-0,036	0,143	**NUP54**	2	-0,153	0,027
NDUFA8	2	0,086	-0,156	**NUP93**	2	0,335	-0,077	**ELP6**	2	0,133	0,243
UTP18	2	-0,168	-0,059	**SRPRB**	2	0,309	1,319	**HEXIM1**	2	-0,547	0,443
PWP1	2	0,045	0,140	**TIMELESS**	2	0,126	0,642	**RTF1**	2	-0,211	0,475
DNMT1	2	0,139	0,405	**COMMD4**	2	0,086	0,354	**EXOC8**	2	-0,198	0,540
B4GALT2	2	0,089	0,648	**PREP**	2	0,142	0,316	**DCAF7**	2	-0,056	0,345
SKIV2L2	2	-0,006	0,281	**RBM25**	2	0,083	0,748	**HAUS5**	2	0,127	-0,194
ABCE1	2	-0,158	0,490	**GINS1**	2	-0,034	0,238	**COPZ1**	2	-0,026	-0,648
DDX39A	2	-0,135	0,203	**CBFB**	2	0,240	0,366	**PRKAG1**	2	0,027	0,143
SOX12	2	0,034	1,062	**PSMD14**	2	-0,054	-0,165	**PPWD1**	2	0,077	0,270
BLMH	2	-0,144	0,559	**KIAA0020**	2	-0,236	-0,171	**MRPL32**	2	-0,064	-0,366

MINPP1	2	0,247	0,402	**DHX8**	2	-0,059	1,026	**KCTD20**	2	0,070	0,648
GFM1	2	-0,233	-0,159	**CTNND1**	2	-0,097	0,572	**SDC2**	2	0,187	-0,333
CLINT1	2	-0,209	-0,270	**HKR1**	2	-0,059	0,155	**MTMR12**	2	-0,017	0,848
HJURP	2	0,007	0,336	**SMARCD1**	2	0,018	0,346	**PTPN1**	2	-0,034	-0,369
SEC31A	2	-0,080	-0,161	**TRIP12**	2	0,043	0,239	**CCDC59**	2	-0,121	-0,455
USP10	2	0,210	-0,330	**ARID1A**	2	-0,178	0,361	**KBTBD7**	2	-0,140	1,150
MTCH2	2	-0,016	-0,130	**MET**	2	0,166	0,048	**MRPS24**	2	-0,210	1,071
MIS12	2	-0,131	1,240	**PABPN1**	2	-0,093	0,604	**PDE12**	2	0,022	0,264
METTL13	2	-0,190	0,864	**ACTN1**	2	0,135	0,012	**NFX1**	2	-0,017	0,511
C5orf15	2	0,081	-0,364	**ARL3**	2	0,015	0,427	**COPS5**	2	0,042	0,092
NEK9	2	-0,025	0,244	**SUN1**	2	-0,007	0,217	**PLEKHM2**	2	-0,175	2,137
BTG3	2	0,047	0,062	**SAMD4B**	2	-0,443	0,031	**HOXB9**	2	-0,093	-0,525
AAGAB	2	0,019	-0,154	**KEAP1**	2	-0,102	0,215	**CDCA5**	2	-0,156	0,521
GOPC	2	0,129	0,248	**SSR1**	2	-0,037	-0,163	**SLC6A15**	2	-0,350	-0,102
PITHD1	2	-0,340	-0,331	**HSBP1**	2	0,324	-0,144	**OSBP**	2	-0,042	0,075
KNSTRN	2	-0,207	-0,080	**CMSS1**	2	-0,341	0,249	**RABEP1**	2	-0,020	0,464
MOB1A	2	0,186	0,127	**SCD5**	2	-0,030	0,304	**HS6ST2**	2	-0,021	-0,191
PLAA	2	-0,341	0,479	**YTHDF3**	2	0,233	0,270	**SCAMP1**	2	-0,051	0,089
RBM28	2	0,249	0,356	**SLC39A6**	2	-0,137	0,188	**RNF219**	2	-0,125	0,171
NAA35	2	0,055	-0,053	**BTAF1**	2	-0,240	0,340	**MORC4**	2	0,189	0,012
PGM3	2	-0,125	0,305	**VMA21**	2	0,129	0,558	**CRKL**	2	-0,226	0,274
RDX	2	0,078	-0,496	**UBE2K**	2	0,010	0,210	**ARFGAP1**	2	0,211	1,029
ADCK3	2	-0,128	0,085	**GLE1**	2	-0,117	0,015	**TAF4**	2	-0,058	1,178
ENAH	2	-0,043	0,236	**LARP4**	2	-0,116	-0,175	**SEC11C**	2	-0,003	0,155
PHF6	2	-0,052	-0,060	**GUF1**	2	0,087	0,183	**ZNF274**	2	0,088	0,216
CHERP	2	-0,040	0,107	**EEF1E1**	2	-0,010	-0,056	**EML4**	2	0,145	0,091
SEPHS2	2	0,104	-0,423	**ETS2**	2	-0,168	0,113	**HAUS6**	2	-0,094	0,484
THOP1	2	-0,097	0,307	**YIF1A**	2	-0,086	-0,341	**CBS**	2	0,339	-0,030
ZCCHC17	2	-0,085	0,506	**C21orf59**	2	0,000	-0,438	**STXBP3**	2	0,112	-0,245
UPF1	2	-0,188	0,338	**THUMPD3**	2	0,104	-0,296	**DIAPH3**	2	-0,071	0,265
ANAPC7	2	0,165	-0,477	**KTI12**	2	-0,058	0,107	**H1F0**	2	-0,375	-1,218
FAF2	2	-0,071	0,408	**GRPEL2**	2	-0,167	0,979	**USF1**	2	0,023	0,283
SPDL1	2	0,119	-0,105	**TRABD**	2	-0,076	0,008	**TTC19**	2	-0,130	-0,107
UBQLN1	2	-0,232	0,156	**SART3**	2	-0,114	-0,279	**SMEK1**	2	-0,225	-0,214
WDR61	2	0,081	0,678	**PREPL**	2	-0,012	-0,315	**PGRMC2**	2	-0,152	0,106
MTPAP	2	-0,059	-0,184	**H2AFY**	2	0,069	0,259	**MAPK1**	2	0,025	0,038
SEC63	2	0,178	0,181	**SBF1**	2	0,143	1,321	**DCTN5**	2	0,271	0,308
SUPT6H	2	-0,104	0,186	**RBM6**	2	0,063	0,240	**CRTAP**	2	0,164	0,773
TIAL1	2	-0,333	-0,371	**NUFIP2**	2	-0,096	0,153	**SMARCC2**	2	-0,036	-0,555
RAD50	2	0,157	-0,045	**IPO9**	2	-0,157	-0,332	**SNAP23**	2	-0,062	-0,129
MRPS18C	2	0,302	0,120	**PTDSS1**	2	-0,147	0,226	**TBC1D20**	2	-0,072	0,415
MMS19	2	-0,152	0,388	**SPPL2A**	2	-0,013	-0,137	**MAPRE2**	2	0,176	0,279
MUT	2	0,309	0,226	**LIMA1**	2	0,087	-0,323	**SLC39A10**	2	-0,031	0,618
WDR5	2	-0,181	0,074	**NOM1**	2	-0,032	0,682	**SLC25A38**	2	-0,386	-0,298
XIAP	2	0,015	0,334	**SNX27**	2	-0,232	0,402	**CAMK1D**	2	0,041	0,333
DDX20	2	-0,204	0,107	**HMGN1**	2	0,307	-1,056	**EIF4ENIF1**	2	-0,308	0,945
ZNF121	2	-0,104	0,060	**DIP2B**	2	-0,101	0,273	**DEPDC1B**	2	-0,030	0,171
NUP50	2	-0,078	0,700	**GADD45A**	2	-0,478	-0,595	**ATAD5**	2	-0,141	-0,537
BRMS1	2	0,062	1,008	**TUBGCP3**	2	-0,168	0,263	**SPINT2**	2	0,468	-1,856
KDELR2	2	-0,013	0,094	**CAST**	2	0,083	0,125	**MAP4K4**	2	0,095	0,776
FBXO21	2	0,062	0,102	**CDC27**	2	-0,052	-0,369	**TMEM165**	2	-0,015	0,193
PPP1CB	2	-0,102	-0,005	**FOXK1**	2	-0,169	0,197	**ZNF607**	2	0,249	-0,099
RANBP9	2	-0,077	-0,153	**ZNF260**	2	-0,018	0,386	**C16orf58**	2	0,245	-0,119
FZD8	2	-0,219	1,370	**ESYT2**	2	0,060	-0,021	**BRD4**	2	0,031	0,293
SP1	2	-0,226	0,585	**MAN1B1**	2	-0,176	0,733	**CLPTM1L**	2	-0,015	0,777
DIAPH1	2	-0,046	-0,089	**TAF1**	2	-0,020	0,222	**LTN1**	2	0,220	-0,261
NET1	2	-0,285	0,105	**R3HDM2**	2	0,461	0,637	**SMNDC1**	2	-0,047	-0,355
TRAPPC3	2	0,145	-0,256	**PDPN**	2	0,114	0,269	**ATP13A2**	2	0,317	0,361
CD2AP	2	0,127	0,326	**BRIP1**	2	-0,129	0,286	**COL2A1**	2	1,036	0,696
RSRC2	2	-0,057	0,124	**EPB41L2**	2	0,262	0,217	**DPYSL3**	2	-0,256	0,062
WDR74	2	-0,162	0,223	**TM9SF4**	2	0,029	-0,211	**KIF1C**	2	0,125	0,652
IQGAP2	2	-0,115	0,494	**TTF2**	2	0,159	0,173	**CAPN2**	2	0,182	-0,457
PARP2	2	0,096	0,078	**B3GAT3**	2	-0,129	0,171	**ROCK2**	2	0,205	0,666
SUV39H2	2	0,029	0,971	**DOHH**	2	-0,308	0,233	**RMDN1**	2	0,206	0,490
UBE2A	2	-0,071	-0,707	**GOLGA3**	2	0,036	0,371	**TMEM208**	2	0,381	-0,601
ZMYM3	2	0,170	0,163	**ARPC2**	2	0,015	-0,050	**FAR1**	2	-0,037	-0,547
FXR1	2	-0,178	0,286	**EPN1**	2	-0,087	1,071	**EPS15**	2	-0,040	0,030
TROVE2	2	-0,039	0,191	**TROAP**	2	0,018	-0,513	**NAF1**	2	-0,223	-0,060
ATP6V0A1	2	-0,053	0,174	**CNPY3**	2	0,116	0,251	**CTDNEP1**	2	-0,235	0,269
CENPL	2	-0,353	0,247	**UNC50**	2	-0,211	0,637	**UFL1**	2	0,107	-0,992
SDCCAG3	2	-0,156	0,522	**YTHDC2**	2	0,088	-0,243	**MAN1A1**	2	-0,053	0,190
GTF2F2	2	-0,004	-0,653	**CTBP2**	2	-0,185	0,032	**UACA**	2	0,108	0,396
UBE2V2	2	0,034	-0,124	**NIPA2**	2	0,011	0,050	**ATG13**	2	0,016	0,079
DHX36	2	-0,162	0,121	**C8orf33**	2	-0,057	-0,249	**PI4KB**	2	-0,033	-0,157
DNAJC2	2	-0,042	-0,474	**CHMP7**	2	0,041	0,744	**PPP1R15A**	2	-0,552	0,037
MAPK1IP1L	2	0,004	-0,069	**KLC2**	2	-0,011	0,587	**STIL**	2	-0,006	0,088
EDC3	2	0,108	0,496	**CD59**	2	0,037	-0,309	**RBL1**	2	-0,123	0,055
RND3	2	0,038	0,705	**FSTL1**	2	0,251	0,745	**DNAJC21**	2	0,042	-0,295
FAM134C	2	-0,066	0,163	**PIBF1**	2	0,053	0,794	**RNMT**	2	-0,212	0,182
SRA1	2	-0,200	0,170	**LSM6**	2	0,158	-0,638	**SPPL3**	2	-0,174	0,347

TRIM8	2	-0,048	0,903	**WDFY1**	2	0,248	0,993	**PERP**	2	0,364	-1,080
LATS1	2	-0,122	0,170	**FAM217B**	2	-0,054	0,219	**KIF21A**	2	0,018	-0,062
POGZ	2	-0,176	0,314	**TIMP3**	2	-0,008	-0,124	**LHFP**	2	-0,067	1,060
C12orf29	2	-0,104	-0,125	**BAIAP2L1**	2	0,141	-1,082	**ENTPD4**	2	0,008	-0,343
PRKCA	2	-0,027	0,754	**GALK2**	2	-0,028	-0,681	**MLXIP**	2	-0,092	0,546
UBE2D3	2	-0,065	-0,350	**BAHD1**	2	-0,124	0,947	**RNF149**	2	0,103	0,545
MED14	2	-0,011	-0,140	**ITPR3**	2	0,036	0,236	**DNAJC10**	2	0,105	0,025
RAD54L	2	-0,232	-0,413	**KRAS**	2	-0,068	-0,428	**WRB**	2	0,288	0,669
C10orf12	2	-0,052	0,191	**PLOD2**	2	0,223	0,182	**ZBTB24**	2	0,025	-0,528
MARVELD3	2	0,423	-0,666	**PICALM**	2	-0,121	-0,561	**KBTBD4**	2	-0,290	-0,639
PDCL	2	0,220	0,089	**STK39**	2	0,040	-0,043	**VPS4A**	2	0,220	-0,461
PAPOLA	2	-0,109	0,120	**AMMECR1L**	2	-0,088	0,526	**FDXR**	2	0,076	0,666
BIRC6	2	0,055	0,408	**IFT57**	2	0,198	0,468	**MID1**	2	0,246	0,681
TWSG1	2	-0,023	0,703	**PIGX**	2	0,062	-0,763	**KCNK1**	2	-0,126	1,825
CDC42BPB	2	-0,050	0,895	**DPYSL5**	2	0,365	0,120	**GATA3**	2	-0,057	1,174
PPP2R1B	2	0,236	-0,141	**MYO10**	2	0,147	-0,063	**PDCD2**	2	0,248	0,022
NADK2	2	-0,051	-0,259	**CNNM1**	2	-0,115	-0,172	**SMG7**	2	-0,217	0,067
GGPS1	2	-0,157	-0,722	**PATL1**	2	-0,161	-0,140	**VPS13A**	2	0,090	-0,059
TOM1L1	2	-0,013	0,652	**PPAN**	2	0,000	-0,586	**FNBP1**	2	0,047	-0,003
TRIP11	2	-0,236	0,340	**NACC1**	2	0,052	-0,268	**PPME1**	2	0,014	-0,157
PAK2	2	-0,139	-0,453	**PIN4**	2	-0,036	-1,109	**ABI2**	2	0,145	-0,042
NUP214	2	-0,039	0,145	**PHF20**	2	-0,037	-0,209	**SUDS3**	2	0,045	-0,491
SLC33A1	2	-0,062	-0,265	**FAM63B**	2	-0,081	0,178	**TSC22D4**	2	-0,065	-0,498
RDH14	2	0,087	1,303	**LRRC8A**	2	-0,067	1,170	**SAV1**	2	-0,277	1,095
GPD2	2	0,449	0,732	**ADNP2**	2	0,265	-0,113	**RAPGEF1**	2	0,049	0,294
BAG3	2	-0,160	-0,872	**FBXW11**	2	0,010	0,282	**SFSWAP**	2	-0,325	-0,296
SENP6	2	0,048	0,277	**TTC33**	2	0,078	-0,443	**RHOBTB3**	2	-0,080	-0,022
FAR2	2	0,164	0,107	**FBXO7**	2	-0,074	-0,368	**KDM2A**	2	-0,241	-0,008
TRIM13	2	-0,065	-0,049	**ZCCHC11**	2	-0,005	0,133	**PHLPP1**	2	-0,063	0,343
HAGH	2	0,118	0,085	**ASH1L**	2	-0,174	-0,011	**ZNF318**	2	0,034	-0,278
OSBPL9	2	-0,197	0,127	**KLHL8**	2	-0,004	-0,547	**ZNF367**	2	0,186	0,357
CDKN2B	2	0,271	0,431	**PANK2**	2	-0,066	-0,463	**CLCN3**	2	0,042	0,121
ATG9A	2	0,140	0,688	**PINK1**	2	0,280	-0,161	**TACC1**	2	0,514	0,614
KLHL9	2	0,012	0,152	**N4BP2L2**	2	-0,173	-0,561	**ROCK1**	2	-0,052	-0,439
KIF1A	2	0,094	0,426	**MON2**	2	0,006	-0,338	**KLHL23**	2	-0,027	-0,768
FAM49B	2	0,069	0,520	**APPBP2**	2	0,122	-0,182	**ATP2C1**	2	0,263	0,360
POMT1	2	-0,031	-0,033	**GDE1**	2	0,226	0,238	**DNAJC5**	2	-0,127	0,693
SNRNP48	2	-0,048	0,238	**HMBS**	2	-0,124	0,009	**PROSER1**	2	-0,298	0,293
TRIM24	2	-0,032	-0,621	**ERCC8**	2	-0,100	0,154	**RIT1**	2	-0,083	0,429
TMEM30A	2	0,302	-0,345	**TIAM1**	2	0,139	0,021	**SPIDR**	2	0,467	0,285
RWDD1	2	0,138	0,161	**SMO**	2	0,083	1,043	**GXYLT2**	2	0,588	-0,533
WDR11	2	0,011	-0,392	**PPIE**	2	-0,146	-0,148	**EFCAB14**	2	-0,157	0,475
TPD52L2	2	-0,069	-0,294	**NSMCE2**	2	0,147	-1,096	**TAB1**	2	-0,033	-0,297
PNMA2	2	0,586	0,119	**FHIT**	2	0,297	0,237	**NFAT5**	2	0,267	-0,383
HOOK3	2	-0,092	-0,179	**STK11**	2	-0,111	0,720	**PRKAA2**	2	0,044	0,751
PTPRS	2	0,005	-0,095	**RPS6KB1**	2	-0,164	-0,044	**PTBP2**	2	-0,284	-0,418
SLC19A1	2	0,293	0,111	**SS18L2**	2	-0,192	-0,513	**CDIPT**	2	0,243	-0,472
UQCC1	2	0,025	0,232	**SCRN3**	2	0,088	-0,047	**PELO**	2	-0,046	-1,276
MNX1	2	-0,186	1,414	**ZZZ3**	2	-0,056	0,643	**DIDO1**	2	-0,023	0,422
GPATCH3	2	-0,482	0,617	**CENPJ**	2	-0,185	-0,767	**DCAF6**	2	0,128	-0,553
CCDC117	2	-0,152	0,140	**GPBP1L1**	2	-0,121	-0,202	**FAM64A**	2	0,130	-0,288
ZNF326	2	-0,028	-0,589	**NADK**	2	0,069	0,379	**REPIN1**	2	0,001	-0,164
SETD5	2	-0,127	0,535	**MED13**	2	-0,001	0,808	**AUTS2**	2	-0,201	1,435
EP400	2	0,022	0,106	**BAG1**	2	-0,539	-0,444	**TRPM7**	2	-0,108	-0,115
HERC2	2	-0,283	0,125	**LEPROTL1**	2	-0,109	-0,450	**SNX19**	2	0,178	0,896
ACVR1B	2	0,078	0,603	**ANKS1A**	2	0,146	0,268	**C2CD3**	2	-0,040	-0,708
TM2D3	2	-0,125	0,088	**CPSF4**	2	-0,063	-0,169	**UBN2**	2	-0,065	0,409
UBE2E3	2	-0,009	-0,187	**FLT1**	2	0,345	0,245	**SETD1B**	2	-0,129	0,084
TMOD3	2	-0,051	-0,492	**EZH1**	2	-0,117	-0,267	**RMND5B**	2	-0,001	0,457
ADD3	2	0,139	-0,385	**DOCK7**	2	0,039	-0,790	**PCDH7**	2	0,267	-0,821
SERP1	2	-0,056	0,230	**AVL9**	2	0,047	0,340	**RASA1**	2	0,077	-0,263
CADM1	2	-0,177	-0,695	**MGAT1**	2	-0,124	0,344	**TMED5**	2	0,060	-1,038
ZBTB11	2	-0,044	0,394	**HGSNAT**	2	0,239	0,486	**EFNA5**	2	-0,150	0,576
DLC1	2	-0,023	0,992	**PPM1K**	2	-0,005	-0,375	**USP13**	2	-0,220	-0,400
EPHA2	2	0,040	-0,228	**ATXN7**	2	-0,154	2,406	**NRCAM**	2	0,149	0,717
CCNI	2	0,059	-0,470	**RALA**	2	0,197	-0,053	**RNF145**	2	-0,221	-0,829
RBBP6	2	0,024	0,081	**SENP2**	2	-0,192	-0,075	**ZKSCAN8**	2	0,132	0,157
N6AMT2	2	0,087	-0,524	**SLC48A1**	2	0,229	0,638	**LMBR1**	2	0,141	-0,044
MSL1	2	-0,082	1,208	**ATP9A**	2	0,144	1,164	**USP34**	2	-0,177	-0,078
C19orf47	2	-0,050	0,019	**PLCE1**	2	-0,020	0,643	**SLC25A14**	2	-0,001	-0,085
BCDIN3D	2	0,082	1,947	**STIM1**	2	0,057	0,512	**CDK17**	2	-0,277	-0,134
BLOC1S2	2	-0,136	-0,307	**FBXO28**	2	-0,107	-0,504	**GPCPD1**	2	-0,349	0,222
C6orf62	2	0,021	-0,186	**TANGO6**	2	0,277	-0,499	**DUSP16**	2	-0,140	0,052
AKAP11	2	0,053	1,199	**RICTOR**	2	0,082	-0,004	**ITGA6**	2	0,437	-0,612
NRAS	2	0,142	-0,333	**BCAS3**	2	-0,110	0,984	**GPD1L**	2	-0,028	0,299
SSX2IP	2	-0,128	0,544	**LRRFIP1**	2	-0,025	-0,187	**BARD1**	2	0,111	0,194
TPRG1L	2	0,106	0,866	**DYNLL2**	2	0,180	-0,107	**JOSD1**	2	0,028	-0,148
VPS33B	2	-0,147	0,073	**INADL**	2	0,108	0,140	**BCORL1**	2	-0,131	-0,487
SPRTN	2	0,026	-0,619	**TMX3**	2	-0,111	-0,453	**ZNF217**	2	0,275	-0,684
STK24	2	-0,136	0,024	**MAP4K5**	2	-0,109	-0,639	**ETV3**	2	-0,243	-0,250

NFIB	2	-0,006	0,239	**STK40**	2	0,071	0,876	**UBC**	1	-0,047	0,508
CD47	2	0,051	-0,789	**ATP7B**	2	-0,083	0,265	**ENO1**	1	-0,186	0,439
CBLL1	2	-0,170	-0,945	**ZNF512**	2	-0,111	-0,785	**LSM4**	1	0,180	0,256
TM9SF1	2	-0,009	-0,867	**RHOU**	2	0,074	-0,958	**TRIP10**	1	-0,313	3,091
PPP1R26	2	-0,019	0,735	**TCP11L1**	2	0,056	0,467	**RPS4X**	1	-0,137	-0,041
FURIN	2	0,216	0,731	**LYSMD3**	2	0,000	-0,198	**ACTB**	1	0,107	-0,144
NIPAL3	2	0,105	0,476	**BPGM**	2	-0,020	-0,945	**MT-CO2**	1	0,369	1,563
CCDC174	2	-0,159	-0,764	**NDST1**	2	-0,014	0,170	**GNB2L1**	1	0,015	0,162
TRAPPC11	2	0,166	-0,674	**SLC22A5**	2	-0,149	0,246	**RPL5**	1	-0,041	-0,208
ITPR2	2	0,251	-0,116	**NCOA2**	2	0,059	-0,221	**TCEB2**	1	-0,115	0,381
UCK1	2	0,071	-0,213	**NPNT**	2	0,049	0,294	**PCNA**	1	-0,142	-0,088
PFKFB3	2	0,163	0,472	**ADCY6**	2	0,270	-0,608	**PTMA**	1	0,259	0,276
OTUD1	2	-0,156	1,304	**SLC20A2**	2	0,040	0,422	**PPIA**	1	0,017	0,243
RAD18	2	-0,214	-0,971	**PTBP3**	2	-0,380	-0,904	**HIST1H2BJ**	1	-0,115	-0,192
GALNT11	2	0,160	0,970	**MDFIC**	2	-0,242	-0,899	**YWHAE**	1	0,117	0,226
CANT1	2	-0,064	-0,516	**DIRAS1**	2	-0,168	1,132	**UCHL1**	1	-0,113	-0,121
FAM129A	2	0,037	-0,831	**MYO18A**	2	0,252	0,251	**ILF2**	1	0,001	0,247
WWC1	2	-0,403	0,077	**SESN3**	2	-0,011	0,009	**RPL3**	1	0,022	0,225
PTPN13	2	-0,177	-0,862	**ARHGEF11**	2	0,031	0,027	**RPL36AL**	1	0,226	-0,012
MLK4	2	-0,035	0,456	**FAM111A**	2	0,520	0,164	**HNRNPAB**	1	0,016	0,167
USP6NL	2	-0,114	-0,461	**PPM1H**	2	0,230	1,404	**SOD1**	1	0,335	0,057
C6orf106	2	0,035	0,021	**EXOC6B**	2	-0,054	-0,278	**ALDOA**	1	0,052	0,154
FRAT2	2	-0,199	1,217	**TTYH3**	2	0,113	0,074	**RPL13**	1	0,065	-0,098
TAF12	2	-0,031	0,349	**SARS2**	2	-0,053	-0,958	**H2AFZ**	1	-0,078	0,125
DENND5A	2	-0,054	0,737	**TSPYL4**	2	0,343	-0,534	**CKS2**	1	-0,176	0,215
PKIB	2	-0,151	-0,434	**RGMB**	2	0,007	-0,210	**LDHA**	1	0,042	0,092
STK10	2	-0,095	-0,544	**ATRNL1**	2	-0,454	0,929	**RPL32**	1	-0,235	-0,056
BNIP2	2	0,139	-1,174	**FOXA1**	2	0,125	-0,776	**RPS3**	1	-0,169	0,340
PPM1L	2	-0,227	0,991	**NIPA1**	2	0,052	-0,612	**RPSA**	1	-0,181	0,695
COA1	2	-0,076	-0,481	**WWOX**	2	0,233	-1,249	**ALYREF**	1	-0,025	0,094
NRARP	2	-0,223	-0,208	**KHNYN**	2	0,198	0,113	**PEBP1**	1	-0,072	0,503
TGFBR3	2	-0,002	-0,860	**HHAT**	2	0,046	-0,359	**TUBB2A**	1	-0,127	0,368
PTEN	2	0,030	0,772	**ORMDL3**	2	-0,130	-1,085	**ARF1**	1	-0,020	0,491
ZDHHC17	2	-0,121	-0,067	**ABLIM1**	2	0,041	-0,442	**ANP32B**	1	0,222	0,273
UBE2H	2	0,171	-0,113	**PPM1A**	2	-0,205	0,470	**SET**	1	-0,149	0,353
CDKN1A	2	0,021	-0,546	**SH3PXD2A**	2	0,153	0,044	**GNAZ**	1	-0,344	2,308
ARF3	2	0,104	0,935	**PPAPDC2**	2	0,354	1,084	**HSPA5**	1	-0,063	0,089
YAF2	2	0,056	-0,151	**KBTBD11**	2	0,066	0,125	**RPL26**	1	-0,058	-0,027
ATRN	2	-0,161	-0,608	**MAP3K3**	2	0,000	-0,819	**VIM**	1	-0,026	0,482
TPRN	2	-0,153	-0,458	**ZNF462**	2	-0,099	-0,037	**MCM3**	1	0,040	0,682
KLF5	2	-0,440	0,120	**MGAT5**	2	-0,216	-0,429	**RPL18**	1	-0,248	0,050
SLC44A1	2	-0,033	0,505	**NINL**	2	0,121	0,231	**PRDX6**	1	-0,070	0,010
EPC1	2	-0,206	-0,152	**CHD6**	2	0,073	-0,649	**SSH1**	1	0,286	0,584
TTC17	2	0,044	0,180	**TMTC2**	2	-0,312	1,398	**ATP5C1**	1	-0,034	0,271
CGGBP1	2	0,009	-0,232	**FAM69A**	2	0,027	-2,338	**HPRT1**	1	0,174	-0,037
USP53	2	-0,057	-0,336	**B3GNT5**	2	-0,323	-0,523	**MT-ND4**	1	0,467	-0,526
UBN1	2	-0,272	0,533	**C12orf49**	2	-0,210	-1,150	**FARSA**	1	-0,054	0,350
PIKFYVE	2	-0,075	0,605	**SLAIN2**	2	-0,218	-0,645	**NUDC**	1	0,037	0,202
RNF215	2	0,006	0,816	**EIF4EBP2**	2	0,082	-1,329	**UQCRQ**	1	-0,195	0,538
ATP11A	2	0,172	0,622	**SMAD2**	2	-0,270	-1,455	**VDAC1**	1	0,179	0,486
PTPN23	2	-0,094	-0,259	**SYDE2**	2	-0,068	-2,011	**PDIA3**	1	0,005	-0,001
E2F2	2	-0,046	-1,161	**CCNJ**	2	0,028	-1,598	**TAGLN2**	1	0,107	-0,225
CDIP1	2	-0,015	-0,299	**DBNDD2**	2	0,042	-0,609	**PSMB1**	1	0,097	0,163
ZNF608	2	-0,019	0,255	**RAB31**	2	0,014	-0,241	**NDUFB7**	1	-0,010	0,792
RALGPS2	2	-0,151	-0,121	**RFX7**	2	-0,048	-0,959	**NME1**	1	-0,069	1,100
GPR161	2	-0,032	0,711	**LRRC8C**	2	-0,199	-0,781	**GLO1**	1	0,233	0,367
SCOC	2	0,216	-1,024	**FUT10**	2	-0,003	-1,344	**KHDRBS1**	1	0,000	0,095
ORMDL1	2	-0,285	-0,951	**C2orf43**	2	0,089	-1,645	**ECHS1**	1	0,115	0,276
TBCK	2	0,205	0,353	**ERBB4**	2	0,170	0,803	**PAF1**	1	0,033	0,672
LMTK2	2	-0,047	-1,002	**NCK2**	2	0,119	-1,560	**SNRPD1**	1	0,186	0,117
C5orf24	2	-0,138	-0,434	**ZNF71**	2	-0,038	-0,791	**PPIB**	1	0,113	0,078
ZCCHC14	2	0,155	0,217	**SMAD3**	2	0,003	-1,807	**TOP2A**	1	0,041	0,354
SETD7	2	0,191	-0,266	**GJA3**	2	0,248	-0,272	**RANBP1**	1	-0,087	0,165
CTSZ	2	0,705	0,377	**ZNF23**	2	0,364	-0,443	**PSMA7**	1	-0,063	0,123
AGFG1	2	-0,061	0,223	**C19orf12**	2	-0,093	0,855	**SRP9**	1	0,073	0,024
RERE	2	-0,143	-0,281	**HIPK3**	2	-0,074	-2,693	**ERH**	1	-0,341	-0,291
TRAF5	2	0,098	-0,619	**BMI1**	2	-0,097	-3,032	**PRDX3**	1	-0,007	-0,135
WDTC1	2	0,020	0,676	**ZNF395**	2	0,380	-0,228	**COX5A**	1	0,113	-0,581
ANKRD30BL	2	-0,146	-0,352	**MVB12B**	2	-0,239	0,031	**NDUFAB1**	1	0,326	-0,323
GPR63	2	-0,104	-0,492	**MAFG**	2	-0,219	0,000	**COX5B**	1	-0,030	0,099
MAN1A2	2	0,009	-0,339	**BOC**	2	0,084	-0,989	**PTMS**	1	0,144	0,757
CSNK1G3	2	-0,173	-0,910	**IFFO2**	2	-0,066	-0,885	**PSMB6**	1	-0,033	0,247
IER3IP1	2	0,000	-0,646	**MGAT2**	2	-0,114	0,000	**PRKCSH**	1	0,086	0,792
DGKH	2	-0,012	-0,384	**ZHX1-C8orf76**	2	0,519	0,000	**NOC2L**	1	-0,049	0,598
PCGF5	2	0,070	-0,159	**HOXC13**	2	-0,024	0,000	**RCC2**	1	-0,108	0,291
NBEA	2	-0,261	0,178	**TICAM2**	2	-2,438	0,000	**COX7A2**	1	0,069	-0,134
ITPR1	2	-0,077	0,089	**ANKHD1-EIF4EBP3**	2	-0,301	0,000	**STRAP**	1	0,050	-0,123
CEP350	2	-0,076	-0,640	**RAB12**	1	-0,111	2,952	**APEX1**	1	0,119	-0,239
LRP3	2	0,212	0,025	**CDK6**	1	-0,227	4,701	**PABPC1**	1	0,014	0,256
SFI1	2	-0,018	-0,514	**HIST1H1C**	1	0,015	-0,010	**GLRX3**	1	0,102	0,237

YWHAQ	1	0,082	0,123	**PSAT1**	1	-0,324	-0,652	**UBE2E1**	1	-0,108	-0,114
UXT	1	-0,333	0,200	**CS**	1	-0,055	0,018	**PSMA5**	1	0,007	0,399
EIF1	1	-0,262	-0,069	**NUP107**	1	0,007	0,198	**SLMO2**	1	0,195	-0,104
PDIA4	1	0,087	0,425	**PEG10**	1	0,010	0,626	**MRPL41**	1	-0,009	0,252
CHD3	1	-0,552	1,068	**MRPL37**	1	0,015	0,037	**SRSF5**	1	0,145	0,245
RPL37	1	-0,096	-0,040	**RRP36**	1	0,170	0,998	**YARS**	1	-0,010	0,109
HNRNPL	1	-0,044	0,431	**MDH1**	1	0,072	-0,016	**NDUFA12**	1	-0,084	-0,452
U2AF2	1	-0,120	0,606	**NAA38**	1	-0,019	0,728	**SMARCA4**	1	-0,143	0,780
MRPL28	1	0,093	0,666	**ARF4**	1	0,145	0,080	**ADH5**	1	-0,003	0,587
ARF5	1	0,092	0,341	**SLBP**	1	-0,061	-0,159	**RPF2**	1	-0,018	0,059
MRPL3	1	0,159	0,938	**RNASEH2A**	1	-0,103	-0,310	**PSME1**	1	0,214	-0,251
PTBP1	1	-0,024	0,418	**EIF6**	1	-0,264	0,065	**KCTD1**	1	-0,212	2,459
PSMC2	1	-0,045	0,251	**FDPS**	1	0,032	0,001	**ICT1**	1	0,003	0,128
PRPF19	1	0,002	0,367	**ZBED4**	1	-0,146	1,116	**POLR2H**	1	-0,318	0,715
IMPDH2	1	-0,156	0,038	**GNAS**	1	0,002	0,307	**PPP4C**	1	0,171	-0,162
HMGN3	1	0,172	0,408	**SARS**	1	-0,173	-0,023	**MRPS2**	1	-0,124	0,310
PHGDH	1	-0,133	0,226	**SPAG7**	1	0,165	1,974	**MRPL9**	1	0,074	0,184
CENPW	1	0,013	0,039	**RRP1**	1	0,206	0,264	**SRSF4**	1	-0,021	0,613
DDT	1	0,057	0,679	**ETFA**	1	0,225	0,152	**RNF40**	1	0,122	0,697
EIF3L	1	-0,200	0,148	**DDB1**	1	-0,240	0,537	**NDUFA4**	1	0,081	-0,060
DDX1	1	0,056	0,062	**PFAS**	1	-0,116	1,254	**SEC61B**	1	0,101	0,319
MRPS26	1	-0,026	0,846	**IMMT**	1	0,027	0,266	**RAB1B**	1	0,098	0,735
RBMX	1	-0,068	0,171	**EBPL**	1	0,080	0,695	**MFAP1**	1	-0,019	-0,004
CYC1	1	-0,223	0,589	**HNRNPR**	1	-0,086	-0,109	**BPNT1**	1	0,172	0,207
ANXA5	1	-0,045	0,180	**AHSA1**	1	0,003	0,047	**FANCI**	1	-0,176	0,294
BOD1	1	-0,367	2,754	**NCAPG**	1	-0,234	0,079	**AK2**	1	-0,095	0,102
LAMTOR4	1	0,118	0,079	**COX4I1**	1	0,444	-0,198	**VPS25**	1	0,052	0,466
COPS6	1	-0,133	0,215	**UTP6**	1	0,100	0,660	**BCL11A**	1	-0,086	2,306
SF3B5	1	0,035	-0,567	**KIF22**	1	0,023	-0,087	**TARS2**	1	-0,084	0,381
MYC	1	0,127	0,651	**IMP3**	1	-0,185	0,178	**TIMM8B**	1	0,179	0,278
CDC123	1	-0,145	0,122	**KIAA1279**	1	0,088	0,274	**RAD23B**	1	0,029	0,718
PDHA1	1	0,016	0,402	**GSR**	1	-0,038	0,388	**NKX6-1**	1	-0,372	0,707
ATP5G2	1	-0,013	0,328	**HAX1**	1	-0,256	0,397	**JTB**	1	-0,365	0,561
SRSF7	1	-0,029	-0,142	**GLUD2**	1	0,751	0,310	**RAD51AP1**	1	-0,052	0,554
GSTO1	1	0,089	-0,370	**PCBP2**	1	-0,187	0,193	**GPRIN1**	1	-0,081	0,302
PRPS1	1	-0,168	0,242	**H1FX**	1	0,133	0,288	**MRPL24**	1	0,054	0,288
RPA2	1	-0,116	0,347	**UBAP2L**	1	-0,048	0,153	**NCAPH**	1	0,076	0,557
SNRPF	1	0,228	-0,150	**MRPS35**	1	0,120	-0,219	**C14orf2**	1	0,048	-0,113
LTV1	1	0,207	0,153	**RECQL**	1	0,195	-0,015	**TXNDC17**	1	0,054	0,032
PSMC3	1	0,094	0,187	**EFTUD2**	1	0,056	0,845	**KIF23**	1	-0,101	0,186
LINC00493	1	-0,081	0,037	**CUL1**	1	0,013	0,542	**MRPS9**	1	0,102	0,329
MRPL15	1	0,172	0,493	**SF3A1**	1	0,002	0,573	**DYNLL1**	1	-0,033	-0,588
MRPL47	1	-0,227	0,864	**BCAS2**	1	-0,031	-0,567	**SRP54**	1	0,212	-0,280
PCMT1	1	0,126	-0,068	**STOML2**	1	-0,061	-0,336	**MRI1**	1	0,105	0,237
THRAP3	1	-0,167	0,550	**CAPRIN1**	1	-0,030	0,149	**CYCS**	1	0,096	-0,290
MAEA	1	0,090	0,460	**NAA20**	1	0,032	0,245	**CAD**	1	0,043	0,432
CFL1	1	-0,057	-0,120	**EMC7**	1	-0,070	0,314	**TDP1**	1	-0,042	0,381
SDHC	1	-0,074	-0,361	**LAPTM4B**	1	-0,071	0,084	**GLOD4**	1	0,017	0,415
COPS3	1	-0,067	-0,024	**DHFR**	1	0,170	-0,260	**CHMP5**	1	-0,002	-0,189
SSB	1	-0,059	-0,316	**BLVRA**	1	0,074	0,125	**KLHDC3**	1	0,107	0,152
GART	1	0,441	-0,149	**RPF1**	1	-0,088	-0,401	**TBCE**	1	-0,035	-0,251
IK	1	0,146	0,206	**RIOK1**	1	-0,469	0,879	**HIF1A**	1	0,155	-0,058
RUVBL2	1	-0,186	0,293	**BMS1**	1	-0,022	0,576	**DDX18**	1	-0,025	0,439
ASNS	1	-0,405	-0,591	**AP2M1**	1	-0,159	-0,024	**VCL**	1	0,158	0,200
MRPL14	1	-0,114	0,335	**WDR18**	1	0,057	0,105	**GEMIN4**	1	-0,142	1,039
EIF4A3	1	-0,161	0,182	**ZMPSTE24**	1	0,119	-0,217	**GNL2**	1	-0,030	0,097
PPP2R1A	1	-0,100	0,108	**DCTPP1**	1	0,007	0,484	**MRPS16**	1	-0,031	0,566
RPL7L1	1	-0,036	0,412	**CALU**	1	-0,013	0,001	**EXOSC6**	1	0,131	0,113
TIPIN	1	0,131	-0,188	**GSPT1**	1	0,173	-0,146	**ARL2**	1	0,220	0,827
MRTO4	1	-0,246	0,282	**APOA1BP**	1	0,050	0,466	**CSTF2**	1	0,017	0,345
PRELID1	1	-0,106	0,283	**KRR1**	1	-0,068	-0,137	**CDC23**	1	-0,050	0,463
EN2	1	0,173	3,470	**AKIRIN2**	1	0,139	0,913	**RCL1**	1	-0,190	0,865
SDHB	1	0,007	0,522	**PSPC1**	1	-0,031	0,412	**DDX54**	1	0,217	1,025
PPP1R9B	1	0,174	3,048	**YME1L1**	1	0,041	0,162	**CEBPZ**	1	0,015	0,556
HDAC1	1	-0,121	0,434	**CSNK1A1**	1	-0,045	-0,084	**NUP43**	1	0,126	-0,120
GNL3L	1	0,171	0,344	**CD320**	1	-0,130	0,399	**CDC16**	1	0,000	0,392
EIF1AX	1	-0,110	0,190	**MRPL55**	1	0,030	0,520	**PSME3**	1	-0,027	0,035
LMAN2	1	-0,167	0,523	**CHMP2A**	1	-0,011	0,252	**PSMF1**	1	-0,061	0,422
MCM2	1	0,217	0,059	**ASF1B**	1	0,099	0,118	**DCTN6**	1	-0,007	0,155
PMPCA	1	-0,106	0,636	**AAMP**	1	0,191	0,530	**SAFB2**	1	-0,008	0,304
NOP2	1	-0,097	0,604	**LYAR**	1	0,125	0,598	**DHCR7**	1	0,266	1,051
HIST4H4	1	-0,069	-0,379	**KDELR1**	1	0,073	-0,263	**MTHFD2**	1	-0,055	-0,631
YWHAB	1	-0,053	-0,604	**AKR1B1**	1	0,059	-0,088	**PSMG1**	1	0,051	-0,791
FAM98A	1	0,275	1,200	**BUD31**	1	-0,144	-0,330	**MRPL54**	1	-0,155	-0,171
TYMS	1	-0,239	-0,140	**MTA2**	1	-0,269	0,556	**CLNS1A**	1	0,149	-0,098
ZMYND19	1	-0,207	1,568	**ERI3**	1	-0,061	1,104	**NELFB**	1	-0,084	1,459
DARS2	1	-0,062	-0,306	**UFC1**	1	-0,213	0,502	**HSD17B4**	1	0,091	0,593
EIF3J	1	-0,015	0,404	**PSMD12**	1	0,048	-0,154	**NKRF**	1	-0,097	0,410
ABCF2	1	0,176	0,938	**HDGFRP3**	1	0,030	1,575	**TECR**	1	0,134	0,125
XRN2	1	-0,036	0,062	**MRPS18A**	1	0,056	0,067	**MTX2**	1	0,151	0,283

AIP	1	-0,163	0,205	**RFC5**	1	-0,115	-0,259	**NPEPPS**	1	0,156	0,010
C19orf43	1	-0,010	0,315	**MAD2L1**	1	-0,050	-0,015	**GRB2**	1	-0,009	-0,030
MRPL36	1	0,371	-0,304	**CPNE3**	1	0,083	0,322	**API5**	1	-0,054	0,068
MIS18A	1	0,148	0,079	**ESPL1**	1	-0,184	0,557	**TIPRL**	1	0,037	-0,422
GPX1	1	-0,025	-0,222	**GTF2H3**	1	-0,042	0,365	**SGCE**	1	0,263	0,338
SGTA	1	0,022	0,490	**UROD**	1	-0,119	0,131	**MRPL43**	1	0,149	1,517
ALDH9A1	1	0,094	0,161	**MZT2A**	1	-0,079	0,453	**ATP1B1**	1	0,001	0,321
CDKN1B	1	-0,210	0,178	**ARF6**	1	-0,085	0,004	**HSD17B12**	1	0,194	0,269
ZNF503	1	-0,405	0,751	**ZNF850**	1	-0,017	0,042	**CYR61**	1	0,086	1,182
GOT1	1	0,101	0,069	**SLC29A1**	1	-0,149	0,112	**CDCA7L**	1	0,188	1,138
SPAG5	1	-0,086	0,406	**IDH3A**	1	0,049	0,541	**DNAJB11**	1	0,070	0,278
MRPL18	1	-0,053	-0,375	**C9orf64**	1	0,047	0,543	**RRBP1**	1	0,189	0,955
TMEM160	1	-0,332	0,724	**DLST**	1	-0,018	0,172	**PDCD11**	1	1,274	0,323
COIL	1	-0,091	0,680	**SFXN4**	1	0,077	0,318	**BRD8**	1	-0,144	0,664
RAB1A	1	0,001	0,424	**NVL**	1	0,040	0,124	**NDUFC1**	1	0,177	-0,368
TRMT1	1	-0,248	0,217	**PAPSS1**	1	0,150	0,318	**ZC3H4**	1	0,167	1,421
PITPNB	1	-0,025	0,122	**PRPF40A**	1	-0,012	0,190	**FXR2**	1	-0,079	0,281
PLEKHJ1	1	0,049	0,501	**DYNC1I2**	1	0,045	-0,170	**POLD2**	1	-0,080	0,296
MLF2	1	-0,100	-0,078	**CRNKL1**	1	0,033	0,619	**SERPINH1**	1	-0,035	0,699
ZIC2	1	-0,576	0,574	**KPNA3**	1	0,048	1,425	**CD276**	1	0,012	1,216
NANOS1	1	-0,269	1,966	**GEMIN5**	1	0,017	0,284	**DFFA**	1	0,114	0,637
CSNK2A1	1	-0,135	0,035	**DNAJC1**	1	-0,281	0,409	**YRDC**	1	-0,040	-0,189
CCNA2	1	-0,098	-0,668	**YIF1B**	1	-0,009	0,469	**POLR3A**	1	-0,165	0,619
CDC25B	1	-0,340	0,518	**YIPF3**	1	-0,017	0,439	**NIPSNAP1**	1	0,252	-0,218
PDCD2L	1	-0,098	-0,017	**CUL4A**	1	0,039	0,249	**SLC35F6**	1	0,072	0,142
FANCL	1	-0,030	0,135	**LEO1**	1	-0,003	-0,237	**RAC3**	1	-0,269	-0,015
DYNC1LI2	1	0,246	1,533	**TACO1**	1	0,100	0,102	**VPS4B**	1	-0,359	0,077
VPS72	1	-0,032	0,310	**NCSTN**	1	-0,180	0,332	**RBBP5**	1	-0,063	0,383
EMC4	1	-0,061	0,252	**AASS**	1	-0,024	0,759	**PPP2R2A**	1	0,037	0,220
ACTR1A	1	0,070	0,278	**UBE2R2**	1	0,025	1,452	**TMEM209**	1	-0,010	-0,128
RNMTL1	1	-0,378	0,189	**PNPO**	1	0,058	0,610	**PARL**	1	-0,164	0,247
CPE	1	0,231	0,262	**RSL24D1**	1	-0,306	-0,815	**OSTC**	1	-0,027	-0,732
SRP72	1	-0,089	0,399	**CENPB**	1	0,013	1,175	**NFATC2IP**	1	0,212	0,602
AP1S1	1	-0,060	-0,290	**ADSL**	1	-0,016	-0,040	**SDF2L1**	1	0,069	-0,345
ABRACL	1	0,248	0,386	**C1GALT1C1**	1	0,064	0,173	**RAB5B**	1	0,049	-0,046
USP14	1	0,052	-0,311	**OXA1L**	1	-0,003	-0,399	**CLIC4**	1	-0,062	-0,123
TELO2	1	-0,070	0,163	**CDCA4**	1	-0,073	0,649	**LETM1**	1	0,027	0,545
MRPL23	1	0,084	0,739	**FAM47E-STBD1**	1	0,787	2,525	**SDHAF1**	1	-0,067	0,081
NDUFB4	1	0,014	-0,880	**MEPCE**	1	-0,303	0,602	**CLPP**	1	-0,038	-0,144
LSM12	1	-0,003	0,329	**GTF3C5**	1	-0,058	0,373	**RGS10**	1	-0,055	0,734
PLD3	1	0,019	-0,208	**MAP2K1**	1	-0,036	0,134	**FAM98B**	1	-0,087	0,815
OLA1	1	-0,064	0,317	**ELOVL5**	1	-0,119	0,270	**TSNAX**	1	0,026	0,077
POLR1C	1	-0,143	0,674	**AP1B1**	1	-0,008	0,264	**SMG8**	1	0,052	0,619
EID2	1	-0,037	-0,848	**NDUFV3**	1	0,322	0,159	**ADK**	1	-0,018	-0,204
AP3D1	1	-0,073	0,953	**LRRC42**	1	0,007	0,909	**HOXC4**	1	0,004	0,627
PDLIM1	1	0,098	-0,020	**PTOV1**	1	-0,217	-0,002	**MTCH1**	1	-0,119	0,030
NAE1	1	0,297	-0,749	**NOSIP**	1	-0,244	-0,059	**RTN3**	1	0,017	-0,532
CLUH	1	-0,012	0,539	**POLD1**	1	-0,180	0,726	**SKP1**	1	0,120	-0,053
CTSL	1	0,207	0,644	**SRP68**	1	-0,205	0,325	**NCBP1**	1	0,056	-0,179
MRPS28	1	0,353	0,455	**PITRM1**	1	0,103	0,656	**RPAIN**	1	0,046	0,282
UBE2D2	1	-0,015	-0,023	**EIF3H**	1	-0,019	0,264	**WDR36**	1	-0,150	-0,018
EXOSC2	1	-0,122	-0,044	**CBX1**	1	0,039	0,525	**SCML2**	1	-0,140	0,470
AAR2	1	-0,065	0,862	**ACBD3**	1	-0,233	0,365	**MTG2**	1	0,029	0,730
CNIH1	1	0,077	0,446	**COL4A1**	1	0,185	0,922	**HMMR**	1	0,073	-0,398
APMAP	1	-0,182	0,328	**NOL9**	1	-0,215	-0,033	**RFWD3**	1	0,153	-0,065
C1orf43	1	0,053	0,651	**NME3**	1	-0,343	-0,802	**MRPL21**	1	-0,092	0,332
ZNF224	1	-0,055	0,643	**C17orf75**	1	0,187	1,734	**UAP1**	1	-0,119	0,088
CD151	1	0,048	-0,075	**TTK**	1	-0,140	0,118	**NCAPH2**	1	-0,064	0,054
NUCB1	1	0,230	0,459	**MRPL17**	1	0,084	0,262	**GPALPP1**	1	0,280	0,902
HK1	1	0,031	0,076	**DPYSL2**	1	0,171	0,867	**UMPS**	1	0,062	0,192
MAFK	1	-0,191	1,783	**TTC27**	1	-0,020	0,800	**H2AFV**	1	-0,001	-0,084
TMX2	1	0,011	-0,427	**UBR7**	1	0,112	0,766	**HOXB6**	1	-0,701	1,257
HMCES	1	0,185	1,374	**TTC13**	1	0,124	-0,030	**BCCIP**	1	0,034	-0,698
CHCHD3	1	0,062	-0,074	**PEF1**	1	0,122	-0,003	**QSOX2**	1	-0,198	0,845
HMOX2	1	-0,176	0,508	**MOGS**	1	0,121	0,440	**SCML1**	1	-0,002	-0,320
MAGED2	1	0,459	0,249	**UBE2O**	1	-0,113	0,743	**WRNIP1**	1	-0,017	0,630
SEPHS1	1	0,037	0,744	**SLC25A13**	1	-0,095	-0,270	**CDK5RAP1**	1	-0,007	0,262
FTH1	1	0,089	-0,172	**SSNA1**	1	-0,090	0,164	**PM20D2**	1	0,343	0,329
SPC24	1	0,139	0,516	**RPRD2**	1	-0,186	0,221	**DNAJA3**	1	-0,043	0,503
ELP5	1	-0,114	0,734	**POLA1**	1	-0,042	0,379	**PRPF4**	1	-0,006	0,047
FUBP1	1	0,076	-0,455	**OGDH**	1	0,139	0,890	**C11orf58**	1	0,034	-0,381
GMPS	1	-0,136	0,113	**FSCN1**	1	-0,351	-0,557	**WDR70**	1	-0,093	0,927
YEATS4	1	0,139	-0,213	**S100A11**	1	0,328	-1,206	**TCEB1**	1	-0,068	-0,456
ADRBK1	1	-0,064	0,390	**CTR9**	1	-0,093	0,228	**DENR**	1	0,131	-0,224
SSSCA1	1	-0,142	-0,395	**PHAX**	1	0,086	-0,214	**DPY30**	1	0,117	-0,162
VPS29	1	-0,021	-0,161	**CTNNBL1**	1	-0,090	0,259	**TNFRSF10D**	1	-0,191	0,461
OIP5	1	-0,066	0,245	**DROSHA**	1	0,062	0,216	**VPS26A**	1	-0,076	-0,465
PMF1	1	0,000	0,849	**PCGF6**	1	-0,036	-0,150	**NEK2**	1	-0,113	-0,415
TMEM50A	1	0,010	-0,522	**ESF1**	1	-0,081	0,208	**DNAL1**	1	0,064	1,591
RPAP3	1	-0,001	0,077	**MAP2K2**	1	0,038	0,322	**GNS**	1	0,181	0,566

PDCD7	1	-0,175	1,143	**ZNF546**	1	-0,211	-0,281	**C16orf91**	1	-0,082	1,425
GPN3	1	-0,147	-0,514	**ZWILCH**	1	0,031	0,013	**ANAPC16**	1	0,185	-0,181
POLR2C	1	0,146	-0,387	**CUL3**	1	0,091	0,430	**RAB10**	1	-0,016	0,101
GSTA4	1	0,261	1,206	**IPO8**	1	-0,409	0,454	**IST1**	1	0,136	-0,573
GLG1	1	0,145	-0,187	**DBR1**	1	0,008	0,074	**ABHD17C**	1	-0,164	1,995
SYPL1	1	0,023	-0,469	**NCAPD3**	1	-0,011	-0,186	**GOLPH3**	1	-0,065	-0,214
TRA2B	1	-0,146	-0,321	**COX11**	1	0,031	0,932	**MRPL13**	1	-0,023	-0,338
COG4	1	0,180	0,321	**COTL1**	1	-0,162	-0,755	**RFC1**	1	0,242	0,177
SIRT1	1	-0,426	0,797	**TEX10**	1	-0,036	0,127	**POLH**	1	-0,028	0,387
UTP3	1	0,009	-0,455	**PKN2**	1	-0,091	0,053	**C10orf2**	1	-0,130	0,470
GRWD1	1	-0,052	0,135	**FAM120A**	1	-0,017	0,859	**WDR1**	1	-0,002	0,357
DDX51	1	0,049	0,307	**DNM1L**	1	-0,024	0,082	**MAT2B**	1	-0,040	-0,099
MTR	1	0,023	0,401	**PRKAR2A**	1	-0,088	0,828	**MPC2**	1	0,214	-0,218
GIPC1	1	0,133	0,514	**SAMD11**	1	-0,251	0,874	**POLR1E**	1	-0,249	-0,623
YBEY	1	0,217	-0,628	**CPSF3L**	1	-0,140	0,114	**TMEM115**	1	0,089	0,896
HSF2	1	0,084	-0,578	**THOC5**	1	0,109	0,147	**BID**	1	-0,205	0,693
TRMT5	1	0,136	0,361	**WHAMM**	1	0,266	1,129	**SLC25A19**	1	-0,193	-0,078
RRN3	1	-0,031	-0,877	**YIPF5**	1	0,028	-0,115	**NPLOC4**	1	0,166	0,075
SAMM50	1	0,242	0,032	**RAB5C**	1	-0,107	0,057	**DNAJC14**	1	0,098	0,474
CD9	1	0,229	-0,158	**ZC3HC1**	1	-0,036	0,011	**TRIM65**	1	-0,228	0,223
TPM4	1	0,339	-0,128	**TBC1D4**	1	0,041	0,860	**IGF2R**	1	0,077	0,131
HEXB	1	0,208	0,083	**TOMM34**	1	0,148	-0,598	**TNKS2**	1	-0,034	0,149
ZRANB2	1	-0,093	-0,375	**CKS1B**	1	-0,247	-0,869	**DSCC1**	1	0,065	0,559
SMARCD2	1	0,041	0,180	**FTSJ2**	1	0,058	0,389	**KAT7**	1	0,017	0,439
PRPS2	1	0,012	-0,195	**C17orf89**	1	0,143	0,285	**FUBP3**	1	-0,130	0,168
VAMP3	1	0,078	1,460	**HRAS**	1	0,050	-0,086	**HGS**	1	-0,182	0,338
RBM23	1	0,096	-0,128	**PTRF**	1	0,054	0,540	**DNAJC9**	1	-0,118	0,364
ATL2	1	-0,064	-0,052	**LSG1**	1	-0,232	0,535	**DNTTIP2**	1	-0,164	-0,233
PKMYT1	1	-0,196	0,149	**WDR12**	1	-0,061	-0,123	**C1orf35**	1	0,274	0,539
WBP11	1	-0,098	-0,485	**HOXA10**	1	-0,193	-0,109	**PRIM2**	1	0,067	0,121
PSMD6	1	-0,036	-0,098	**SMG9**	1	-0,350	-0,205	**TES**	1	-0,076	-0,645
CASC3	1	-0,089	0,465	**HSPA4L**	1	-0,019	0,042	**TCTN3**	1	0,084	0,486
MCM3AP	1	0,228	0,089	**PGM2**	1	0,109	-0,102	**NUDT15**	1	0,096	0,298
NAMPT	1	0,068	-0,474	**AP1M1**	1	0,004	0,614	**BCKDHB**	1	0,449	0,564
CHMP2B	1	0,017	0,332	**HADH**	1	-0,095	0,352	**UIMC1**	1	0,078	0,640
AAMDC	1	0,232	-0,304	**FAM162A**	1	-0,223	0,054	**ZNF526**	1	-0,173	1,078
MICU2	1	-0,072	-0,202	**CAMLG**	1	-0,246	-0,261	**PPP3CA**	1	-0,008	0,994
UNC45A	1	0,034	0,704	**SEC23IP**	1	0,182	-0,178	**TMEM205**	1	0,144	-0,666
PLRG1	1	-0,116	-0,185	**BCKDHA**	1	-0,186	-0,150	**CAPZA2**	1	0,217	-0,287
BRI3	1	-0,080	0,843	**BABAM1**	1	-0,013	0,421	**CCNF**	1	-0,146	0,885
MRPL22	1	-0,124	0,476	**CARM1**	1	0,021	0,263	**ZNF221**	1	-0,051	0,104
SUMF2	1	0,080	0,205	**SPOP**	1	-0,305	0,554	**SUGP2**	1	0,025	0,322
SNX3	1	0,088	-0,374	**WDR34**	1	-0,153	-0,225	**DHX38**	1	0,275	-0,035
ABCC4	1	-0,113	0,911	**AARS2**	1	0,183	0,248	**GTF3C3**	1	0,071	1,009
FHL1	1	-0,114	0,163	**KCTD9**	1	-0,160	0,713	**IPO11**	1	-0,003	-0,261
PRPSAP2	1	-0,078	-0,042	**TMEM192**	1	0,066	-0,011	**CUL4B**	1	0,006	-0,337
LAMP2	1	0,134	-0,549	**RAB21**	1	0,172	0,553	**LMNA**	1	0,072	-0,043
ARL1	1	0,158	0,085	**ZNF329**	1	0,074	0,015	**UGGT1**	1	0,064	0,046
CMTR1	1	0,210	0,734	**RBX1**	1	-0,035	-0,342	**SUN2**	1	-0,104	0,774
MYEOV2	1	-0,091	0,223	**GINS2**	1	0,049	-0,247	**BTG1**	1	0,043	0,412
ZC3H14	1	-0,025	0,666	**MPLKIP**	1	0,022	0,222	**MAP1S**	1	-0,402	0,955
ZNF483	1	-0,102	0,478	**TTC3**	1	0,337	1,000	**WIBG**	1	0,015	0,640
CNPY2	1	-0,033	-0,338	**PRPF38A**	1	-0,030	-0,073	**PCNT**	1	0,116	0,314
ZNF234	1	0,036	0,385	**NELFCD**	1	-0,015	0,379	**OGFR**	1	-0,150	0,605
TP53BP2	1	-0,214	0,275	**CLCC1**	1	0,073	-0,535	**NT5C2**	1	-0,199	0,044
COPS2	1	-0,018	0,096	**CYP51A1**	1	-0,095	-0,758	**ALDH5A1**	1	0,414	0,768
ATP6V0B	1	-0,279	-0,240	**PCIF1**	1	-0,046	1,573	**AGO4**	1	0,015	1,020
CLN6	1	-0,207	1,070	**ARIH2**	1	0,169	-0,249	**IRF2BP1**	1	-0,167	0,309
TRMT2A	1	-0,137	0,570	**SMARCA1**	1	0,309	0,400	**QTRTD1**	1	-0,056	-0,014
TCEB3	1	0,039	0,309	**SNX1**	1	-0,012	0,438	**EXOC3**	1	0,051	0,739
PRR11	1	-0,049	0,353	**WARS**	1	0,049	-0,547	**GPN2**	1	-0,212	-0,026
IDE	1	-0,133	-0,034	**TOMM5**	1	-0,148	0,446	**WDR76**	1	0,068	-0,484
MPDU1	1	-0,068	0,183	**BAG2**	1	0,011	0,578	**SYMPK**	1	-0,154	0,535
MED27	1	-0,010	-0,894	**LUC7L**	1	0,043	0,710	**NLE1**	1	-0,135	0,413
ANAPC5	1	0,048	0,079	**OGT**	1	-0,074	0,172	**CIRBP**	1	0,016	-0,277
RHOT2	1	-0,340	-0,075	**IRF3**	1	-0,084	-0,224	**ZNF222**	1	-0,053	0,650
MAPK9	1	0,072	1,257	**PRKAA1**	1	0,012	0,167	**DCTN4**	1	-0,097	-0,171
ISOC1	1	-0,073	-0,474	**SNX6**	1	0,268	-0,645	**XBP1**	1	-0,262	-0,470
MAD2L1BP	1	0,036	0,151	**PPP2CB**	1	-0,112	0,103	**GOLPH3L**	1	-0,079	0,002
RNPS1	1	-0,161	-0,167	**HMGN4**	1	0,313	-0,046	**CALCOCO2**	1	0,040	-0,209
CEP55	1	-0,099	0,507	**WDR62**	1	-0,059	0,627	**EXOC2**	1	0,609	1,142
METAP1	1	-0,043	0,057	**APOPT1**	1	-0,472	-0,331	**OGFOD1**	1	0,129	-0,774
NFKBIB	1	-0,668	-0,968	**COMMD2**	1	-0,060	-1,830	**SCARB2**	1	0,016	0,280
NDUFAF4	1	-0,020	-0,602	**SEC62**	1	-0,305	0,396	**ZC3HAV1**	1	0,061	0,130
EXO1	1	-0,168	-0,325	**TFG**	1	-0,083	-0,347	**ACBD5**	1	0,278	0,451
VIMP	1	-0,066	0,467	**NANS**	1	-0,043	-0,128	**CDCA2**	1	0,028	-0,042
ZKSCAN1	1	-0,028	-0,189	**LIMS1**	1	0,000	0,300	**TMEM41B**	1	0,093	-0,161
UQCRB	1	0,278	0,026	**ARRB2**	1	-0,108	0,327	**NUDT9**	1	-0,087	0,580
VEZT	1	0,094	1,161	**ABCB10**	1	-0,011	0,513	**PHF23**	1	-0,208	0,975
CAMK1	1	0,008	0,214	**ZFP30**	1	0,007	0,199	**TAF8**	1	0,062	0,222

GCDH	1	0,198	0,696	**TNRC18**	1	-0,044	0,552	**KPNA1**	1	0,068	0,244
ZNF567	1	0,112	0,271	**MBD2**	1	0,022	1,351	**FERMT2**	1	0,098	0,017
CRLF3	1	0,035	-0,198	**ECSIT**	1	-0,287	0,034	**C9orf40**	1	0,115	1,288
BBC3	1	-0,087	1,149	**PPIG**	1	0,027	-0,024	**L3MBTL2**	1	-0,141	0,405
CHCHD4	1	0,161	0,320	**GNE**	1	-0,043	0,113	**FOXJ3**	1	-0,213	-0,033
CENPE	1	0,043	0,131	**TSPAN13**	1	0,058	-0,181	**ZNF431**	1	0,093	-0,539
RABGGTB	1	-0,089	-0,439	**MSMO1**	1	0,327	-0,580	**TJP1**	1	0,238	0,044
SIX1	1	-0,012	1,168	**UCHL5**	1	0,115	-0,042	**MRPS22**	1	-0,209	-0,308
METTL7A	1	0,631	0,130	**IRF2BP2**	1	-0,251	0,573	**DENND4B**	1	0,072	3,003
C2orf15	1	0,127	0,297	**RSRC1**	1	-0,236	0,055	**GRHPR**	1	-0,125	0,639
CTTN	1	0,151	0,157	**PPP1R12A**	1	-0,047	0,427	**RANBP3**	1	0,018	0,100
DDX10	1	-0,224	0,086	**KCMF1**	1	-0,075	0,764	**STK25**	1	-0,117	0,715
RAB14	1	-0,172	-0,145	**GBAS**	1	0,243	0,375	**SAMHD1**	1	0,066	-1,049
PSMA2	1	0,024	-0,119	**RGS16**	1	-0,175	0,248	**LPCAT1**	1	0,054	0,575
FAM213A	1	1,238	0,478	**GNA11**	1	0,079	0,753	**BLOC1S3**	1	-0,463	0,525
FUNDC1	1	-0,097	-0,416	**BCAT1**	1	-0,191	0,057	**CDC42SE1**	1	-0,052	0,891
ESCO2	1	-0,191	0,019	**PRCC**	1	-0,035	-0,253	**PGLS**	1	-0,067	0,714
KCTD5	1	-0,131	1,103	**ELP3**	1	-0,067	-0,221	**DNAJC22**	1	0,225	0,360
RPS27L	1	0,000	-0,259	**CFL2**	1	0,612	-0,395	**HIBADH**	1	0,123	0,306
C11orf68	1	-0,102	0,511	**UBE2G1**	1	-0,011	0,216	**PBRM1**	1	-0,037	0,198
CHEK1	1	0,044	-0,096	**FANCA**	1	0,122	-0,478	**FBXL15**	1	-0,195	2,219
SERF2	1	0,000	-0,807	**GTPBP1**	1	-0,119	0,547	**RPL22L1**	1	-0,587	0,144
ALAS1	1	-0,150	-0,066	**C14orf119**	1	-0,104	-0,105	**BFAR**	1	0,159	-0,172
PPP6R1	1	-0,349	0,273	**ARGLU1**	1	0,062	0,035	**ALCAM**	1	0,056	0,913
MED4	1	-0,124	0,434	**AGPAT5**	1	-0,093	0,042	**RABL6**	1	-0,217	0,739
NDUFAF1	1	0,018	-1,077	**TUFT1**	1	-0,158	-0,129	**SGPP1**	1	0,454	0,430
ABHD10	1	0,142	0,115	**METTL21A**	1	-0,015	0,123	**MNAT1**	1	0,267	0,452
UGDH	1	0,197	-0,044	**KIAA0907**	1	-0,190	-0,055	**NEDD1**	1	0,074	-0,289
BEX4	1	0,569	-0,909	**AFMID**	1	0,225	-0,284	**EMC2**	1	0,117	-0,431
ANLN	1	-0,017	-0,399	**PARPBP**	1	-0,071	0,306	**MIS18BP1**	1	0,055	0,205
C4orf29	1	0,097	0,570	**RMI2**	1	0,230	1,344	**C1orf109**	1	-0,182	-0,633
SNX17	1	0,191	-0,102	**SMPD4**	1	0,057	0,239	**PAXBP1**	1	0,321	0,315
TRAF3IP1	1	-0,057	0,307	**HAUS3**	1	-0,115	0,475	**AEBP2**	1	-0,229	0,295
COG8	1	0,149	-0,041	**PPID**	1	0,255	-0,117	**SCP2**	1	0,087	-0,420
BLM	1	-0,313	0,067	**PSME2**	1	0,119	-0,855	**THAP4**	1	-0,097	0,644
NDRG1	1	-0,336	-0,109	**HEATR3**	1	0,242	-0,378	**PTK7**	1	0,060	0,543
FBXL3	1	0,001	1,081	**RTN4IP1**	1	0,095	0,150	**CTSC**	1	-0,011	0,232
UBAP1	1	0,063	0,251	**CPT2**	1	0,111	0,464	**JAG2**	1	-0,181	0,478
COPS7A	1	-0,226	-0,403	**FKBP11**	1	-0,194	0,142	**COL14A1**	1	0,278	0,301
SKI	1	-0,207	0,988	**METTL16**	1	-0,297	0,610	**C9orf78**	1	0,062	-0,291
BRCA1	1	0,274	-0,026	**FAM221A**	1	0,247	-0,047	**MND1**	1	0,053	-0,477
ZNHIT2	1	-0,321	2,050	**MANBAL**	1	0,035	-0,095	**ITCH**	1	-0,148	-0,322
TRIAP1	1	-0,062	-0,822	**SPRYD7**	1	-0,129	-0,220	**FXN**	1	0,041	0,094
ERF	1	-0,817	0,214	**EXO5**	1	-0,044	0,646	**HIATL2**	1	-0,453	-0,026
CWC27	1	-0,141	-0,325	**PYCR1**	1	-0,166	-0,353	**ZNF543**	1	-0,080	-0,307
FAM96A	1	-0,031	-0,204	**DGCR8**	1	-0,132	1,283	**MKRN1**	1	-0,039	-0,320
PACSIN2	1	0,068	-0,348	**FAM177A1**	1	0,366	-0,035	**ZUFSP**	1	-0,007	0,155
INIP	1	0,006	0,479	**TGOLN2**	1	0,086	0,587	**DBN1**	1	0,155	0,135
CPD	1	-0,010	-0,188	**KPNA5**	1	0,183	0,567	**SLC35A4**	1	-0,195	0,904
TRIT1	1	-0,032	0,188	**ADPGK**	1	-0,031	-0,051	**KANSL3**	1	-0,065	0,356
H2AFY2	1	0,014	-0,446	**CYFIP2**	1	0,039	0,367	**APLP1**	1	-0,049	0,866
SUGT1	1	-0,129	0,426	**MRPL1**	1	-0,231	-0,228	**IQCC**	1	0,050	-0,066
ELF2	1	-0,068	0,341	**DHTKD1**	1	-0,121	-0,478	**PON2**	1	-0,037	0,880
HAUS2	1	-0,064	-0,155	**SHISA2**	1	-0,548	1,606	**LIG4**	1	0,035	0,607
TMA16	1	0,081	0,155	**GPC4**	1	-0,056	-0,137	**TLX1**	1	-0,026	2,046
COMTD1	1	-0,008	-0,475	**TTI1**	1	-0,065	0,024	**LRIG2**	1	0,123	0,623
GAS6	1	0,177	1,542	**PIAS1**	1	-0,087	0,206	**XRCC2**	1	0,095	0,320
SLC50A1	1	-0,359	-1,087	**EYA3**	1	-0,059	0,896	**NUPL2**	1	-0,041	0,249
ATF7IP	1	-0,129	-0,132	**APOE**	1	-0,111	-0,373	**MTOR**	1	0,018	0,544
NEO1	1	0,145	-0,053	**RBM34**	1	-0,082	-0,974	**XPNPEP3**	1	-0,040	-0,191
ATF6	1	-0,067	0,222	**MEAF6**	1	0,045	0,038	**LIN7C**	1	-0,042	-0,154
ALKBH2	1	-0,278	0,140	**ECHDC1**	1	0,000	0,041	**SLC31A1**	1	0,021	-0,104
ZNF766	1	0,082	-0,372	**RTCA**	1	0,105	-0,381	**TSPAN6**	1	0,439	-0,621
DYM	1	-0,094	0,239	**GPC3**	1	-0,262	-0,511	**NLN**	1	0,189	0,406
AGK	1	0,220	0,139	**ORC2**	1	0,044	0,363	**TMEM43**	1	0,048	0,387
TMEM65	1	-0,009	1,033	**ZNHIT6**	1	-0,089	0,275	**STK4**	1	-0,018	-0,010
GFER	1	-0,351	0,725	**FOXO3**	1	-0,064	0,109	**VPS16**	1	-0,319	0,324
SMG5	1	-0,326	0,572	**DUS3L**	1	-0,134	-0,195	**TRRAP**	1	0,021	0,057
GATAD1	1	0,031	0,353	**POLG**	1	-0,050	0,277	**ATXN2**	1	-0,033	0,803
NCDN	1	-0,067	0,622	**ZNF226**	1	-0,137	0,150	**ZDHHC6**	1	0,306	0,401
SGOL1	1	-0,088	0,557	**KNTC1**	1	-0,278	-0,065	**ZNF557**	1	-0,020	0,152
SRCAP	1	-0,078	0,357	**TUBGCP4**	1	0,004	-0,088	**AP2A1**	1	-0,032	-0,011
ALDH1A2	1	-0,315	0,457	**MTO1**	1	0,221	-0,315	**ZFAND5**	1	-0,255	0,117
CSK	1	-0,164	0,492	**ZNF544**	1	0,079	0,609	**TTC9C**	1	-0,043	-0,623
GRPEL1	1	0,084	0,215	**CDKN2C**	1	-0,173	0,092	**CECR5**	1	-0,077	0,800
MDM4	1	-0,191	0,118	**GFPT1**	1	0,038	-0,393	**BTBD2**	1	0,305	0,133
TAX1BP1	1	0,047	0,437	**NEIL3**	1	0,071	-0,478	**HERPUD2**	1	-0,083	0,687
GPBP1	1	-0,327	0,314	**TNRC6A**	1	0,237	0,250	**FAM73A**	1	0,173	0,287
DNA2	1	-0,022	0,218	**CORO2A**	1	0,051	1,331	**PDP2**	1	0,203	0,144
UBE3A	1	-0,063	0,188	**IFFO1**	1	-0,044	0,592	**ANXA11**	1	0,271	0,149

NIPBL	1	-0,356	-0,037	**ELOVL4**	1	0,190	-0,444	**KRTCAP2**	1	-0,236	-0,676
SNX11	1	-0,088	-0,194	**OBSL1**	1	0,087	0,917	**SMIM7**	1	0,006	-0,272
RELA	1	-0,309	0,576	**TBC1D24**	1	0,405	0,036	**TRIM11**	1	-0,027	0,628
DZIP1	1	0,283	0,429	**RNFT2**	1	0,144	0,312	**LRRC27**	1	0,055	0,317
SLC39A1	1	-0,183	-0,846	**ZNF136**	1	-0,052	0,290	**ERCC3**	1	0,021	0,320
PLEKHA2	1	-0,067	0,131	**WBP4**	1	0,128	1,139	**MYH14**	1	0,008	0,911
TRAF2	1	-0,440	0,111	**HEATR6**	1	-0,184	0,907	**LZIC**	1	-0,083	-0,264
EXOC4	1	0,180	0,488	**PSMD9**	1	0,059	-0,256	**STRIP1**	1	0,027	0,156
GMPR2	1	0,273	0,249	**DDX47**	1	-0,033	0,549	**SHOC2**	1	-0,051	-0,021
ZNF639	1	-0,424	-0,061	**SNTB1**	1	0,191	0,613	**SRBD1**	1	-0,005	0,569
CDK9	1	0,038	0,016	**UBE2J2**	1	0,007	-0,013	**DUS1L**	1	-0,154	0,489
DIS3L	1	0,116	-0,469	**THAP6**	1	0,287	0,378	**UGP2**	1	0,203	0,612
THAP5	1	-0,006	-0,051	**TRIM37**	1	0,081	0,348	**PODXL**	1	0,221	0,625
NCKAP1	1	-0,053	0,056	**NRBP1**	1	0,077	-0,114	**BCL7A**	1	-0,148	0,034
PSMA6	1	-0,037	-0,273	**SNAPC5**	1	0,067	-0,097	**DVL2**	1	-0,099	0,116
CDR2	1	0,143	0,034	**NFATC3**	1	0,019	0,321	**OCRL**	1	-0,106	-0,256
CAPN7	1	0,081	-0,180	**MAPK8IP2**	1	-0,270	0,110	**MED9**	1	-0,065	0,842
CEP170	1	0,094	-0,009	**SSU72**	1	-0,006	-0,720	**COG2**	1	-0,139	-0,041
BAMBI	1	0,048	0,545	**KRTAP19-1**	1	-0,721	0,000	**PIGP**	1	0,487	0,111
SMIM4	1	0,062	-0,612	**COQ7**	1	0,096	-0,327	**RIMS4**	1	-0,246	1,241
LONP2	1	0,225	-0,431	**ZNF302**	1	0,228	-0,393	**PEX6**	1	0,211	0,603
RAB5A	1	-0,077	-0,107	**MAP7**	1	0,372	0,153	**ZNF638**	1	0,066	0,267
PRNP	1	0,059	-0,518	**CEP85**	1	0,131	-0,202	**CENPA**	1	-0,095	0,292
ETFDH	1	-0,062	-0,027	**WDR35**	1	-0,069	0,406	**NPC1**	1	-0,210	-0,298
ARIH1	1	0,062	0,098	**ANKRD28**	1	0,032	0,701	**MAP2K7**	1	0,022	-0,315
IFIT5	1	-0,017	0,277	**GALNT7**	1	0,122	0,232	**ZSCAN29**	1	-0,013	0,361
DEAF1	1	-0,384	-0,776	**LASP1**	1	-0,039	0,204	**ANKZF1**	1	-0,089	0,023
INTS2	1	-0,001	-0,154	**MAP3K7**	1	0,110	0,757	**EED**	1	-0,220	0,573
AMACR	1	0,217	0,873	**DCAKD**	1	0,216	1,041	**EVI5**	1	0,162	0,107
TM2D1	1	0,109	-0,060	**SCO2**	1	-0,071	-2,045	**FBXO11**	1	-0,047	-0,008
HERC4	1	0,107	0,211	**NR2C2**	1	-0,143	0,380	**PCSK6**	1	-0,139	0,624
CDC73	1	-0,032	-0,412	**EMP2**	1	-0,153	0,160	**APOL2**	1	-0,129	-0,453
TOB1	1	-0,045	-0,897	**CASC5**	1	-0,395	0,153	**RBM17**	1	0,101	0,210
RAB4A	1	0,076	0,983	**PRCP**	1	0,273	-0,208	**FBXO9**	1	0,090	-0,231
MYEF2	1	0,533	0,510	**GUCD1**	1	0,028	0,182	**SIMC1**	1	0,029	0,142
GMPPB	1	-0,286	0,920	**TOX4**	1	0,007	-0,482	**B4GALT3**	1	-0,122	1,258
PROSC	1	0,010	0,177	**FIBP**	1	-0,174	0,074	**BUD13**	1	0,081	0,423
C16orf62	1	0,325	0,130	**DUSP1**	1	-0,094	-0,087	**EXT2**	1	-0,091	-0,372
MARK3	1	-0,111	0,332	**CARS2**	1	0,019	0,171	**KIF7**	1	0,077	0,651
OSER1	1	-0,203	-1,098	**MRPL50**	1	0,092	-0,252	**CNKSR3**	1	0,091	0,132
HTT	1	-0,102	0,274	**PHLDB3**	1	-0,124	0,240	**QSOX1**	1	0,191	-0,299
HDAC3	1	0,078	0,272	**MFSD11**	1	-0,197	0,208	**UBXN7**	1	-0,382	0,294
FIGNL1	1	-0,213	-0,267	**RAB34**	1	-0,116	-0,288	**RNASEH2B**	1	-0,208	0,045
KIAA1429	1	-0,010	0,078	**INTS5**	1	0,026	0,612	**MKLN1**	1	-0,219	-0,222
ARNT	1	-0,076	0,368	**TGFBR1**	1	0,000	0,756	**KANK2**	1	0,083	-0,006
RBM4	1	-0,019	2,407	**RHNO1**	1	0,112	-0,517	**CYB5D1**	1	-0,204	1,386
LMO4	1	-0,410	-0,324	**TMEM106C**	1	0,020	-1,056	**ZNF74**	1	-0,052	0,659
NFS1	1	-0,100	-0,087	**GCLC**	1	-0,010	0,220	**VPS53**	1	-0,091	0,120
ERLIN2	1	-0,077	0,039	**IRAK4**	1	0,019	0,596	**C1orf52**	1	-0,024	-0,443
FECH	1	0,042	0,551	**TAF11**	1	0,163	-0,098	**ZNF655**	1	-0,129	-0,404
TXNL1	1	-0,311	-0,101	**ZNF7**	1	-0,024	-0,157	**LYRM4**	1	-0,007	-0,388
PANK4	1	-0,106	0,717	**TOR3A**	1	-0,132	-0,201	**AGPAT2**	1	-0,099	0,510
TBC1D10B	1	0,079	0,095	**MKS1**	1	0,131	0,786	**THAP11**	1	0,054	0,781
SNX14	1	0,301	0,149	**SLC25A4**	1	0,058	-0,221	**FBXO18**	1	0,148	0,264
HOOK1	1	-0,444	0,104	**PPP1R35**	1	0,224	-1,223	**MICALL1**	1	0,050	0,131
GOLIM4	1	0,006	0,085	**SULF2**	1	0,037	0,209	**SIK2**	1	-0,194	0,162
HINT3	1	0,080	-0,021	**KIF15**	1	-0,179	-0,180	**TGDS**	1	-0,025	-0,083
GSK3A	1	-0,143	0,043	**TRIM4**	1	0,044	0,045	**ARHGAP17**	1	0,247	0,164
GGA1	1	0,038	0,077	**CD55**	1	-0,145	-0,316	**SUV420H2**	1	-0,223	0,128
PACSIN3	1	-0,211	1,839	**C1orf131**	1	0,301	-0,010	**SNAP47**	1	0,002	-0,235
EGFL7	1	-0,308	-0,067	**POT1**	1	-0,085	-0,008	**CASC4**	1	0,115	-0,062
ZNF687	1	-0,095	0,624	**ISG20L2**	1	-0,021	-0,506	**KREMEN1**	1	0,159	-0,198
TBCD	1	-0,229	0,381	**PKN3**	1	-0,155	-0,228	**LCLAT1**	1	0,192	-0,027
WEE1	1	-0,189	0,018	**SNAP29**	1	0,000	0,501	**F2R**	1	0,321	0,249
TNFRSF1A	1	0,241	0,512	**RPS6KA3**	1	0,009	0,041	**STAT5B**	1	0,051	0,330
R3HCC1L	1	-0,258	0,090	**LRBA**	1	-0,200	0,134	**ZNF780B**	1	0,046	-0,114
FRA10AC1	1	0,242	0,837	**RAD1**	1	-0,065	-0,011	**GID4**	1	-0,135	0,795
MYCBP2	1	-0,111	0,902	**RDH11**	1	0,343	0,018	**ATP6V0A2**	1	0,114	0,358
COL6A1	1	0,310	0,285	**DDB2**	1	0,207	-0,022	**ZNF24**	1	-0,100	-0,402
ZNF829	1	0,041	-0,026	**AGRN**	1	0,299	0,211	**EID1**	1	0,196	2,552
GNPDA1	1	-0,038	-0,256	**SIN3B**	1	-0,052	0,550	**POLR3D**	1	0,293	-0,444
GUCY1B3	1	0,049	0,700	**TAF5**	1	-0,063	-0,336	**MAVS**	1	0,189	-0,278
CCDC12	1	-0,070	0,666	**ALDH3A2**	1	-0,052	0,174	**CHST12**	1	-0,149	1,157
PUS7L	1	0,119	-0,231	**TARSL2**	1	0,144	0,003	**DVL3**	1	-0,186	0,581
SCFD1	1	0,099	-0,314	**C1orf123**	1	-0,223	0,290	**SLC27A4**	1	0,010	0,026
TMEM183A	1	-0,087	1,130	**FKBP5**	1	0,331	0,210	**MB21D2**	1	-0,263	0,954
PCNP	1	-0,020	-0,789	**KIAA0100**	1	-0,041	0,515	**VPS41**	1	0,026	0,650
ARID3A	1	-0,344	0,943	**SGK3**	1	0,076	0,383	**PCDHGC3**	1	0,317	0,654
SMARCA2	1	0,054	0,418	**TM2D2**	1	0,369	0,806	**WDR48**	1	-0,142	0,123
CCDC23	1	-0,082	2,879	**FZD6**	1	0,154	0,612	**C7orf50**	1	0,184	0,338

DOCK4	1	-0,050	0,242	**HAPLN3**	1	0,319	2,719	**AGO2**	1	0,093	0,687
NOP9	1	0,260	0,264	**ARHGAP11A**	1	0,132	-0,623	**RCCD1**	1	0,590	0,188
PRMT3	1	0,150	0,087	**TRIM33**	1	-0,063	-0,167	**PARD6B**	1	-0,066	-0,544
ARFGAP3	1	0,069	-0,067	**MACROD1**	1	-0,149	0,657	**NUDCD3**	1	-0,006	0,621
USP47	1	-0,050	0,545	**PVR**	1	0,078	-0,506	**TMOD2**	1	-0,037	1,077
ARHGAP5	1	0,128	0,057	**NRDE2**	1	-0,141	-0,031	**TMEM9B**	1	0,009	-0,453
FSD1	1	-0,236	-0,716	**FAM20B**	1	-0,076	0,282	**KLHL5**	1	0,160	0,190
KIAA0355	1	-0,106	0,345	**ATM**	1	-0,191	0,108	**ZNF444**	1	-0,273	-0,231
CIZ1	1	-0,216	-0,227	**MSRB3**	1	-0,056	0,902	**RHOB**	1	0,050	-0,656
LSM14B	1	0,036	-0,065	**FANCE**	1	0,258	0,748	**TSEN54**	1	-0,255	-0,236
HOXA13	1	0,199	0,916	**NFE2L3**	1	-0,120	0,746	**PPM1E**	1	-0,185	-0,144
CUL5	1	0,096	0,054	**DTNBP1**	1	0,114	-0,014	**GTF2A1**	1	0,030	-0,645
IMPACT	1	-0,190	0,801	**SLC35G2**	1	0,024	-0,091	**LRRC58**	1	-0,003	0,015
BSDC1	1	0,252	0,850	**NBN**	1	-0,016	-0,699	**CHCHD5**	1	0,273	-0,295
EAF1	1	-0,303	0,525	**PSRC1**	1	-0,018	-0,304	**HMGCL**	1	0,198	0,040
COMMD10	1	-0,212	0,374	**SPIN1**	1	0,018	0,128	**LAMA5**	1	0,200	0,530
SH3GLB2	1	-0,077	0,137	**CCND3**	1	0,032	0,156	**IFT140**	1	-0,262	1,817
YIPF2	1	-0,179	-0,076	**NEDD4**	1	0,064	0,436	**NCOA7**	1	0,041	-0,456
LACTB	1	-0,208	-0,079	**C22orf39**	1	-0,092	-0,028	**F11R**	1	0,122	0,171
ANKRD27	1	0,156	-0,085	**IFRD1**	1	-0,378	-0,491	**TBK1**	1	-0,197	-0,653
TMEM41A	1	-0,206	-0,030	**ANGEL2**	1	-0,034	-0,342	**YKT6**	1	-0,172	0,294
INSM1	1	-0,354	0,846	**PIK3C3**	1	0,026	0,222	**EIF4E2**	1	0,078	-0,555
DCAF10	1	0,139	0,527	**SNUPN**	1	-0,121	-0,754	**FTO**	1	0,370	-0,268
C16orf87	1	0,182	-0,046	**EEF2K**	1	0,263	0,314	**CEP250**	1	0,051	0,458
NR2F1	1	-0,316	-0,261	**SPTSSA**	1	0,367	-0,236	**ZNF264**	1	-0,363	-0,082
MYO9B	1	0,326	0,932	**CMTM8**	1	0,099	0,588	**CAMKK2**	1	0,029	0,330
ZNF251	1	0,225	0,676	**ACAP2**	1	-0,416	0,441	**POC1A**	1	-0,030	0,254
ZNF568	1	-0,007	-0,448	**ZMYM2**	1	-0,069	-0,427	**ZNF232**	1	0,222	1,656
PROCR	1	0,055	-1,158	**RAB2A**	1	0,050	0,065	**FARS2**	1	0,065	0,627
FOXO1	1	-0,808	1,043	**ATG3**	1	-0,202	-0,255	**DOT1L**	1	-0,131	0,452
SFT2D2	1	0,067	-0,124	**ZMYND11**	1	-0,050	0,298	**MADD**	1	-0,250	0,453
EME1	1	0,305	0,555	**ZNF451**	1	-0,051	0,408	**FBXL19**	1	0,047	0,608
PUSL1	1	-0,204	-0,691	**SRPK2**	1	-0,127	-0,519	**SESN2**	1	-0,570	-0,797
USP24	1	-0,192	-0,226	**SLC6A6**	1	0,413	0,299	**DNAJC13**	1	0,526	1,568
NDE1	1	0,250	-0,360	**TRMT1L**	1	0,105	-0,162	**NRN1**	1	0,282	-0,302
SMIM12	1	0,049	0,111	**WASF2**	1	-0,088	0,159	**ARFGEF2**	1	0,022	0,114
RAD54B	1	0,070	0,718	**PUM2**	1	-0,174	-0,525	**ZC3H7A**	1	0,106	-0,449
GUCY1A2	1	0,076	2,015	**ZNF131**	1	-0,088	0,058	**H6PD**	1	0,182	0,115
GID8	1	-0,087	-1,479	**DDAH1**	1	-0,009	0,243	**TMSB4X**	1	0,100	-1,356
ZNF266	1	-0,039	-0,185	**ZFYVE21**	1	-0,079	0,202	**BORA**	1	-0,049	-0,457
ING3	1	-0,270	-0,141	**DHRS3**	1	-0,035	-0,340	**BLOC1S4**	1	0,163	-0,289
GON4L	1	-0,073	-0,268	**KAT6A**	1	-0,173	0,418	**SDC4**	1	0,155	-0,779
SNF8	1	0,004	-0,455	**SLC25A10**	1	-0,019	0,263	**ARHGEF7**	1	-0,045	-0,017
RPAP1	1	0,146	-0,094	**FBXO17**	1	0,112	0,760	**GOLGA5**	1	0,001	-0,802
RAB35	1	-0,162	-0,390	**TNFAIP8**	1	0,198	0,534	**XYLT2**	1	0,253	0,503
KIAA0319L	1	0,031	0,376	**LRP8**	1	0,016	0,089	**BTG2**	1	0,143	0,337
TRIB1	1	-0,155	0,032	**FMNL2**	1	-0,085	0,912	**ZNF772**	1	0,101	-0,439
PTGR2	1	0,516	0,238	**ACTR5**	1	-0,252	0,569	**NEK4**	1	0,040	-1,009
IFNAR1	1	0,167	-0,521	**MARK2**	1	-0,130	0,321	**PDE6A**	1	-0,224	0,123
TFDP2	1	-0,343	-0,060	**NUDT3**	1	0,000	0,017	**SLC35F5**	1	0,268	0,147
YEATS2	1	-0,300	0,135	**MYO5A**	1	-0,093	0,388	**AFF4**	1	-0,027	-0,267
INF2	1	0,086	0,337	**TCF3**	1	-0,263	-0,731	**TMEM243**	1	0,012	1,183
PIK3C2A	1	-0,160	-0,307	**KAT6B**	1	-0,061	1,116	**ARHGEF2**	1	-0,179	-0,344
RECQL4	1	-0,382	0,399	**CCNL2**	1	-0,266	-0,693	**PEX5**	1	-0,011	-0,319
ESRP2	1	0,479	-0,049	**SIKE1**	1	-0,174	0,024	**NEK6**	1	-0,001	1,271
CEP290	1	0,154	1,055	**MMS22L**	1	0,013	0,003	**USP12**	1	0,001	1,869
ATP6V1H	1	0,013	-0,726	**DNMT3B**	1	0,264	0,129	**AHCYL2**	1	-0,136	0,018
CASP3	1	-0,027	-0,947	**SALL2**	1	0,378	-0,086	**RNF216**	1	-0,129	0,347
DOPEY2	1	0,424	-0,079	**THADA**	1	0,009	0,099	**TAF5L**	1	-0,037	0,757
BRF1	1	-0,066	0,028	**CEP97**	1	-0,359	0,376	**NAPG**	1	-0,021	-0,055
RNF8	1	0,237	-0,243	**OXR1**	1	0,250	0,268	**FAM174A**	1	-0,230	0,041
ZNF35	1	-0,109	0,923	**SLC25A30**	1	0,186	-0,179	**PNKP**	1	-0,219	-0,004
B3GALNT2	1	-0,090	-0,248	**PDF**	1	0,348	-0,749	**TENM3**	1	-0,348	0,553
RBBP9	1	-0,053	-0,321	**POC5**	1	0,122	0,048	**NFYA**	1	-0,088	0,673
ATP8B2	1	0,133	0,374	**VRK3**	1	-0,101	-0,121	**TP53I13**	1	0,255	0,597
C12orf65	1	-0,086	0,450	**TEX2**	1	-0,103	1,240	**NBPF1**	1	-0,002	-0,045
SATB2	1	-0,419	0,509	**EFNB1**	1	-0,768	-0,069	**GPSM2**	1	-0,248	-0,124
VPS18	1	-0,030	0,377	**FAM208A**	1	0,142	-0,108	**MFSD3**	1	0,123	-0,524
RWDD2B	1	0,493	-0,688	**ANKRD13A**	1	0,115	-0,106	**ZMYM5**	1	0,178	-0,495
FDX1	1	0,031	-0,602	**CYB5A**	1	-0,171	0,274	**MBD1**	1	-0,266	0,448
ABI1	1	-0,220	-0,410	**PTPRA**	1	-0,228	0,412	**SNX7**	1	0,035	-0,245
PIK3R2	1	-0,139	0,744	**SELT**	1	0,027	0,980	**UPF2**	1	-0,173	-0,729
TPM1	1	0,243	-0,100	**CIC**	1	-0,081	1,018	**SH3GLB1**	1	-0,041	-0,783
FAM91A1	1	-0,176	0,451	**PRKAR2B**	1	0,245	0,563	**SCAP**	1	-0,123	0,361
XPO6	1	0,161	-0,488	**CENPC**	1	0,001	0,100	**PLD6**	1	-0,138	-0,167
HOXB2	1	0,535	0,439	**TSC2**	1	-0,264	0,305	**BCAP29**	1	-0,152	-0,065
E2F3	1	0,041	0,143	**POLR1D**	1	-0,042	0,473	**ARPP19**	1	-0,287	-0,323
ZNF77	1	0,292	0,314	**JUND**	1	-0,238	-0,032	**PAQR4**	1	-0,127	-0,702
ATP6V0E2	1	0,311	0,976	**NRSN2**	1	0,188	-0,099	**SLC25A15**	1	0,292	-0,176
UBOX5	1	-0,071	0,300	**C1orf174**	1	-0,071	-0,586	**YIPF6**	1	0,090	-0,159

SERPINB6	1	0,238	-0,563	**RPRD1A**	1	-0,136	0,063	**ZCCHC7**	1	-0,004	0,027
GSTCD	1	0,100	-0,558	**AGAP3**	1	-0,058	1,809	**JPH1**	1	-0,376	0,911
SUSD5	1	-0,188	0,321	**GPT2**	1	0,002	-0,434	**USP36**	1	-0,144	0,107
JMJD1C	1	-0,163	-0,013	**ZNF432**	1	-0,279	-0,463	**MRPL38**	1	-0,128	0,300
KIAA1715	1	0,013	0,615	**SMC6**	1	0,200	-0,730	**QSER1**	1	0,026	0,294
ARRDC4	1	-0,138	0,479	**TUT1**	1	-0,190	0,544	**ZFAND3**	1	-0,032	-0,425
BCL2L13	1	0,140	-0,047	**RUFY2**	1	-0,164	0,095	**ATG16L1**	1	-0,036	0,878
SUPT20H	1	0,115	0,667	**RHBDF2**	1	0,071	-0,033	**BRMS1L**	1	0,164	-0,776
STOM	1	0,100	-0,585	**RBM20**	1	0,081	0,654	**METTL9**	1	0,181	-0,370
MTMR4	1	0,060	0,288	**RSAD1**	1	-0,202	-0,154	**SS18**	1	-0,048	-1,103
CSNK1G2	1	-0,012	0,223	**ZFP36L2**	1	-0,296	-0,310	**TUB**	1	0,255	1,350
SLC38A10	1	0,091	0,847	**ERBB2IP**	1	0,117	-0,432	**SLC25A12**	1	0,241	0,178
DGCR2	1	-0,121	0,272	**RLF**	1	-0,117	-0,625	**KCTD10**	1	0,092	0,203
RCBTB1	1	-0,095	1,456	**MYB**	1	0,065	0,057	**KLHL12**	1	0,004	-0,345
EXTL3	1	-0,117	-0,261	**EP400NL**	1	0,124	-0,349	**GOLGA4**	1	-0,143	-0,156
TAB2	1	-0,034	0,311	**NF1**	1	-0,045	0,156	**KAT8**	1	0,050	-0,151
LRIG3	1	-0,002	-0,532	**FBXO42**	1	0,112	0,510	**VEGFB**	1	0,025	0,182
PTPN14	1	-0,074	-0,036	**ENTPD7**	1	0,052	0,390	**HPS5**	1	-0,240	-0,096
ATG5	1	-0,021	0,284	**ZHX2**	1	-0,039	1,667	**CRLS1**	1	-0,055	0,952
BAP1	1	-0,008	0,097	**MAN2C1**	1	-0,082	-0,195	**IRAK1BP1**	1	0,024	0,632
RGP1	1	0,015	0,969	**WNT5A**	1	-0,313	0,811	**EPT1**	1	-0,072	-0,709
RIPK4	1	0,204	0,270	**E2F7**	1	-0,041	0,424	**CTPS2**	1	0,278	0,340
PPAP2A	1	-0,019	-0,679	**NPTX2**	1	-0,225	-0,344	**TOP1MT**	1	-0,236	0,630
ATF1	1	-0,276	-0,676	**CACTIN**	1	-0,304	0,720	**TCF7L2**	1	0,273	-0,487
GDAP2	1	0,200	0,384	**MAPK14**	1	0,109	-0,664	**TBC1D7**	1	0,197	0,794
KLC4	1	0,215	0,365	**B4GALT5**	1	-0,216	0,014	**CDK13**	1	0,018	-0,255
FAM210A	1	-0,143	-0,433	**ISL2**	1	-0,396	-0,621	**ADIPOR1**	1	-0,047	-0,058
LSM10	1	-0,061	-0,070	**BLOC1S1**	1	0,205	-1,296	**ATP11B**	1	-0,216	-0,046
IP6K2	1	-0,082	-0,273	**LZTR1**	1	-0,057	0,673	**PTTG1IP**	1	0,484	-0,841
CEP78	1	-0,023	0,295	**RAP2C**	1	0,159	0,151	**DENND5B**	1	0,060	0,618
CEP72	1	-0,150	-0,665	**KANK1**	1	0,054	0,003	**MTMR6**	1	-0,170	-0,671
TAF2	1	-0,004	-0,378	**SLC35C2**	1	-0,133	0,394	**NUP62CL**	1	0,075	-0,771
MCFD2	1	0,014	-0,092	**CCDC127**	1	0,160	0,013	**CDC42EP4**	1	-0,270	1,995
MIER3	1	-0,256	0,574	**LRRC8E**	1	0,153	-0,488	**IFT27**	1	0,554	0,699
BAG4	1	-0,071	-0,473	**ATG12**	1	-0,242	-0,088	**HIBCH**	1	0,023	-0,352
ALMS1	1	-0,581	0,255	**ZNF480**	1	0,214	-0,759	**ARMC1**	1	0,140	-0,752
SPIRE1	1	-0,131	0,143	**AMPD2**	1	-0,091	0,079	**FAM131A**	1	-0,287	-0,391
SLC18B1	1	0,214	0,139	**PPCDC**	1	-0,405	-0,395	**HOXC6**	1	0,271	2,669
CPNE8	1	-0,173	-0,830	**BBS7**	1	0,009	-0,499	**CMTM6**	1	0,203	-0,765
CBR3	1	0,403	-0,744	**ZNF445**	1	-0,011	-0,456	**NFYB**	1	0,190	-0,545
ELOVL7	1	0,211	-0,654	**TGIF2**	1	-0,026	0,506	**FNIP1**	1	-0,090	0,350
WDR60	1	0,068	0,313	**ZNF397**	1	-0,192	-0,328	**C3orf38**	1	0,017	0,494
BLOC1S5	1	0,270	-0,180	**ANKRD40**	1	-0,066	-0,808	**PI4K2B**	1	0,053	-0,239
FAM53C	1	-0,242	-0,591	**TRIQK**	1	0,139	0,516	**RASSF8**	1	-0,081	0,269
PPP1R12B	1	-0,064	0,530	**KCTD2**	1	0,055	1,423	**LDOC1L**	1	-0,055	0,320
ZFYVE27	1	0,032	-0,246	**PAN2**	1	0,174	0,443	**ALG12**	1	0,087	1,006
MAN2A1	1	-0,179	0,031	**FIG4**	1	0,294	-0,021	**CCP110**	1	0,241	-0,371
OTUD4	1	-0,085	0,264	**TRAPPC13**	1	0,058	-0,101	**FAM118A**	1	-0,060	-0,189
PTPN12	1	-0,290	-0,222	**ARHGEF10**	1	-0,070	0,246	**SYK**	1	0,046	-0,798
SETX	1	-0,039	-0,046	**ZNF37A**	1	-0,244	0,397	**FZD3**	1	-0,317	-0,462
ARHGAP26	1	0,040	0,222	**BCR**	1	0,050	0,497	**CASC10**	1	0,378	0,589
HELZ	1	0,129	0,138	**C6orf120**	1	0,438	0,347	**SEC22C**	1	-0,033	-0,102
HPS1	1	0,007	1,096	**POLR3H**	1	-0,169	-0,674	**ACSL1**	1	0,276	-0,479
AK3	1	-0,132	-0,685	**TRIM23**	1	0,036	-1,062	**HAUS8**	1	-0,111	-0,866
CIT	1	0,086	0,180	**SMUG1**	1	0,127	-0,352	**CNOT8**	1	0,038	-1,224
CXXC1	1	-0,034	-0,479	**ZMAT3**	1	-0,105	-0,003	**PPP2R5A**	1	-0,140	-0,277
SNTB2	1	0,256	-0,167	**RAMP1**	1	1,071	-0,176	**PEX10**	1	0,022	1,779
AKAP13	1	-0,127	0,248	**KLHDC10**	1	-0,078	0,164	**ANKRD18A**	1	0,057	0,524
PEX16	1	-0,091	-0,199	**RFXAP**	1	-0,194	-0,094	**TOPORS**	1	-0,016	-1,043
CHPT1	1	0,031	-0,248	**NEK7**	1	0,056	1,591	**TMEM57**	1	0,216	-0,938
NSUN4	1	-0,109	0,033	**TMED3**	1	-0,246	-1,245	**FAM69B**	1	-0,028	1,056
KATNAL1	1	0,031	0,301	**LIN28B**	1	0,171	0,311	**FAN1**	1	0,187	-0,311
ATG4C	1	0,475	-1,136	**TMEM38B**	1	0,175	-0,327	**PRMT6**	1	0,057	-0,394
KLHL29	1	-0,006	1,459	**RAPGEF6**	1	-0,801	-0,524	**LRP12**	1	0,020	-0,302
HOXC11	1	0,191	3,349	**MTFR1**	1	0,037	-0,230	**AP1AR**	1	-0,026	0,308
DENND4C	1	-0,131	0,091	**ENTPD6**	1	0,122	-0,304	**ACTR3B**	1	0,410	0,179
LONRF3	1	-0,005	0,042	**EIF2AK4**	1	0,116	0,484	**JAM3**	1	0,110	-0,179
HPS4	1	0,047	0,569	**UPP1**	1	0,028	1,019	**ZBTB48**	1	0,017	-0,285
TMEM242	1	-0,206	0,235	**ZNF512B**	1	0,190	0,487	**C3orf58**	1	-0,115	-0,072
RREB1	1	0,133	1,368	**EHMT1**	1	-0,093	0,163	**CDON**	1	0,137	0,629
FYN	1	0,120	0,019	**NDEL1**	1	-0,098	0,163	**CSRP2BP**	1	0,043	2,500
LPL	1	0,361	1,294	**FAM160B2**	1	0,214	0,215	**CDADC1**	1	0,011	1,157
PALLD	1	0,290	0,105	**TBC1D9B**	1	-0,093	-0,066	**STX6**	1	0,118	0,579
VASP	1	-0,019	-0,171	**NR3C1**	1	-0,018	-0,116	**PCYT1A**	1	-0,308	0,029
ZNF12	1	0,184	-0,520	**FAM13B**	1	-0,224	0,223	**STXBP2**	1	0,144	0,233
METTL8	1	0,233	-0,061	**CDYL**	1	0,061	0,146	**PSEN1**	1	-0,131	-0,187
COX20	1	-0,041	0,280	**UGCG**	1	0,027	0,810	**ZNRF3**	1	-0,059	0,736
SCYL2	1	-0,119	0,128	**IQGAP3**	1	-0,096	0,002	**GAN**	1	-0,085	-0,135
C4orf3	1	0,467	-0,660	**FREM2**	1	0,150	1,057	**PSMG4**	1	0,037	-0,035
L3MBTL3	1	-0,025	-0,217	**KIAA1958**	1	-0,064	-0,153	**TNIP2**	1	-0,043	0,271

SOX9	1	0,217	0,937	**PLK4**	1	-0,058	-0,111	**ARHGAP21**	1	0,087	-0,466
VAV2	1	0,144	0,667	**TMCO3**	1	-0,168	0,183	**ANKRD26**	1	0,355	-0,876
GPATCH2	1	0,029	-0,212	**THAP3**	1	-0,305	0,929	**RABGAP1L**	1	0,109	0,081
PPAP2B	1	0,048	-0,508	**ZIK1**	1	0,023	-1,044	**DGKE**	1	0,026	-0,158
DNMBP	1	-0,267	1,249	**VPS39**	1	0,193	0,494	**RFNG**	1	-0,099	0,049
RAB3IP	1	-0,168	0,456	**CHST8**	1	-0,361	1,250	**FKBP15**	1	0,005	0,403
DNAJB12	1	-0,085	0,305	**BMPR2**	1	0,026	0,226	**ZBTB40**	1	-0,256	0,310
SPATA2L	1	0,084	0,220	**RHBDD1**	1	0,035	0,601	**CELF2**	1	-0,023	-0,102
LEPR	1	-0,051	-0,540	**MFSD2A**	1	-0,061	0,037	**RUNX1**	1	0,226	-0,021
ASAP2	1	-0,114	0,382	**RNF168**	1	-0,325	0,238	**RCAN3**	1	0,763	-0,309
GADD45B	1	-1,371	-1,965	**KMT2C**	1	0,074	0,090	**RAB11FIP4**	1	-0,372	-0,094
MVP	1	0,188	0,385	**SLC16A14**	1	0,049	-0,401	**HDHD2**	1	-0,061	0,104
MMAB	1	0,111	-0,784	**KLHL36**	1	0,293	1,059	**CNOT7**	1	-0,013	-0,054
FBXO3	1	-0,063	-0,129	**TMEM177**	1	-0,023	-0,110	**CEP128**	1	-0,019	0,203
TBC1D5	1	0,372	0,397	**CHCHD6**	1	-0,110	-0,079	**PAPD4**	1	0,044	-1,718
CDS2	1	-0,046	-0,430	**FBXO46**	1	-0,184	-0,292	**LSAMP**	1	1,487	-0,254
RAB23	1	-0,027	-1,115	**IFNAR2**	1	0,169	0,063	**TBC1D9**	1	0,150	-0,047
FAM204A	1	-0,043	-1,194	**EYA4**	1	-0,085	0,688	**KIF5A**	1	-0,024	-0,343
FAM104A	1	-0,117	1,214	**PIP4K2A**	1	-0,150	0,273	**TTC39B**	1	0,124	-0,256
SIPA1L2	1	-0,335	0,009	**CREB3L2**	1	-0,067	-0,512	**MBTD1**	1	-0,016	-0,256
WDR78	1	0,482	0,511	**GALNT6**	1	0,401	-0,598	**PLA2G16**	1	1,025	-0,112
REXO1	1	-0,483	-0,076	**CCNG2**	1	0,085	0,695	**CDC42BPA**	1	-0,007	-0,274
MON1B	1	0,336	0,070	**ZFAND4**	1	-0,132	0,239	**ZRANB3**	1	0,048	-0,718
SLC16A2	1	0,461	0,857	**CBL**	1	-0,018	-0,313	**ZHX1**	1	-0,042	-0,125
ZNF346	1	0,287	0,137	**VPS37B**	1	0,011	-0,434	**INTU**	1	0,122	0,235
TTC28	1	-0,547	0,463	**SLC44A2**	1	-0,028	-0,833	**SLC35A1**	1	-0,021	1,977
GIGYF1	1	-0,236	0,523	**DPY19L1**	1	-0,065	-1,081	**KIAA0895**	1	-0,256	-0,146
MAP3K1	1	0,012	-0,206	**ITGAE**	1	0,130	-0,131	**TMEM246**	1	0,131	0,027
PALD1	1	0,124	-0,198	**RAB40C**	1	-0,448	0,475	**SLC12A4**	1	0,364	-0,040
CCDC113	1	0,080	0,972	**APEX2**	1	0,547	-1,265	**MAGI3**	1	-0,195	0,343
COQ2	1	-0,071	-0,116	**RBM33**	1	-0,170	0,408	**PTPN9**	1	0,033	-0,096
PPP6R2	1	-0,047	0,131	**BRF2**	1	-0,138	-2,027	**ZNF696**	1	-0,228	-0,083
ELMO2	1	0,296	0,244	**CCDC25**	1	0,140	-1,490	**DCPS**	1	-0,227	-0,776
WHSC1L1	1	-0,072	0,335	**INPPL1**	1	0,294	-0,022	**ACVR2A**	1	0,040	-0,385
PCSK5	1	-0,243	0,939	**KLF16**	1	-0,191	-0,037	**TTL**	1	0,078	0,004
ZNF420	1	0,041	-1,195	**TLDC1**	1	0,310	-0,104	**ZNF783**	1	0,116	-0,222
PYGO2	1	-0,086	1,204	**FUZ**	1	-0,010	-1,263	**EXT1**	1	-0,082	0,817
ENC1	1	-0,096	-0,567	**KIF3B**	1	-0,065	-0,385	**MAD1L1**	1	-0,083	-0,890
ACSF3	1	0,121	0,324	**UBXN2B**	1	-0,130	-0,291	**FBXW4**	1	0,257	-0,369
EPHA3	1	-0,028	0,077	**BRWD3**	1	0,618	0,454	**ACVR2B**	1	-0,157	0,687
WASF1	1	-0,334	-0,326	**BRPF3**	1	0,270	0,423	**ALS2**	1	0,247	-0,237
ATG2B	1	0,052	0,331	**ZNF408**	1	-0,067	0,652	**KIAA1671**	1	0,107	0,176
UXS1	1	0,476	1,117	**DOCK9**	1	-0,102	1,266	**IMP4**	1	-0,234	-2,263
SLC2A4RG	1	-0,057	0,054	**TLE4**	1	-0,178	-0,007	**TMEM237**	1	-0,013	0,315
PPP2R5E	1	0,062	-0,294	**ATG4D**	1	-0,131	-0,080	**RAD54L2**	1	-0,079	0,320
FAM173B	1	0,031	-0,849	**CYTH2**	1	-0,072	-0,660	**SIL1**	1	0,119	-1,008
LPAR3	1	-0,046	0,747	**PDGFRL**	1	0,222	0,196	**MAGI1**	1	-0,174	0,956
ZNF511	1	-0,055	-0,767	**IL13RA1**	1	0,147	-0,718	**TRIM44**	1	0,059	-0,988
GPR107	1	0,257	-0,407	**ZNF623**	1	-0,035	-0,454	**PAG1**	1	0,165	0,286
ZNF805	1	-0,125	-0,976	**USP42**	1	-0,082	0,776	**TAPT1**	1	-0,198	0,419
LRRC45	1	0,096	-0,483	**PRMT2**	1	0,282	-0,119	**TSSC1**	1	-0,103	1,402
USP32	1	0,025	1,327	**C10orf88**	1	0,293	-0,154	**CEP120**	1	0,065	-0,308
MRGBP	1	0,008	-0,351	**ATP1B2**	1	-0,720	-0,724	**WWTR1**	1	0,211	-0,163
CCDC88A	1	-0,075	-0,403	**FMN2**	1	0,051	1,606	**LARP6**	1	0,326	0,788
TRIB2	1	0,124	-0,096	**ITFG3**	1	0,000	-0,015	**BCL11B**	1	0,020	0,645
ZNF268	1	-0,175	-0,659	**NCK1**	1	-0,126	0,264	**E2F6**	1	-0,060	-0,550
SIX5	1	-0,066	0,005	**CDS1**	1	0,092	-0,079	**ST6GALNAC4**	1	-0,723	1,438
PPP3R1	1	-0,076	-0,903	**PAPD5**	1	0,244	0,114	**SCRN1**	1	0,273	-0,920
PCNXL4	1	0,073	0,363	**KLHL14**	1	0,005	1,094	**REEP3**	1	0,336	-1,347
FAM63A	1	0,050	-0,286	**WRAP73**	1	-0,236	-0,241	**MUS81**	1	-0,176	-0,863
SCRN2	1	0,298	-1,380	**RC3H2**	1	0,439	0,079	**RNF169**	1	0,004	-0,363
AP3S2	1	-0,095	-0,211	**GATA4**	1	0,038	-0,340	**NPPC**	1	0,289	-0,565
SMARCE1	1	0,127	-0,380	**NCKIPSD**	1	0,058	-0,423	**PRKG1**	1	-0,215	-0,305
C5orf28	1	-0,104	-0,762	**TMEM167A**	1	-0,037	-0,106	**SCMH1**	1	-0,054	0,727
PPP1R13B	1	0,047	0,356	**AGO1**	1	0,164	0,401	**OTUD6B**	1	-0,012	-0,439
SLC25A46	1	0,169	0,815	**MRPS6**	1	0,400	0,251	**MAX**	1	-0,156	-0,221
KIAA0930	1	0,136	0,023	**IRF2BPL**	1	0,186	-0,156	**MYO9A**	1	0,130	0,016
NUDT2	1	0,087	-0,943	**ANKRD49**	1	0,268	0,893	**MANEA**	1	0,112	-0,092
ADCY7	1	0,177	0,055	**LONRF1**	1	0,173	0,017	**POC1B**	1	0,119	-0,856
OPN3	1	-0,347	-0,397	**CHST11**	1	0,281	0,081	**ENPP5**	1	0,673	0,738
MAPK8	1	-0,067	-0,239	**PRDM2**	1	0,005	-0,053	**GZF1**	1	-0,007	-0,143
SASH1	1	0,024	0,214	**PEAK1**	1	-0,143	-0,138	**HOMER1**	1	-0,204	0,269
PRPF39	1	-0,061	-1,138	**FBLN1**	1	0,317	1,112	**KAZN**	1	-0,111	0,335
BTBD7	1	0,073	0,141	**ZNF471**	1	0,096	1,095	**ABCB6**	1	-0,123	-0,304
UNC5B	1	-0,330	0,092	**B4GALT4**	1	0,170	0,198	**LRP5**	1	0,003	-0,612
G2E3	1	0,231	-0,218	**CA12**	1	-0,195	0,778	**TIMM21**	1	-0,049	-1,324
LMX1B	1	-0,231	-0,516	**MTFR1L**	1	0,045	-0,993	**AXIN1**	1	0,193	1,221
TOB2	1	-0,122	-0,762	**CACUL1**	1	-0,001	-0,422	**SLC9A1**	1	0,182	0,131
TBC1D1	1	0,239	0,607	**DMPK**	1	-0,262	-0,030	**LRIG1**	1	-0,083	-0,176
PDPK1	1	-0,537	-0,839	**HS3ST3B1**	1	-0,196	-0,400	**DUSP4**	1	-0,179	0,951

PTPRU	1	0,369	-0,282	**PRKCH**	1	0,252	0,151	**GSTZ1**	1	0,219	-0,338
ZBTB37	1	0,080	0,658	**VCPIP1**	1	-0,109	-0,696	**USP20**	1	-0,145	-1,055
APBB2	1	-0,211	0,425	**SFMBT1**	1	-0,185	0,258	**TRAK1**	1	0,098	-0,041
USP45	1	0,189	0,232	**TYW3**	1	-0,009	-0,417	**C15orf61**	1	-0,293	-1,417
HDDC3	1	0,132	-1,472	**UVRAG**	1	-0,059	0,287	**SCN9A**	1	0,004	-0,145
SIRPA	1	-0,104	-0,591	**ELK1**	1	-0,136	1,129	**TMEM64**	1	-0,033	0,416
MECOM	1	-0,210	-0,259	**JMY**	1	-0,528	-0,706	**FAM195A**	1	-0,138	-1,170
REV1	1	0,183	0,218	**MALT1**	1	-0,043	-0,913	**C15orf52**	1	0,549	1,621
RNF26	1	-0,099	0,512	**NKTR**	1	-0,060	-0,275	**FAS**	1	0,191	-0,838
CDK8	1	-0,100	-0,708	**FAT4**	1	-0,308	0,643	**AK4**	1	-0,038	-1,354
ULK1	1	-0,243	0,058	**COMMD6**	1	0,098	-0,412	**ARNTL2**	1	0,041	-0,939
PXDN	1	0,278	0,629	**GMCL1**	1	-0,010	-0,984	**RAB8B**	1	0,310	-1,452
PML	1	-0,082	-0,408	**VSIG10**	1	0,562	0,257	**CHN1**	1	0,071	-0,567
FRS2	1	-0,193	0,647	**PROS1**	1	0,209	0,226	**SDK1**	1	0,389	0,532
SLC25A36	1	-0,099	0,925	**BTBD11**	1	-0,440	0,354	**ZNF48**	1	-0,003	-1,593
SCLY	1	-0,026	-0,549	**ZNF324**	1	-0,264	-0,677	**AGAP1**	1	-0,134	1,132
SDK2	1	0,180	0,855	**NEDD4L**	1	0,061	-0,095	**EDEM1**	1	0,079	0,125
TCF12	1	-0,156	-0,120	**SERP2**	1	-0,085	0,979	**RRAGD**	1	0,352	-0,449
TATDN2	1	-0,024	-0,926	**FBXW8**	1	0,223	-0,808	**TMEM189**	1	0,183	0,111
ARHGEF6	1	0,270	-0,125	**ARHGAP32**	1	-0,177	1,044	**UST**	1	0,062	-0,108
DLG3	1	0,211	-0,420	**PLCL2**	1	-0,113	-1,096	**GPATCH2L**	1	-0,017	0,015
TGIF1	1	-0,150	0,196	**KCNJ14**	1	-0,264	-0,481	**SVIL**	1	0,373	-0,454
CDKL2	1	0,039	1,991	**SZRD1**	1	-0,094	-1,390	**CAAP1**	1	0,056	-1,614
CYLD	1	0,063	0,009	**TDRD3**	1	-0,081	-1,117	**TMEM164**	1	0,265	-0,304
PLEKHA1	1	-0,096	-0,696	**RAVER2**	1	-0,047	-0,428	**RADIL**	1	-0,321	0,200
C3orf52	1	0,109	1,290	**UCP2**	1	0,062	-1,826	**FAM161B**	1	-0,155	-1,306
SPRED1	1	0,070	0,006	**ANXA4**	1	0,401	-0,808	**RBM18**	1	-0,152	-0,996
SRC	1	0,126	0,143	**RBAK**	1	-0,112	-0,725	**PLCG2**	1	0,205	-0,174
USPL1	1	-0,171	-0,737	**ERCC6L2**	1	-0,014	0,805	**METTL10**	1	-0,224	-1,135
GNA13	1	-0,050	-0,873	**DPP7**	1	-0,326	2,562	**FBXO34**	1	-0,067	-0,338
CUX1	1	-0,141	0,255	**ACOT8**	1	0,005	-0,994	**SYNE1**	1	0,016	0,144
EVI5L	1	0,334	-0,196	**C9orf69**	1	-0,106	1,921	**TBC1D16**	1	0,362	1,576
NFIL3	1	-0,138	-0,558	**ZNF780A**	1	-0,186	-1,262	**ZNF784**	1	-0,130	2,660
EMB	1	0,038	-0,762	**GPRC5A**	1	0,315	-0,682	**KITLG**	1	-0,038	-1,047
FEZ1	1	0,086	-0,481	**MCF2L**	1	0,053	0,730	**UBP1**	1	-0,046	1,212
AGPAT9	1	0,217	-1,431	**PKP4**	1	-0,062	0,104	**MANBA**	1	0,080	-0,519
HMGA2	1	0,482	-0,123	**AAK1**	1	0,165	0,209	**ATP8A1**	1	-0,156	1,032
RSBN1	1	-0,195	-0,841	**FAM172A**	1	-0,180	-0,173	**TPK1**	1	0,381	0,604
RNF213	1	0,188	-0,102	**TRIM2**	1	0,380	-0,485	**ARHGAP22**	1	0,128	-0,077
GET4	1	-0,096	-1,582	**SUCO**	1	-0,037	-0,699	**PRDM10**	1	0,047	-0,356
STAMBP	1	0,215	-1,023	**USP28**	1	0,187	-1,262	**TRIM56**	1	0,033	-1,281
VEGFA	1	-0,357	0,039	**AFTPH**	1	0,065	-0,867	**TGFBR2**	1	0,056	-0,263
CROCC	1	0,066	-0,100	**ZDHHC5**	1	-0,042	-1,572	**CTDSPL**	1	-0,143	0,500
FAM126A	1	-0,075	-0,221	**GNG12**	1	0,193	-1,273	**ADRA2C**	1	-0,163	0,882
TMEM8B	1	-0,081	-0,316	**CRTC3**	1	0,271	0,306	**TIAM2**	1	0,140	0,387
SERTAD4	1	-0,010	0,203	**PHF2**	1	-0,304	-0,943	**ARL5A**	1	-0,137	0,345
SGMS1	1	-0,091	1,221	**AMOTL2**	1	0,200	2,040	**WDFY2**	1	-0,221	0,689
NYNRIN	1	1,020	0,905	**NACC2**	1	0,240	1,112	**PRSS12**	1	-0,071	-1,036
WDFY3	1	-0,029	0,323	**HOXB3**	1	-0,223	-1,409	**ST8SIA6**	1	-0,177	0,052
LAMTOR3	1	-0,144	-1,090	**MAPK8IP3**	1	-0,259	0,697	**ZDHHC23**	1	-0,009	-0,635
POU2F1	1	-0,084	-0,316	**ADCY1**	1	-0,131	0,544	**ZNF223**	1	-0,103	0,328
ISCU	1	-0,128	-0,536	**IQCE**	1	0,638	0,189	**TRAF3**	1	-0,149	-1,082
POU4F1	1	-0,006	0,762	**FZD7**	1	-0,137	-0,994	**CASZ1**	1	-0,221	-0,290
TMCC1	1	0,322	2,538	**SFMBT2**	1	0,054	-0,870	**MYD88**	1	0,476	-0,530
RAB22A	1	-0,047	-0,610	**TMEM56**	1	-0,268	-0,655	**CMTM3**	1	0,437	0,352
FEM1C	1	-0,147	-0,838	**NKD2**	1	0,337	-0,529	**EBLN2**	1	-0,018	-0,178
AKT1	1	0,137	-0,313	**ANK3**	1	0,026	0,441	**PPP1R9A**	1	-0,017	0,540
CMC2	1	0,305	-1,759	**LIPH**	1	0,090	-1,805	**KLHL42**	1	0,041	-1,202
DCBLD2	1	0,037	0,359	**TRPC1**	1	-0,172	0,041	**ADO**	1	0,089	-0,704
LMBR1L	1	-0,057	-1,103	**PIGC**	1	0,067	-1,376	**DGKI**	1	0,120	1,034
RNF103	1	0,145	-0,406	**COL4A6**	1	0,102	-0,168	**RAP1GAP2**	1	0,129	-0,355
PANK1	1	0,096	-0,508	**SMIM10**	1	0,489	-1,453	**CDH7**	1	0,531	-1,326
TBX2	1	-0,120	1,992	**CMTM4**	1	0,367	0,209	**SORBS3**	1	-0,120	0,325
HIC2	1	-0,060	2,018	**NECAB3**	1	-0,149	0,442	**ELK3**	1	0,312	0,886
NLRX1	1	0,773	1,348	**EIF4E3**	1	0,210	2,382	**OARD1**	1	0,083	-1,036
MTG1	1	0,258	-0,974	**MAP3K9**	1	-0,056	-0,643	**MPP3**	1	0,251	-1,445
MAP3K10	1	0,187	-0,232	**GOLT1B**	1	0,005	-1,678	**WDR27**	1	0,068	-0,322
SYNE2	1	-0,002	-0,225	**RNF44**	1	-0,183	-1,292	**MYO5B**	1	0,043	-0,115
MED13L	1	-0,083	-0,013	**SRP19**	1	0,381	-1,702	**TMTC1**	1	0,200	0,006
GORASP1	1	0,283	0,788	**C17orf59**	1	-0,039	-0,709	**NLGN2**	1	0,066	-0,248
SNX18	1	-0,098	0,922	**ASAP1**	1	0,036	-0,465	**NRIP1**	1	-0,052	-1,404
KLHL22	1	0,189	-0,365	**FAM19A5**	1	0,328	2,238	**ZNF385B**	1	0,523	2,673
ZNF536	1	-0,154	0,414	**PPM1F**	1	0,221	-1,460	**FAM168A**	1	-0,119	-0,323
C12orf75	1	0,138	0,963	**ZNF518B**	1	0,000	0,307	**TCEA2**	1	0,294	-0,949
TMEM39A	1	-0,105	0,310	**EXD3**	1	-0,117	0,408	**ASB1**	1	0,185	-0,967
CEP63	1	0,422	0,193	**DDIT3**	1	-0,809	-3,319	**HSF5**	1	0,732	0,000
FAM8A1	1	0,238	-0,846	**ZGPAT**	1	-0,038	0,872	**RNF11**	1	-0,048	-0,955
L3MBTL4	1	0,335	-0,146	**C15orf41**	1	-0,181	-0,541	**AZI2**	1	-0,033	-2,279
SLCO5A1	1	-0,093	0,039	**ZDHHC2**	1	0,230	-0,563	**CALML4**	1	0,121	2,734
ZNF782	1	-0,053	0,818	**ANKIB1**	1	0,328	0,072	**ZNF248**	1	0,055	-1,473

TMEM18	1	0,028	-1,084	**ABCB4**	1	0,811	0,046	**TDRD6**	1	-0,074	2,661
SULT4A1	1	-0,230	0,600	**TANC2**	1	-0,070	-1,260	**PRPF40B**	1	-0,164	-1,941
KCNQ5	1	-0,028	-0,660	**FGF13**	1	0,287	-1,609	**LATS2**	1	-0,311	-1,466
P4HTM	1	-0,043	-1,025	**OLFM2**	1	0,458	-0,629	**MPND**	1	-0,433	-5,735
CTNNBIP1	1	0,742	0,884	**ING2**	1	0,078	-1,019	**SPRY4**	1	0,445	-0,941
TMEM55B	1	0,536	-1,902	**SH3BP5L**	1	0,163	0,729	**TMEM178B**	1	-0,294	-0,994
SSC5D	1	0,203	0,681	**TPST1**	1	0,173	-2,160	**PID1**	1	0,027	-2,021
PAIP2B	1	-0,183	-1,003	**MFSD6**	1	0,312	-1,932	**DNAH5**	1	-0,151	-2,166
FAM214A	1	0,003	-0,910	**KLF9**	1	-0,110	-1,371	**IPO4**	1	0,146	-5,459
SNX25	1	-0,056	-1,192	**CDX2**	1	-0,430	-2,248	**TMEM132D**	1	0,000	0,000
IQCJ-SCHIP1	1	-0,236	-2,489	**SLC35G1**	1	-0,052	-2,558	**HIST1H3D**	1	-0,224	0,000
PPM1J	1	-0,092	1,734	**EPHB1**	1	0,725	0,343	**ATP5I**	1	0,403	0,000
B4GALNT3	1	0,134	-0,358	**ATXN1L**	1	0,082	-0,732	**CTNNA3**	1	0,569	0,000
FBF1	1	0,302	0,000	**SEMA4D**	1	0,317	-1,039	**C8orf58**	1	0,030	0,000
CDC14B	1	0,010	-0,364	**ZNF407**	1	-0,297	-1,040	**MRPL12**	1	0,039	0,000
TC2N	1	0,012	-1,400	**RAB11FIP2**	1	-0,029	-0,932	**CCDC71L**	1	-0,208	0,000
PBX3	1	-0,112	-0,797	**KCNQ2**	1	-0,174	-0,481	**DAPL1**	1	0,000	0,000
ARL4D	1	-0,192	-2,913	**CHIC1**	1	-0,132	-1,831	**ILK**	1	-0,046	0,000
KMT2E	1	-0,244	-2,170	**MTMR7**	1	0,147	-2,006	**ACBD6**	1	0,006	0,000
ARNTL	1	-0,304	0,310	**TMEM74**	1	-0,503	-1,134	**PMEPA1**	1	-0,617	0,000
PDE4D	1	-0,108	-0,088	**MFAP3L**	1	-0,375	4,177	**AURKC**	1	-0,583	0,000
UNC93B1	1	-0,005	-0,832	**PLEKHA8**	1	0,024	-0,306	**ZBTB34**	1	-0,175	0,000
BCL2	1	-0,150	0,134	**WSB2**	1	0,268	-2,065	**GFRA1**	1	0,262	0,000
FRMPD4	1	0,014	0,609	**VANGL2**	1	0,408	-1,974	**PLCXD2**	1	-0,317	0,000
EPHA5	1	-0,120	-1,198	**ZC3H10**	1	-0,093	0,262	**ADAMTS7**	1	0,550	0,000
FGF9	1	0,124	-2,274	**DNAJB2**	1	-0,359	-0,444	**THEGL**	1	1,104	0,000
C1orf159	1	0,110	-0,442	**CTSH**	1	0,682	-0,802	**KMT2B**	1	0,000	0,000
SESTD1	1	0,151	-0,983	**PCLO**	1	0,569	-0,322	**AC010642.1**	1	0,074	0,000
PDE8B	1	-0,153	0,441	**CHMP3**	1	0,141	1,323	**NDST2**	1	-0,046	0,000
BLCAP	1	-0,076	-1,489	**NTN4**	1	0,195	-1,213	**ATP6V0C**	1	-0,119	0,000
INSIG2	1	0,190	0,498	**REEP1**	1	-0,254	-0,963	**GPR149**	1	-0,823	0,000
ADAM19	1	0,621	3,621	**DMRT3**	1	-0,091	-0,151	**NDUFV2**	1	-0,060	0,000
CTXN1	1	0,142	-3,286	**ARHGAP19**	1	0,147	0,931	**C15orf38-AP3S2**	1	0,253	0,000
PDE5A	1	-0,019	-0,989	**WNT5B**	1	0,118	-2,341	**CDK14**	1	-0,433	0,000
PDGFA	1	0,113	-0,465	**PTPN21**	1	-0,068	0,641	**CEBPA**	1	0,255	0,000
USP44	1	0,296	-0,442	**TENM4**	1	-0,209	0,000	**CDR2L**	1	-0,124	0,000
MEX3B	1	-0,136	-1,194	**CELSR3**	1	-0,246	-1,978	**COX8A**	1	0,018	0,000
RIMKLA	1	-0,192	-1,743	**ZCCHC24**	1	0,205	-1,069	**ZBED6**	1	-0,072	0,000
TRAK2	1	0,011	-0,993	**RORA**	1	-0,004	-1,156	**LRRC24**	1	-0,639	0,000
ETV5	1	0,093	-2,551	**PRKCE**	1	-0,122	-2,250	**TMEM251**	1	-0,025	0,000
STARD13	1	0,029	-0,343	**PKDCC**	1	0,052	-1,899	**MRPL53**	1	-0,008	0,000
FAM171A2	1	-0,216	-0,477	**NPR3**	1	-0,074	-2,121	**PTP4A3**	1	0,194	0,000
PPP2R2C	1	0,679	2,120	**ZBTB7B**	1	-0,159	-2,724	**MINOS1-NBL1**	1	0,000	0,000
CNNM2	1	0,169	-0,607	**KIAA1549L**	1	0,238	-1,305	**RP11-286N22.8**	1	0,383	0,000
CD44	1	0,325	-0,854	**SCAMP5**	1	-0,201	-3,094	**IL4I1**	1	0,424	0,000
FAM107B	1	0,004	-1,253	**GRAMD4**	1	0,264	-2,115	**CREBL2**	1	0,178	0,000
CCDC6	1	-0,201	-2,471	**HFM1**	1	0,415	-2,056				

5 Materials and Methods:

5.1 General equipment

Table 5.1 Equipment and instruments

Equipment and instruments	Manufacturer
Centrifuge Eppendorf 5417R	Eppendorf
Centrifuge Eppendorf 5424	Eppendorf
Centrifuge Eppendorf 5810R	Eppendorf
Centrifuge Avanti J-26 XP	Beckman Coulter
CFX96 Real-Time system	Bio-Rad
Eraser for imaging plates	Molecular Dynamics
Gel documentation system ChemiDox XRS	Bio-Rad
Gel dryer Bio-Rad Model 583	Bio-Rad
Heating block Eppendorf comfort	Eppendorf
Horizontal electrophoresis system Compact S,M,L	Biometra
Imaging plates BAS-IP MS 2025, 2040	Fujifilm
Inverted microscope Axiovert 25	Carl Zeiss
Nanodrop NanoVue plus	GE Healthcare
Nunc Galaxy S CO_2 incubator	RS Biotech
Phosphoimager Typhoon FLA7000	GE Healthcare
Pipetman P2, P20, P200, P1000	Eppendorf
Piston Gradient Fractionator	Biocomp
Semi-dry electroblotter	Thermo
Shaking incubator innova 44	New Brunswick Scientific
Thermocycler TProfessional Trio	Biometra
UV-cross linker Bio-Link BLX 365	Peqlab
Ultra centrifuge Optima L-80 XP	Beckman Coulter
Vertical electrophoresis system Mini-Protean	Bio-Rad
Vortex-Genie 2	Scientific Industries

5.2 Consumables

Table 5.2 Consumables

Consumables	Manufacturer
G-25, G-50 MicroSpin columns	GE Healthcare
Hybond-N+ for nucleic acid transfer	GE Healthcare
Nitrocellulose transfer membrane	GE Healthcare
Protein-G dyna beads	Life Technologies
Safe-lock tubes 1.5 ml, 2 ml	Eppendorf
Spectrophotometer cuvettes	Sarstedt
Sterile filters (0.2 µm, 0.5 µm)	Whatman
Tissue culture plates Cellstar 15 cm, 10 cm	VWR
Tissue culture muti-ll plates 6, 12,24 wells	VWR

5.3 Chemicals and commercially available systems

Table 5.3 Chemicals and commercially available systems

Chemicals and commercially available systems	Manufacturer
4-thio uridine	Chemistry Dept.
Acrylamide bis tris	Serva
Albumin Fraction V	Roth
Ampicillin sodium salt	Roth
Bradford reagent	Biorad
Dimethyl sulfoxide (DMSO)	Roth
Coomassie Brilliant Blue G-250	Serva
EDTA	Roth
EGTA	Roth
Ethanol	Sigma
Formamide (99.5%)	Roth
Glycerol (99.5%)	Sigma
Glycine	Roth
GlycoBlue	Ambion
H_2O_2 30%	AppliChem
Isopropanol	Fischer Scientific
Kanamycin sulfate	Roth

Lipofectamine RNAiMax	Invitrogen
Lipofectamine 2000	Invitrogen
Luminol	Serva
Methanol	Roth
Milk powder (Blotting grade)	Roth
PCR purification kit	Analytik Jena
Mini-prep kit	Analytik Jena
Nanofectin	GE healthcare
Gel extraction kit	Analytic Jena
p-Coumaric acid	Sigma
Phenol(pH:4,7)	Roth
Random hexamers	Invitrogen
RiboZero magnetic kit	Illumina
RNA library preparation kit (ultra directional)	NEB
Rotihporese gel 40 (19:1)	Roth
Rotiphorese gel 40 (37.5:1)	Roth
SUPERscriptII reverse transcription kit	Invitrogen
SUPERscriptIII reverse transcription kit	Invitrogen
SYBR green mix	Bio-Rad
TEMED	Roth
Tetracycline	Sigma
TRIzol Reagent	Invitrogen
γ-^{32}P-ATP (222TBq(6000Ci)/mmol 370MBq	Hartmann Analytic

5.4 Enzyme and size markers

Table 5.4 Enzymes and size markers

Enzymes*	Manufacturer
Calf intestinal phosphatase (CIP)	NEB
DNase I	Fermentas
Polynucleotide kinase (PNK)	Fermentas
Phusion High-Fidility DNA polymerase	Fermentas
Proteinase K	AppliChem
RNase I	Fermentas

RNase T1	Fermentas
RNA polymerase	Home made
Shrimp alkaline phosphatase	Fermentas
T4 RNA ligase I	Fermentas
T4 RNA ligase 2 trauncated	NEB
T4 DNA ligase	Fermentas
*All restriction enzymes were purchased from Fermentas	
Taq polymerase	Takara
Size marker	**Manufacturer**
GeneRuler™ DNA ladder mix	Fermentas
GeneRuler™ 100 bp plus DNA ladder	Fermentas
Gene Ruler 1kB plus	Fermentas
PageRuler™ prestained protein ladder	Fermentas
PageRuler™ unstained protein ladder	Fermentas

*All restriction enzymes were purchased from Fermentas and NEB, unless otherwise stated.

5.5 Buffers and solutions

All buffers below were made in house with DEPC water.

Buffer	Composition
DNA loading buffer (6x)	30% glycerol 0.25% bromophenol blue 0.25% xylene cyanol FF
Native loading buffer (5x)	50% (v/v) glycerol 0.5x TBE 0.02% (w/v) bromophenol blue
Phosphate buffer saline (PBS) (10x)	
Protein sample buffer (6x)	300 mM Tris-Cl pH 6.8

	6 % (w/v) SDS 30 % (v/v) glycerol 0.03% (w/v) bromophenol blue 300 mM DTT
RNA sample buffer (2x)	8 M urea 10 mM EDTA 0.04% (w/v) bromophenol blue
Tris/EDTA/borate (TBE) (5x)	445 mM TRIS-HCl, pH-8.3 445 mM Boric Acid 10 mM Na_2EDTA
Towbin buffer (10x)	0.25 M Tris 1.92 M Glycine 0.1% (w/v) SDS final pH: 8.6
Tris buffer saline tween (TBST)	250 mM Tris 150 mM NaCl 2 mM KCl final pH: 7.4
TE buffer (1x)	100 mM Tris-Cl (pH 8) 10 mM EDTA
Transfer buffer (1x)	1x towbin buffer 20% methanol

5.6 Media and media stocks

Table 5.6.1 Bacterial media

All the media below were made in house. By adding respective antibiotics in the following concentrations; Ampicillin-100 µg/ml, Kanamycin- 50 µg/ml, Chloramphenicol- 50 µg/ml selection media was made. Agar plates were generated by adding 2% (w/v) bacto-agar.

Media	Composition
Luria broth (LB)	1.0 % (w/v) tryptone 1.0 % (w/v) NaCl 0.5 % (w/v) yeast extract
Terrific broth (TB)	1.2 % (w/v) tryptone 2.4 % (w/v) yeast extract 0.4 % (v/v) glycerol 17 mM KH_2PO_4 72 mM K_2HPO_4

Table 5.6.2 Mammalian cell culture media and consumables

Media	Manufacturer
Dulbecco's modified eagle media (DMEM)	Gibco
OPTI-MEM	Gibco
Fetal bovine serum (FBS)	Gibco
Blasticidin	InvivoGen
Zeocin	InvivoGen
Hygromycin	InvivoGen
Trypsin	Gibco
Penicillin/streptomycin	Gibco

5.7 Cell lines and strains

Table 5.7.1 Bacterial strains

Stock name	Strain	Plasmid	Details on strain	Source
SJS-104	*E. coli* BL21 Plyss	pET-M11	Transformed with plasmid pETM-11 containing CNBP Isoform-4 right after the His-tag.	This study
SJS-105	*E. coli* BL21 Plyss	pET-M11	Transformed with plasmid pETM-11 containing CNBP Isoform-3 right after the His-tag.	This study
SJS-110	*E. coli* DH5α	pFRT-FLAG-HA	Transformed with plasmid pFRT-FLAG-HA containing CNBP Isoform-6.	This study
SJS-111	*E. coli* DH5α	pFRT-FLAG-HA	Transformed with plasmid pFRT-FLAG-HA containing CNBP Isoform-2.	This study
SJS-114	*E. coli* DH5α	pFRT-FLAG-HA	Transformed with plasmid pFRT-FLAG-HA containing CNBP Isoform-3.	This study
SJS-115	*E. coli* DH5α	pFRT-FLAG-HA	Transformed with plasmid pFRT-FLAG-HA containing CNBP Isoform-5.	This study
SJS-116	*E. coli* DH5α	pET-M11	Transformed with plasmid pETM-11 containing CNBP Isoform-6 right after the His-tag.	This study
SJS-121	*E. coli* DH5α	pFRT-FLAG-HA	Transformed with plasmid pFRT-FLAG-HA containing CNBP Isoform-4.	This study
SJS-122	*E. coli* DH5α	pET-M11	Transformed with plasmid pETM-11 containing CNBP Isoform-2 right after the His-tag.	This study
SJS-129	*E. coli* BL21 Plyss	pET-M11	Transformed with plasmid pETM-11 containing CNBP Isoform-2 right after the His-tag.	This study
SJS-105	*E. coli* BL21 Plyss	pET-M11	Transformed with plasmid pETM-11 containing CNBP Isoform-6 right after the His-tag.	This study

Table 5.7.2 Cell lines

Cell line	Source/supplier	Culture media
HEK293	DSMZ (ACC035)	DMEM 10% (v/v) FBS 1% (v/v) Pen Strep
HeLa	ECACC	DMEM 10% (v/v) FBS 1% (v/v) Pen Strep
Flip-In T-Rex 293		DMEM 10% (v/v) FBS 1% (v/v) Pen Strep 10 µg/ml Blasticidin 100 µg/ml Zeocin

Flip-In T-Rex 293 CNBP isoform-1	This study	DMEM 10% (v/v) FBS 1% (v/v) Pen Strep 10 µg/ml Blasticidin 100 µg/ml Hygromycin B
Flip-In T-Rex 293 CNBP isoform-2	This study	Same as isoform-1
Flip-In T-Rex 293 CNBP isoform-3	This study	Same as isoform-1
Flip-In T-Rex 293 CNBP isoform-4	This study	Same as isoform-1
Flip-In T-Rex 293 CNBP isoform-5	This study	Same as isoform-1
Flip-In T-Rex 293 CNBP isoform-6	This study	Same as isoform-1

5.8 Antibodies

Table 5.8

Antibody	Origin	Supplier	Working dilution
Alexa-Fluor 488 F(ab)2 fragment anti mouse IgG	mouse	Invitrogen	1:500
Alexa-Fluor 488 F(ab)2 fragment anti rabbit IgG	rabbit	Invitrogen	1:500
anti-βactin	mouse	Abcam	1:5000
anti-calnexin	mouse	Abcam	1:1000
anti-CNBP	rabbit	Sigma	1:2000
anti-FLAG	mouse	Sigma	1:2000
anti-GAPDH	rabbit	Abcam	1:2000
anti-HA	mouse	Sigma	1:2000
anti-His	rabbit	Sigma	1:1000
anti-Histone H3	rabbit	Abcam	1:2000
anti-mouse;HRP	donkey	SantaCruz	1:5000

conjugated				
anti-rabbit;HRP conjugated	goat	SantaCruz	1:5000	

5.9 Plasmid stocks

Table 5.9

Plasmid name	Expressed element	Comment	Details on construction	Marker	Reference
pFRT CNBP iso1	CNBP	CNBP isoform 1 FLAG-HA	Restriction cloning	Amp	This study
pFRT CNBP iso2	CNBP	CNBP isoform 2 FLAG-HA	Restriction cloning	Amp	This study
pFRT CNBP iso3	CNBP	CNBP isoform 3 FLAG-HA	Restriction cloning	Amp	This study
pFRT CNBP iso4	CNBP	CNBP isoform 4 FLAG-HA	Restriction cloning	Amp	This study
pFRT CNBP iso5	CNBP	CNBP isoform 5 FLAG-HA	Restriction cloning	Amp	This study
pFRT CNBP iso6	CNBP	CNBP isoform 6 FLAG-HA	Restriction cloning	Amp	This study
pETM11 CNBP iso1	CNBP	CNBP isoform 1 His	Restriction cloning	Kan	This study
pETM11 CNBP iso2	CNBP	CNBP isoform 2 His	Restriction cloning	Kan	This study
pETM11 CNBP iso3	CNBP	CNBP isoform 3 His	Restriction cloning	Kan	This study
pETM11 CNBP iso4	CNBP	CNBP isoform 4 His	Restriction cloning	Kan	This study
pETM11 CNBP iso5	CNBP	CNBP isoform 5 His	Restriction cloning	Kan	This study
pETM11 CNBP iso6	CNBP	CNBP isoform 6 His	Restriction cloning	Kan	This study
psiCHK-TMPO	Luciferase	TMPO PAR-CLIP site	Restriction free cloning	Amp	This study

		cloned before Firefly start codon			
psiCHK-LUC7L3	Luciferase	LUC7L3 PAR-CLIP site cloned before Firefly start codon	Restriction free cloning	Amp	This study
psiCHK-HNRNPH3	Luciferase	HNRNPH3 PAR-CLIP site cloned before Firefly start codon	Restriction free cloning	Amp	This study
psiCHK-DDX42	Luciferase	DDX42 PAR-CLIP site cloned before Firefly start codon	Restriction free cloning	Amp	This study

5.10 Synthetic DNA and RNA oligonucleotides

Table 5.10

Synthetic DNA oligonucleotides

NAME	SEQUENCE 5'-3'
SJO-100	AACGGATCCATGAGCAGCAATGAGTGCTTC
SJO-101	GGTCTCGAGTTAGGCTGTAGCCTCAATTGT
SJO-102	GCGCCATGGCCAGCAGCAATGAGTGCTTC
SJO-103	GGTGGTACCTTAGGCTGTAGCCTCAATTGT
SJO-104	GACTCGAGCGAGCAGCAATGAGTGCTTC
SJO-105	GAGGATCCTTAGGCTGTAGCCTCAATTGT
SJO-106	AGCGGATCCATGGAGGAGGCGGAGGAGC
SJO-107	GCGCTCGAGTCAGGTGCCCATCTCCACCT
SJO-108	GCGCCATGGCCGAGGAGGCGGAGGAGC
SJO-109	GGTGGTACCTCAGGTGCCCATCTCCACCT
SJO-110	GGACTCGAGCGGAGGAGGCGGAGGAGC
SJO-111	AGAGGATCCTCAGGTGCCCATCTCCACCT
SJO-112	AGCGGATCCATGGAGGACTCTGAAGCACT
SJO-113	GCGCTCGAGTCAGGAGGGCTTGGCTGTGG
SJO-114	GCGCCATGGCCGAGGACTCTGAAGCACT
SJO-115	GGTGGTACCTCAGGAGGGCTTGGCTGTGG
SJO-116	GGACTCGAGCGGAGGACTCTGAAGCACT
SJO-117	AGAGGATCCTCAGGAGGGCTTGGCTGTGG
SJO-118	GTGATCTTCAGGAGGATGTTGAAGCCTGCTATAACTG
SJO-119	CAGTTATAGCAGGCTTCAACATCCTCCTGAAGATCAC

SJO-120	TTTGGGAACCCGGGAGGGGCGCTTATGGGGAGGGTGGGGAGGGTG
SJO-121	GAGGGGGAGGGGGG
SJO-122	GCTACAACTGTGGCAAACCA
SJO-123	TGACCAGTTTCACCACACCT
SJO-124	AACGGATCCATGCTGCTGCAGCCCGCG
SJO-125	GGTCTCGAGTCACTGCATCCTGTCAGGCT
SJO-126	GCGCCATGGCCCTGCTGCAGCCCGCGCCG
SJO-127	GGTGGTACCTCACTGCATCCTGTCAGGCTGCA
SJO-128	GGTCTCGAGTCAGCCCGTCTGGAGGCTCCGC
SJO-129	GGTGGTACCTCAGCCCGTCTGGAGGCTCCGC
SJO-124-A	AACGGATCCATGCTGCTGCAGCCCGCGCCGTGCG
SJO-125-A	GGTCTCGAGTCACTGCATCCTGTCAGGCTGCAGCT
SJO-130	TTTGTCGTGAGGACGCGCGCAGCGCGTGGTAGGACGTCGAGCGTTGTG
SJO-131	CGGCTACGGCTTCGTGACAATGGCCGACCGGGCGGCA
SJO-132	TGCCGCCCGGTCGGCCATTGTCACGAAGCCGTAGCCG
SJO-126-A	GCGCCATGGCCCTGCTGCAGCCCGCGCCGTGCGCCCC
SJO- 133	CTGTCCCGTCGCTGTCCT
SJO- 134	GGCGGCAGGGTAGCTGTA
SJO-135	ACGCCTCGCTCAGGAAGTA
SJO-136	GTCTTTGCAAGCCCTCTCAG
SJO-137	ATGAAGGTGCTGATGGGCAGTG
SJO-138	TTGACTTGTCGGTCCTGCTGC
SJO-139	GAGTTGAGTCCTTAAGAAAAT
SJO-140	CTCAATCTACAACTCTGGGT
SJO-141	CCAACGTGGCAATTGCAACCG
SJO-142	TTGACCTGGTATTGGGCAGCC
SJO-143	GGCATGTCATTGCAGGATCAT
SJO-144	GCAGTACGCCCAGAAACAATC
SJO-145	GAGAGTGCTTTGGACAAATCTG
SJO-146	CAGCATTGCCTTCTGAGTCC
SJO-147	AAGCCATTTGATGTATGCGGT
SJO-148	GTCCTGAGCCCTGCGATGCT
SJO-149	GCTTTTGATTATTACTGATGGTG
SJO-150	GAATCTCTGCCAAGACACACT
SJO-151	AGAGGGAATTCAAACCAGGAAAC
SJO-152	CTATGTAGAGCCCATCTTGAC
SJO-153	TAGAGTGCTCGGCTGCCCGG
SJO-154	GCTTTGGGAACCCGGGAGGG
SJO-155	ATCGCGACCAACATCGAGCAGATTTTTAGGTCTTTCGTGGTCAGTAAA TTCCGGGAAATTCAACAGGAGCTTTCCAGTGGAAGGAATG
SJO-156	GATCCATTCCTTCCACTGGAAAGCTCCTGTTGAATTTCCCGGAATTTA CTGACCACGAAAGACCTAAAAATCTGCTCGATGTTGGTCGCGAT
SJO-157	ATCGCGACCAACATCTATCAGATTTTTATCTCTTTCCTCCTCAGTAAA TTCCGATCAATTCAACACACTCTTTCCAGTTCGAGGAATG
SJO-158	GATCCATTCCTCGAACTGGAAAGAGTGTGTTGAATTGATCGGAATTTA CTGAGGAGGAAAGAGATAAAAATCTGATAGATGTTGGTCGCGAT
SJO-159	CTGTAGTCTGCATATCCCTGTCCATATCCATAGTTCCCAT AGTTATACCCAGTATAATCATATCCGCCATAGCCCTATAGTGAGTCGTATTAA
SJO-160	CTGTAGTCTGCATAATTCTGATTATAATTATAGTATTCAT AGTTATACCCAGTATAATCATAATTGCCATAGCCCTATAGTGAGTCGTATTAA
SJO-161	CGTTGACAGCTCCGATGTTGTCACCACAGACTGAACAGAG ATCTCCAGCGCCACAGTTCCCTATAGTGAGTCGTATTAA
SJO-162	CGTTGACAGTATTGATGTTGTCACCACAGACTGAACAGAG ATTATTAGCGCCACAGTTCCCTATAGTGAGTCGTATTAA

SJO-163	ATCATTTCGGCCGCGCAGTTGTTGGATGAGTTAATGGGCCGGGACG
SJO-164	GATCCGTCCCGGCCCATTAACTCATCCAACAACTGCGCGGCCGAAATGAT
SJO-165	ATCCCGGAGTTCCTGGAAGACCCCTCGGTCCTGG
SJO-166	GATCCCAGGACCGAGGGGTCTTCCAGGAACTCCGGGAT
SJO-167	ATCAACTGGAATAAAGGTGGTCCTGGCACTAAGCGAGGATTT GGCTTTGGAGGTTTTGCCATCAGTGCTGGGAAAAAGGAGGAAG
SJO-168	GATCCTTCCTCCTTTTTCCCAGCACTGATGGCAAAACCTCCAA AGCCAAATCCTCGCTTAGTGCCAGGACCACCTTTATTCCAGTTGAT
SJO-169	ATCATGGATTGGGTTATGAAACATAATGGTCCAAATGACGCTAG TGATGGGACAGTACGACTTCGTGGACTACCATTTGGTTGCAGCAAAGAGG
SJO-170	GATCCCTCTTTGCTGCAACCAAATGGTAGTCCACGAAGTCGTAC TGTCCCATCACTAGCGTCATTTGGACCATTATGTTTCATAACCCAATCCATGAT
SJO-171	ATCATTTCGGCCGCGCAGTTGTTAATAAAGTTAATGGGCCAAGACG
SJO-172	GATCCGTCTTGGCCCATTAACTTTATTAACAACTGCGCGGCCGAAATGAT
SJO-173	ATCCCTAATTTCCTCATTGACCCCTCGGTCCTGG
SJO-174	GATCCCAGGACCGAGGGGTCAATGAGGAAATTAGGGAT
SJO-175	ATCAACTATTTTAAACCTCGTCCTAACACTAAGCGACCAT TTGGCTTTTTTAGTTTTGCCATCAGTGCTGAATTAAAGGAACTTG
SJO-176	GATCCAAGTTCCTTTAATTCAGCACTGATGGCAAAACTAAAAAAG CCAAATGGTCGCTTAGTGTTAGGACGAGGTTTAAAATAGTTGAT
SJO-177	ATCATCCATTGGGTTATGAAACATAATGGTCCAAATGACGCTAGTG ATGCCACAGTACGACTTCGTTACCTACCATTTGGTTGCAGCAAAGAGG
SJO-178	GATCCCTCTTTGCTGCAACCAAATGGTAGGTAACGAAGTCGTACTG TGGCATCACTAGCGTCATTTGGACCATTATGTTTCATAACCCAATGGATGAT
SJO-179	TTGGCAGAAGCTATGAAACG
SJO-180	GCAACTGCAACTCCGATAAA
SJO-181	GTCCCGGCCCATTAACTCATCCAACAACTGCGCGGCCGAAATCCCTA TAGTGAGTCGTATTAA
SJO-182	CAGGACCGAGGGGTCTTCCAGGAACTCCGGCCCTATAGTGAGTCGTATTAA
SJO-183	TTCCTCCTTTTTCCCAGCACTGATGGCAAAACCTCCAAAGCCAAATCC TCGCTTAGTGCCAGGACCACCTTTATTCCAGTTCCCTATAGTGAGTCGTATTAA
SJO-184	CTCTTTGCTGCAACCAAATGGTAGTCCACGAAGTCGTACTGTCCCATCACT AGCGTCATTTGGACCATTATGTTTCATAACCCAATCCATCCCTATAGTGAGTCGTATTAA
SJO-185	GTCTTGGCCCATTAACTTTATTAACAACTGCGCGGCCGAAATCCCTAT AGTGAGTCGTATTAA
SJO-186	CAGGACCGAGGGGTCAATGAGGAAATTAGGCCCTATAGTGAGTCGTATTAA
SJO-187	AAGTTCCTTTAATTCAGCACTGATGGCAAAACTAAAAAAGCCAAATGGTC GCTTAGTGTTAGGACGAGGTTTAAAATAGTTCCCTATAGTGAGTCGTATTAA
SJO-188	CTCTTTGCTGCAACCAAATGGTAGGTAACGAAGTCGTACTGTGGCATCACT AGCGTCATTTGGACCATTATGTTTCATAACCCAATGGATCCCTATAGTGAGTCGTATTAA
SJO-189	CGGTACTGTTGGTAAAGCCACCATGATTTCGGCCGCGCAGTTGTTGGATGAGTTAATG
SJO-190	GCCCTTCTTAATGTTCTTAGCATCGGCGTCCCGGCCCATTAACTCATCCAACAACTGCG
SJO-191	CGGTACTGTTGGTAAAGCCACCATGATTTCGGCCGCGCAGTTGTTAATAAAGTTAATGGG
SJO-192	GCCCTTCTTAATGTTCTTAGCATCGGCGTCTTGGCCCATTAACTTTATTAACAACTGCGC
SJO-193	CGGTACTGTTGGTAAAGCCACCATGCCGGAGTTCCTGGAAGACCCCTCG
SJO-194	GCCCTTCTTAATGTTCTTAGCATCGGCCAGGACCGAGGGGTCTTCCAGGA
SJO-195	CGGTACTGTTGGTAAAGCCACCATGCCTAATTTCCTCATTGACCCCTCGG
SJO-196	GCCCTTCTTAATGTTCTTAGCATCGGCCAGGACCGAGGGGTCAATGAGGA
SJO-197	CGGTACTGTTGGTAAAGCCACCATGAACTGGAATAAAGGTGGTCCTGGCA CTAAGCGAGGATTTGGCTTTGGAGGT
SJO-198	GCCCTTCTTAATGTTCTTAGCATCGGCTTCCTCCTTTTTCCCAGCACTGAT GGCAAAACCTCCAAAGCCAAATCCTC
SJO-199	CGGTACTGTTGGTAAAGCCACCATGAACTATTTTAAACCTCGTCCTAACACT AAGCGACCATTTGGCTTTTTTAGT
SJO-200	GCCCTTCTTAATGTTCTTAGCATCGGCAAGTTCCTTTAATTCAGCACTGATG GCAAAACTAAAAAAGCCAAATGGTC
SJO-201	CGGTACTGTTGGTAAAGCCACCATGATGGATTGGGTTATGAAACATAATGGTC CAAATGACGCTAGTGATGGGACAGTAC
SJO-202	GCCCTTCTTAATGTTCTTAGCATCGGCCTCTTTGCTGCAACCAAATGGTAGTC CACGAAGTCGTACTGTCCCATCACTAGCG

SJO-203	CGGTACTGTTGGTAAAGCCACCATGATCCATTGGGTTATGAAACATAATGGTC CAAATGACGCTAGTGATGCCACAGTAC
SJO-204	GCCCTTCTTAATGTTCTTAGCATCGGCCTCTTTGCTGCAACCAAATGGTAGGT AACGAAGTCGTACTGTGGCATCACTAGCG
SJO-205	CGCTTAAAAGCTTGGCATTCCGGTAATTTCGGCCGCGCAGTTGTTGGATGAGTTAATG
SJO-206	GGCCATGGTGGCTTTACCAACAGGTCCCGGCCCATTAACTCATCCAACAACTGCG
SJO-207	CGCTTAAAAGCTTGGCATTCCGGTAATTTCGGCCGCGCAGTTGTTAATAAAGTTAATGGG
SJO-208	GGCCATGGTGGCTTTACCAACAGGTCTTGGCCCATTAACTTTATTAACAACTGCGC
SJO-209	GGCGCCATGGCCAGCAGCAATGAGCCTACTGGTGGAGGCCGTGGTCGTGGAATG
SJO-210	TTAGGCTGTAGCCTCAATTGTGCATTCCCGTGCAA
SJO-211	CGGGAATGTCCTACTGGTGGAGGCTTCCAGTTTGTTTCCTCGTCTCTTCCAGAC
SJO-212	Same as 210
SJO-213	GGCGCCATGGCCAGCAGCAATGAGTTCCAGTTTGTTTCCTCGTCTCTTCCAGAC
SJO-214	Same as 210
SJO-215	GGCGCCATGGCCAGCAGCAATGAGTGCTTCAAGTG
SJO-216	TTAGGCTGTAGCCTCAATTGTCTTCACTTTGGTGCAGTCTTTTTGAATGTGTCCG
SJO-217	GATTACGCTGGATCCATGAGCAGCAATGAGCCTACTGGTGGAGGCCGTGGTCGTGGAATG
SJO-218	Same as 210
SJO-219	GATTACGCTGGATCCATGAGCAGCAATGAGTTCCAGTTTGTTTCCTCGTCTCTTCCAGAC
SJO-220	Same as 210
SJO-221	GATTACGCTGGATCCATGAGCAGCAATGAG
SJO-222	GAACCGGACCGAAGCCCGATTTGGATCCGGCGAACCGGATCGAGTCCCGGCCCATTAACTCATCCAACAACTGC GCGGCCGAAATTTGGCCCGAAGGCCCCCTATAGTGAGTCGTATTAA
SJO-223	GAACCGGACCGAAGCCCGATTTGGATCCGGCGAACCGGATCGACAGGACCGAGGGGTCTTCCAGGAACTCCGGT TGGCCCGAAGGCCCCCTATAGTGAGTCGTATTAA
SJO-224	GAACCGGACCGAAGCCCGATTTGGATCCGGCGAACCGGATCGATTCCTCCTTTTTCCCAGCACTGATGGCAAAA CCTCCAAAGCCAAATCCTCGCTTAGTGCCAGGACCACCTTTATTCCAGTTTTGGCCCGAAGGCCCCCTATAGTG AGTCGTATTAA
SJO-225	GAACCGGACCGAAGCCCGATTTGGATCCGGCGAACCGGATCGACTCTTTGCTGCAACCAAATGGTAGTCCACGA AGTCGTACTGTCCCATCACTAGCGTCATTTGGACCATTATGTTTCATAACCCAATCCATTTGGCCCGAAGGCCC CCTATAGTGAGTCGTATTAA
SJO-226	GAACCGGACCGAAGCCCGATTTGGATCCGGCGAACCGGATCGAGTCTTGGCCCATTAACTTTATTAACAACTGC GCGGCCGAAATTTGGCCCGAAGGCCCCCTATAGTGAGTCGTATTAA
SJO-227	GAACCGGACCGAAGCCCGATTTGGATCCGGCGAACCGGATCGACAGGACCGAGGGGTCAATGAGGAAATTAGGT TGGCCCGAAGGCCCCCTATAGTGAGTCGTATTAA
SJO-228	GAACCGGACCGAAGCCCGATTTGGATCCGGCGAACCGGATCGAAAGTTCCTTTAATTCAGCACTGATGGCAAAA CTAAAAAAGCCAAATGGTCGCTTAGTGTTAGGACGAGGTTTAAAATAGTTTTGGCCCGAAGGCCCCCTATAGTG AGTCGTATTAA
SJO-229	GAACCGGACCGAAGCCCGATTTGGATCCGGCGAACCGGATCGACTCTTTGCTGCAACCAAATGGTAGGTAACGA AGTCGTACTGTGGCATCACTAGCGTCATTTGGACCATTATGTTTCATAACCCAATGGATTTGGCCCGAAGGCCC CCTATAGTGAGTCGTATTAA
SJO-230	GAACCGGACCGAAGCCCG
SJO-231	CAGTTCTTCATGCCAGTGCT
SJO-232	AGGCCCTTCTTAGACACGAA
SJO-233	GCGAGATCCCTCTCGTTAAG
SJO-234	ATCTTAGGCAGATCGTCGCT

5.11 Molecular biological methods

5.11.1 Determination of concentration of nucleic acids

DNA and RNA concentration were measured using nanodrop NanoVue plus.

5.11.2 Preparation of plasmid DNA

Plasmid DNA was extracted from bacterial cells using standard Analytic Jena kit as per manufacturer's instruction.

5.11.3 Purification of DNA from agarose gel or PCR reaction

DNA was purified from agarose gel or PCR reaction using standard Analytik Jena kits as per manufacturer's instruction.

5.11.4 Polymerase chain reaction (PCR)

DNA fragments of interest were amplified by PCR reaction using Taq or Phusion polymerase and oligonucleotides given in table above. Below given are the reagents and program used for a standard PCR. Annealing temperature for each reaction depends upon Tm of the oligonucleotides used.

	Taq polymerase	**Phusion polymerase**
Reagents		
DNA template	100-300 ng	>100 ng
Reaction buffer	5 µl (10x)	5 µl (10x)
Forward primer	0.5 µM	0.5 µM
Reverse primer	0.5 µM	0.5 µM
dNTPs	100 µM	100 µM
Polymerase	1 U	0.5 U
Final volume	50 µl with H_2O	50 µl with H_2O

Program	Temp.	Time	Cycles	Temp.	Time	Cycles
Initialization	95 ˚C	5'	1	95 ˚C	5'	
Denaturation	95˚C	30"	30-35x	95˚C	30"	30-35x
Annealing	55-65˚C	30"		55-65˚C	30"	
Elongation	72˚C	1 min/kb		72˚C	30 secs/kb	
Final elongation	72˚C	5 mins	1	72˚C	5 mins	1

5.11.5 Agarose gel electrophoresis

To separate the DNA of various sizes 0.5-2.5% (w/v) agarose gels were made in 1x TBE buffer. To visualize DNA ethidium bromide was added in the solubilized agarose (0.5 µg/ml) before

pouring the gel. Prior to loading the DNA samples were premixed in 6x DNA loading dye boiled at 95˚C, 5mins and separated at 100-130 V for 30-150 mins. If needed the DNA bands were excised from agarose gel using Analytik Jena kit as mentioned above.

5.11.6 Restriction digestion and DNA ligation

For cloning DNA fragment of interest into desired vectors, restriction digestion followed by ligation was performed. 1.5 µg of vector and 500 ng of PCR product were digested with restriction endonuclease followed by dephosphorylation (30 mins, 37˚C, using SAP) of plasmid vector (to avoid re-circularization).

Digested DNA fragments and linearized vectors were ligated by T4 DNA ligase in a molar ratio of 1:1 or 1:3 at 14˚C overnight and were transformed into chemically competent *E. coli* cells.

5.11.7 Transformation of chemically competent *E. coli* cells

Chemically competent *E. coli* cells were transformed with desired vector by heat shock method. ~100 ng of vector DNA was mixed with 100 µl of competent cells on ice. After 30 mins of incubation on ice, the cells were transferred to a 42˚C heating block for 45 secs followed by 5 mins cooling on ice. 900 µl of pre-warmed LB/SOC was added to the cells and incubated at 37˚C for 1 hour. Plating of transformed cells on the desired antibiotic agar plates were performed using sterile glass beads.

5.11.8 Site directed mutagenesis

To introduce mutations or deletions in pre-cloned plasmid PCR based site directed mutagenesis was performed. We used 2-step PCR amplification method. In the PCR amplification-I, the oligonucleotides carrying mutation and the flaking regions around the mutation site was used to amplify the 2 segments of the gene in two different tubes. The two amplified gene regions were run on agarose gel and purified. In amplification step-II the two PCR products containing flanking regions complementary to each other were used to amplify the entire gene. The primers were designed in such a way that the amplified product carries restriction sites at both the ends. The final amplified gene containing mutation was digested with the respective restriction enzymes and cloned into the plasmid of interest.

5.11.9 Restriction free cloning

To introduce mutations or deletions in pre-cloned plasmid restriction free cloning was also performed. As above, we used 2-step PCR amplification method. In the PCR amplification-I, the oligonucleotides carrying mutation and the flaking regions around the mutation site was used to

amplify the 2 segments of the gene in two different tubes. The two amplified gene regions were run on agarose gel and purified. In amplification step-II the two PCR products containing flanking regions complementary to each other were used to amplify the entire plasmid using Pfu DNA polymerase. Subsequently the maternal plasmid was digested by DpnI and incubated for 2 h at 37˚C. The entire reaction mix was transformed into DH5α cells and plated on adequate selection media.

5.11.10 Bacterial cryo-stock preparation

To prepare cryo-stock of *E. coli* for storage 500 µl of overnight grown culture was mixed with sterile 50% glycerol and stored at -80˚C.

5.12 Cell culture methods

5.12.1 Culture and passage of adherent cell lines

Adherent cell line (mostly used in this study: HEK293 and HeLa) were cultured in DMEM containing 10% FBS and 1% Pen/Strep. The modified or stable cell lines generated in this study were grown in media containing appropriate antibiotic. Cells were grown in 10 or 15 cm plates in a Nunc Galaxy S CO_2 incubator (5% CO_2). To split cells, 3ml of 0.25% trypsin-EDTA was added to a 100% confluent 15 cm plate and incubated in the CO_2 incubator for 5 mins. To stop trypinization, DMEM was added to the detached cells and desired amount of cells were seeded into new culture flask/plate.

5.12.2 Generation of Flp-In T-Rex 293 stable cell lines

To generate a stable cell line for gene of interest Flp-In T-Rex cells were used. Cells were grown upto 40-50% confluency in a 10 cm plate containing DMEM (with 10% FBS, 1% P/S)+ 10 µg/ml blasticidin +100 µg/ml zeocin. Nanofectin was used for the transfection (as per manufacturer's instruction) of pFRT/TO/MCS plasmid containing gene of interest along with the helper plasmid pOG44 (in a ratio of 9:1 for a total of 8 µg DNA). Twenty-four hour post transfection, the media was changed to DMEM (with 10% FBS, 1% P/S) containing 10 µg/ml blasticidin+ 100 µg/ml hygromycin for selecting transfected cells. Selection media was changed routinely every 24 hours until clones became visible. Colonies were picked and transferred into 6 well plate containing selection media for further up scaling.

5.12.3 Transient transfection

For the transient transfection of siRNA and vector plasmids Lipofectamine RNAiMax and Lipofectamine 2000 was used respectively as per manufacturers instruction.
Cells were grown in a 6 or 12 well plate till 60% confluency and transfected with appropriate concentration of siRNA/plasmid.

5.12.4 Preparation of cryo-stocks

For the preparation of cryo –stocks, cells were trypsinized and counted using hemocytometer. $2x10^6$ cells per cryo-vials were used for freezing along with 10% DMSO. The vials are first stored at -20˚C for 4 hours followed by 24-48 hours in -80˚C. Finally, the stocks were kept in liquid nitrogen tank until further use.
To use the frozen stocks, cells were thawed in a 37˚C water bath. The cells were re-suspended into a 6 cm plate containing pre-warmed media and thereafter cultured normally.

5.13 Biochemical methods

5.13.1 Bradford assay

Concentration of protein solutions was determined by Bradford method. First, a standard curve was made using BSA of known concentration. A series of dilution of BSA was used to draw the standard curve (2 µl protein+ 998 µl Bradford solution, 1x) by measuring its absorbance at 595 nm. Measuring the absorbance and corresponding to the equivalent standard concentrations determined the concentration of unknown protein sample.

5.13.2 SDS-PAGE

For the separation of protein and peptides based on their molecular weight, denaturing one-dimensional sodium dodecyl sulphate polyacrylamide gel electrophoresis (SDS-PAGE) was utilized. Samples were mixed in 1x Lämmli buffer and denatured for 5 mins at 95˚c prior to loading. Samples were loaded on gels consisting of a 4% PAA stacking gel on top of a 10-15% PAA resolving gel. Samples were run at 100-200 V in the presence of 1x Towbin buffer.

5.13.3 Native PAGE

5.13.4 Coomassie staining of SDS gels

To visualize the SDS-PAGE separated proteins, Coomassie staining was performed. The gels were incubated in Coomassie stain (50% methanol, 10% glacial acetic acid, 0.15% Serva stain R)

for 1 hour. Distaining of Coomassie stained gels were performed with 20% acetic acid until the bands were visible.

5.13.5 Silver staining of SDS gels

Silver staining is a more sensitive method to visualize protein/peptide bands on SDS gels as compare to coomassie staining. PAA gel is quickly rinsed with water followed by fixation for 1 hour in fixer solution (50% methanol, 12% acetic acid, 0.5 ml/l formaldehyde). The gel was washed 3x 20 mins with 50% (v/v) ethanol followed by 1 min sensitizer treatment (0.02g Sodium thiosulphate in 100ml H_2O). The gel was washed 3x 20secs each with ddH_2O and incubated in silver stain (0.2 g $AgNO_3$, 75 µl 27% formaldehyde in 100 ml water) for 20 mins (cover the gel/box with aluminum wrap). Washed the gel with water 2x 20 seconds each. The gel was added with developing solution (6 g anhydrous Na_2CO_3, 50 µl 27% formaldehyde in 100 ml water) till the bands are seen. After washing with 2x 2mins water the reaction was stopped with 25% acetic acid for 10 mins and stored in 50% methanol.

5.13.6 Cellular fractionation (cytoplasmic and nuclear)

Expression of FH-CNBP isoforms 1-6 from stable HEK293 cells (1x, 15 cm plate) was induced with 500 ng/ml tetracycline for 14 hours. Next morning the cells were washed with ice cold PBS (5 ml), scraped and collected by centrifugation. Fractionation of cytoplasmic and nuclear fraction was performed as described in Gagnon KT et al., 2014 protocol unless otherwise stated. In brief, the pelleted cells were resuspended in 1 ml of hypotonic lysis buffer (HLB) (10 mM Tris, pH 7.5, 10 mM NaCl, 3 mM MgCl2, 0.3% NP-40 v/v, 10% glycerol v/v) per 75 mg cell pellet. Resuspended cells were incubated on ice for 10 mins followed by centrifugation at 800g for 8 mins at 4˚C. The supernatant containing cytoplasmic fraction was collected in a fresh tube and NaCl was added to make final concentration 150 mM. The pellet containing nuclear fraction was washed 4x with HLB buffer (collect pellet each time by centrifuging at 200g, 2 mins at 4 ˚C). Finally the pellet was resuspended in nuclear lysis buffer (NLB) (20 mM Tris, pH 7.5, 150 mM KCl, 3 mM MgCl2, 0.3% NP-40 v/v, 10% glycerol v/v). Nuclear fraction was sonicated 2x 40% power, 15 secs each. Finally, both the fractions were spun down at 18000g 15 mins at 4˚C and the supernatants were collected. Samples were taken from both cytoplasmic and nuclear fraction and resolved on SDS-PAGE for western blotting.

5.13.7 Sucrose gradient and fractionation

To prepare the lysate for polysome gradient, HEK 293 cells were grown in a 10 cm plate till approx. 80% confluency. The cells were washed with ice-cold PBS containing 100 µg/ml

cyclohexamide and lysed in lysis buffer (100 mM KCl, 20 mM Tris pH 7.5, 5 mM $MgCl_2$, 0.5% NP-40, 1 mM DTT, protease inhibitors) containing 100 µg/ml cyclohexamide. The extract was clarified by centrifugation (11,200 rpm, 10 mins, 4˚C).

The clarified lysate was loaded onto 5-45% linear sucrose gradient (in 100 mM KCl, 20 mM Tris pH 7.5, 5 mM $MgCl_2$, 0.5% NP-40, 1 mM DTT). To prepare the sucrose gradient 5% sucrose and 45% sucrose was mixed into 1:1 ratio as per Beckmen's gradient maker instructions. The gradient was subjected to centrifugation in an SW60Ti rotor (Beckman) (1:30 h, 34,500 rpm, 4˚C). UV profiling (254 nm) and fractionation of different subunits of ribosomes was done by using fractionator (Biocomp). SDS-PAGE and western blot analyzed the individual fraction.

5.13.8 Protein purification

For the expression of recombinant CNBP, pET-M11 vector containing CNBP (under lac-operon) was transformed into *E. coli* BL21 DE3 (pLysS). Bacteria were grown till OD600 of 0.6 and induced with 0.5 mM IPTG. Three hours after induction the cells were collected, resuspended in lysis buffer (5x w/v of pellet) (500 mM NaCl, 20 mM HEPES, pH 7.5, 5 mM TCEP, 5 mM Imidazole, 10% Glycerol) and lysed by sonication on ice (5x 45 sec pulse with 1 min pause in between). The cell debris was cleared by centrifugation 30,000 rpm, 45 mins and the supernatant was incubated with Ni-NTA agarose (Qiagen) beads for 30 mins at 4˚C. The supernatant was loaded onto a column and the flow through was allowed to pass by gravitational force. The collected beads were washed 3x 10 ml each with wash buffer (lysis buffer+20 mM imidazole) and the CNBP was eluted from the beads in 5 ml, 250 mM imidazole. The eluted protein was concentrated using centricon MWCO 10 kDa. The concentrated protein was run on a Superdex75 Akta column and different fractions were visualized on SDS-PAGE.

5.13.9 CRISPR/Cas9 gene editing

Flp-In T-REx HEK293 cells were reverse transfected with 2 µg CNBP CRISPR/Cas9 KO Plasmid (sc-404090) using LipoD293™ *in vitro* DNA Transfection Reagent (SignaGen® Laboratories). Forty-eight hours after transfection, single cells were screened for expression of GFP and sorted into 96-well tissue culture dishes using the FACSAria™ (BD Biosciences). Dead cells were excluded from the sort using TO-PRO®-3 Iodide (Molecular Probes). Once colonies numbered ~$5x10^5$ cells, knockouts were screened by immunoblotting with anti-CNBP antibody (Sigma SAB2100453). Knockout was confirmed by RNA-sequencing analysis. Individual clones had deletions of variable length spanning a region beginning within exon 3 and ending within exon 4.

5.14 RNA techniques

5.14.1 RNA purification/extraction

To obtain total cellular RNA from samples TRIzol method of RNA extraction was used as per manufacturers guidelines. In detail, the cells are washed with 1x PBS followed by addition of TRIzol (1 ml TRIzol per well for a 6 well plate). The cells were re-suspended and added with 200 µl chloroform per ml TRIzol followed by mixing up and down, 10 seconds. After incubation at room temperature for 5 mins, the samples were spun down at 4˚C for 15 mins full speed. Carefully the aqueous phase containing RNA was taken into a fresh eppendorf and added with equal volume of isopropanol for precipitation. To precipitate, the sample was incubated at -20˚C for >30 mins and centrifuged at 4˚C full speed for 30 mins. The pellet was washed with 70% ethanol and spun for 10 mins at 4˚C. Finally the pellet was air dried and re-suspended in desired volume of water and the concentration was measured on Nanodrop.

To purify RNA from solutions acidic Phenol: Chloroform: Isoamylalcohol (P:C:I, pH 4) was used. Equal volume of PCI was added to the sample and mixed well. The sample was centrifuged at room temperature for 5 mins full speed and the supernatant containing RNA was collected in a fresh eppendorf. To remove the traces of phenol from the sample RNA equal volume of chloroform was added and the above step was repeated. The aqueous phase was mixed with equal volume of isopropanol for precipitation. If the RNA species were small, 1 µl of glycogen was added as carrier for precipitation.

5.14.2 *In vitro* transcription

In vitro transcription was performed using home made T7 RNA polymerase. The DNA template was designed in such a way that it contained T7 promoter sequence. Following reaction mix was used to synthesize RNA of interest in a total of 100 µl reaction mix:

10 µl	10x T7 buffer
5 mM	DTT
1 µM	T7 oligo
1 µM	Template DNA
5 mM	ATP
5 mM	CTP
8 mM	GTP
2 mM	UTP
10 µl	T7 RNA polymerase

Water to make up to 100 µl.

The reaction was incubated at 37˚C for 2 hours and mixed with equal volume of stop mix. The reaction was loaded onto 10-12% urea gel and the RNA was visualized.

5.14.3 5' end labeling of DNA or RNA oligonucleotides

For 5' labeling, 20 pmol of the oligonucleotide was incubated with 25 µCi of γ -ATP in the presence of 1 U polynucleotide kinase (PNK) and 1x PNK buffer and incubated at 37˚C for 30 mins. The labeled DNA/RNA was ran on 12-15% urea gel the corresponding band was excised and eluted. For the labeling of template containing 5' phosphate, first the 5' end was first dephosphorylated using calf intestinal phosphatase (CIP), 10 U, 37˚C, 1 hour.

5.14.4 Elution of DNA/RNA from PAA gel

To elute the labeled DNA/RNA from PAA gel 0.3 M NaCl was used. The gel was dismantled and wrapped in saran wrap. The DNA/RNA to be excised was visualized by direct staining, UV-shadowing or aligned to its 100% image printout. The corresponding bands were marked clearly, excised and cut into small pieces. The gel pieces were weighed and 3 volume (w/v) 0.3% NaCl was added. Passive elution was performed overnight in cold room on a head over tail. Next day the supernatant containing labeled DNA/RNA was precipitated and re-suspended in desired volume of water.

5.14.5 Reverse transcription

To reverse transcribe cDNA from total RNA or specific RNA Superscript III first strand synthesis kit was used as per manufacturer's instruction.

5.14.6 Quantitative RT-PCR

To analyze the efficiency of CNBP knockdown qRT-PCR was used. Briefly, total RNA was isolated using TRIzol method and its concentration was measured using nanodrop. 2 µg of RNA was subjected to reverse transcription using Super script III. Expression of CNBP mRNA was quantitatively assessed by qRT-PCR in a CFX96 RealTime System with GAPDH as the reference gene. For each reaction (20 µl total volume), 10 µl of SYBR Green mix (Bio-Rad), 5 ng cDNA and 0.4 µM of each oligo were used. Each reaction was performed in triplicates and the following reaction program was used;

PCR-program (40 cycles)

95˚C for 30 secs, 95 for 5 secs, 58˚C for 30 secs

5.14.7 Electrophoretic mobility shift assay and Filter binding assay

In vitro interaction of CNBP to its target mRNAs was analyzed by gel shift assays. 5' end labeled target RNA (2 nmol) was incubated with gradually increasing concentration purified CNBP in 1x binding buffer (given in figure legends). The reaction mix was incubated on ice for 45 mins and added with native loading buffer prior to loading on a 0.4% agarose or native gel (6%). Gels were dried and signals were analyzed on the Typhoon FLA 7000 phosphoimager.

For filter binding assays 2 nmol of radiolabelled oligoribonucleotides were incubated with recombinant CNBP as described above. To separate the bound RNA protein complex from unbound RNA the samples were applied to a dot blot apparatus (BioRad). The unbound RNA was retained on a Hybond N+ membrane (GE Healthcare), whereas the RNA-protein complex was retained on a Hybond ECL membrane (GE Healthcare). The bound and unbound spots were quantified using ImageQuant (GE Healthcare) and their relative K_ds were calculated using Prism software (GraphPad).

5.14.8 RNA sequencing

RNA from three different clones of CNBK KO cells and three biological replicates of the parental Flp-In T-REx HEK293 was isolated using TRIzol reagent according to the manufacturer's instructions. The Ribo-Zero rRNA removal kit (Illumina) was used to deplete ribosomal RNA followed by cDNA library preparation using NEBNext mRNA Library Prep Master Mix Set for Illumina (NEB). cDNA was amplified using NEBNext Multiplex Oligos for Illumina (NEB) and sequencing was performed on Illumina HiSeq 2500 platform. After sequencing the reads were aligned to the human genome version hg19 using TopHat (Trapnell et al. 2012). Cufflinks and Cuffdiff were used to quantify transcripts and determine differential expression (Trapnell et al. 2012).

5.14.8 Ribosome profiling

Ribo-seq was performed as described in (Ingolia et al. 2012). Essentially, single 10 cm plates of Flp-In T-REx HEK293 (either wt or CNBP KO) at 60-80% confluence were treated for translation inhibition with either 100 µg/ml Cycloheximide (CHX), or with 2 µg/ml Harringtonine (HRN) followed by addition CHX, as described in (Ingolia et al. 2012). Treated plates were immediately placed on ice, media was aspirated, cells were washed with ice-cold PBS, and overlaid with 400 µl of ribosome footprinting buffer (20 mM Tris pH 7.4, 150 mM NaCl, 4 mM $MgCl_2$, 1 mM DTT, 100 µg/ml CHX) supplemented with 1% NP40 and 25 U/ml Turbo DNaseI. Cells were then scraped, collected to pre-chilled 1.5 ml microcentrifuge tubes and extracted by incubation on ice for 10 mins. Cell extracts were triturated by passing 10 times through a 26-G needle, and cleared of debris by centrifugation at 4°C and 20000g for 10 mins. Then, 7.5 µl of RNase I (100 U/µl, 2.5

U/µl final concentration) were added to 300 µl of the recovered cell extracts and incubated for 45 mins, at room temperature with gentle mixing. Next, 10 µl of SUPERaseIn (20 U/µl) was added in order to stop RNaseI, and the extracts were ultracentrifuged for 4 h (TLA 100.3 rotor at 70000 RPM) through a 900 µl sucrose cushion (footprinting buffer with 20 U/ml SUPERasIN and 1 M sucrose). The ultracentrifugation supernatant was discarded and the ribosome- and footprint-containing pellets were resuspend in 150 µl of footprinting buffer supplemented with 20 U/ml SUPERasIN. RNA was purified by phenol-chloroform extraction, followed by ethanol precipitation. The precipitated RNA was washed twice with 75% ethanol, air-dried, and resuspended in 15 µl DEPC-treated water. NGS sequencing libraries of ribosome footprints were constructed as described for PAR-CLIP (see above) and in (Hafner et al. 2012b), with the following modifications: **a.** Prior to 3' adapter ligation, purified RNAs (~300 ng, reaction volume of 15 µl) were dephosphorylated by 10 units of Calf Intestinal Phosphatase (CIP, M0290, NEB) according to the manufacturer's instructions. Then, the dephosphorylated RNA was loaded on a 15% Urea-PAGE for exclusion of CIP and selection of 20-35 bases long fragments. **b.** After 3' adapter ligation (but before size selection of adapter-ligated RNA fragments) purified RNA was resuspended in 17 µl of DEPC-treated water and phosphorylated at 37 °C for 30 min by 10 Units of T4 - Polynucleotide Kinase (M0201, NEB, reaction volume of 20 µl) in the presence of T4 DNA ligase buffer (B0202, NEB). Sequencing was performed on Illumina HiSeq 2500 platform. After sequencing the reads were aligned to the human genome version hg19 using TopHat (Trapnell et al. 2012). RNAcounter was used to quantify transcript-mapped footprints. Translational inhibition with CHX, or CHX and HRN resulted in equivalent results and in Fig. 5C-E data from experiments using CHX were presented.

5.15 Immunobiological techniques

5.15.1 Western blotting

To detect the protein of interest separated on SDS gels (using protein/tag specific antibody) western blotting was performed. According to length and width of the SDS gel to be transferred, 6x Whatman paper and 1x nitrocellulose membrane were cut. For semi-dry transfer, the membrane and the Whatman paper were dip into 1x transfer buffer (1x Towbin+ 20% methanol) and were stacked in semi dry chamber in the order of 3x Whatman paper, 1x nitrocellulose membrane, SDS-gel and 3x Whatmann paper from the bottom to top. The transfer was done at length x width x 0.8 mA for 90 mins.

After the transfer membrane was blocked in TBST+5% milk solution for 1 hour. Rinsed the membrane 2x in TBST and incubated in primary antibody for 1 hour at room temperature or

overnight in the cold room. Washed membrane 3x in TBST 15 mins each and added with secondary antibody. After 2 hour incubation at room temperature washing was performed same as above and the membrane was developed using enhanced chemiluminescence system (ECL) (GE healthcare) or home made mix (0.2 mM coumaric acid+1.25 mM Luminol+0.3% H_2O_2.

5.15.2 Immuno-precipitation

Immuno-precipitation (IP) was performed using protein-G dyna beads. For each milliliter of cell lysate 20 µl of dyna beads were used. First, the beads were washed 2x with NP-40 lysis buffer (50 mM HEPES, pH 7.5, 150 mM KCl, 2 mM EDTA, 0.5% NP-40, protease inhibitor cocktail) and incubated with IgG anti-FLAG antibody for 1 hour at room temperature. The FLAG-bound beads were washed 3x with NP-40 lysis buffer to get rid of unbound antibody.

To prepare cell lysate, the cells were collected after scraping or trypsinization and washed 1x with ice cold PBS. The cell pellet was re-suspended in 3 volumes of NP-40 lysis buffer and incubated on ice for 10 mins. To clear debris the cell suspension was centrifuged for 15 mins at 4˚C at full speed and the supernatant was collected in a fresh eppendorf. The cleared lysate was mixed with FLAG-tagged magnetic beads and was incubated at 4˚C for 2 hours on head over tail rotor. Using a magnetic rack, the magnetic beads were collected from the lysate and washed 3x with NP-40 lysis buffer.

The protein bound to the magnetic beads were eluted either with boiling, 95˚C 5 mins or by peptide elution. For the later, the beads were incubated with 200 µg/ml FLAG-peptide for 30 mins in the cold room and the flow-through containing protein was collected. The eluted protein/proteins were analyzed on SDS-gel.

5.15.3 PAR-CLIP

Photoactivatable ribonucleoside-enhanced cross-linking and immunoprecipitation (PAR-CLIP) was performed as previously described {Hafner:2012gh, Hafner:2010ft, Hafner:2010kr} with minor modifications. Briefly, ten 15-cm tissue culture plates (per isoform) with stable cell lines for CNBP over-expression were grown till 80% confluent. Fourteen hours before harvesting, cells were fed with 100 µM 4SU and induced with 500 ng/ml tetracycline. Cells were cross-linked using UV-strata 365 nm crosslinker with 1 J/cm^2 energy and pelleted until further use. Cell pellets were resuspended in NP-40 lysis buffer (50 mM HEPES, pH 7.5, 150 mM KCl, 2 mM EDTA, 0.5% NP-40, protease inhibitor cocktail) and lysis was performed by incubating cells on ice for 10 mins followed by 15 mins centrifugation, 13000 rpm, 4˚C. The lysates were digested with 1 U/µl RNaseT1 at room temperature for 15 mins and added with Ni-NTA magnetic beads coupled with FLAG- antibody for immunoprecipitation. Two hours after incubating lysates with

the beads at 4˚C, the beads conjugated with CNBP RNA-protein complexes, were washed with NP-40 lysis buffer. The RNA in RNA protein-complex was further digested with 1 U/µl RNaseT1 and the 3' ends were de-phosphorylated using calf intestinal phosphatase (0.5 U/µl) (NEB). The RNA fragments were radioactively end labeled using T4 polynucleotide kinase (Fermentas) and the protein-RNA complexes were resolved on 4-12% NuPAGE gel (Invitrogen). The gel was exposed to phosphoimager screen and the protein-RNA complex running at expected size is excised. After gel elution the protein in the complex was digested using proteinase K (5 mg/ml) and the RNA was isolated by P:C:I.

The isolated hot RNA was first run on a 15% urea gel along with the 19 & 35-nt RNA size marker for size selection. The RNA species between 19 & 35-nts were cut out of the band and isolated with 0.3 M NaCl. The precipitated RNA was then subjected to 3' barcoded adapter ligation. Ligated RNA along with the ligated marker was run on a 15% urea gel and corresponding bands were excised. The process is repeated for 5' adapter ligation followed by reverse transcription.

To avoid the over-saturation of one cDNA species a pilot PCR (100 µl total volume with 10 µl cDNA) was performed with the cDNA obtained above. The PCR samples were collected at different cycles (10 µl each time) (12, 15, 18, 21, 24, 27 & 30 cycles) and run on a 2.5% agarose gel. Finally, a large scale PCR was performed (300 µl reaction volume with 30 µl cDNA) up to the appropriate cycle number and the cDNA was isolated from 2.5% agarose gel.

PAR-CLIP cDNA libraries were sequenced on an Illumina HiSeq 2500 platform. Clusters of overlapping sequence reads mapped against the human genome, hg19, were generated using the PARalyzer software {Corcoran:2011bp} incorporated into a pipeline (PARpipe; https://ohlerlab.mdc-berlin.de/software/PARpipe_119/) with default settings. Binding sites were categorized using the GRCh37.p13 GTF annotation (gencode.v19.chr_patch_hapl_scaff.annotation.gtf).

5.15.4 Arsenite stress and Immunofluorescence microscopy

To check the localization of CNBP under stress condition sodium arsenite was used to induce oxidative stress in HEK 293 cells and the localization of CNBP was determined using fluorescence microscopy. Cells were grown in a 6 well plate containing cover slips up to 50-60% confluency. The cells were added with 1 mM sodium arsenite for 90 mins. For harvesting, the media was removed and coverslips were fixed with 4% (v/v) formaldehyde (37% in 1x PBS) for 10 mins at room temperature. Cover slips were washed with 1x PBS and incubated in 0.2% Triton X-100; 1% (w/v) BSA (mixed in 1x PBS) for 30 mins to permeabilize the cell membrane and block unspecific antigens. The cover slips were washed once with 1x PBS and incubated with primary antibody (in PBS and 1% BSA) overnight at 4˚C. Next day the cells were washed

carefully in 1x PBS for 5 mins and incubated with fluorescent secondary antibody for 3 hours at room temperature. The coverslips were washed again as above and were analyzed in light fluorescence microscope.

6 References

Armas, P., S. Nasif and N. B. Calcaterra (2008). "Cellular nucleic acid binding protein binds G-rich single-stranded nucleic acids and may function as a nucleic acid chaperone." J Cell Biochem **103**(3): 1013-1036.

Ascano, M., M. Hafner, P. Cekan, S. Gerstberger and T. Tuschl (2012). "Identification of RNA-protein interaction networks using PAR-CLIP." Wiley Interdiscip Rev RNA **3**(2): 159-177.

Backe, P. H., A. C. Messias, R. B. Ravelli, M. Sattler and S. Cusack (2005). "X-ray crystallographic and NMR studies of the third KH domain of hnRNP K in complex with single-stranded nucleic acids." Structure **13**(7): 1055-1067.

Baltz, A. G., M. Munschauer, B. Schwanhausser, A. Vasile, Y. Murakawa, M. Schueler, N. Youngs, D. Penfold-Brown, K. Drew, M. Milek, E. Wyler, R. Bonneau, M. Selbach, C.

Dieterich and M. Landthaler (2012). "The mRNA-bound proteome and its global occupancy profile on protein-coding transcripts." Mol Cell **46**(5): 674-690.

Beckmann, B. M., R. Horos, B. Fischer, A. Castello, K. Eichelbaum, A. M. Alleaume, T. Schwarzl, T. Curk, S. Foehr, W. Huber, J. Krijgsveld and M. W. Hentze (2015). "The RNA-binding proteomes from yeast to man harbour conserved enigmRBPs." Nat Commun **6**: 10127.

Beuth, B., S. Pennell, K. B. Arnvig, S. R. Martin and I. A. Taylor (2005). "Structure of a Mycobacterium tuberculosis NusA-RNA complex." EMBO J **24**(20): 3576-3587.

Borgognone, M., P. Armas and N. B. Calcaterra (2010). "Cellular nucleic-acid-binding protein, a transcriptional enhancer of c-Myc, promotes the formation of parallel G-quadruplexes." Biochem J **428**(3): 491-498.

Boyadjiev, S. A. and E. W. Jabs (2000). "Online Mendelian Inheritance in Man (OMIM) as a knowledgebase for human developmental disorders." Clin Genet **57**(4): 253-266.

Braddock, D. T., J. L. Baber, D. Levens and G. M. Clore (2002). "Molecular basis of sequence-specific single-stranded DNA recognition by KH domains: solution structure of a complex between hnRNP K KH3 and single-stranded DNA." EMBO J **21**(13): 3476-3485.

Brett, D., H. Pospisil, J. Valcarcel, J. Reich and P. Bork (2002). "Alternative splicing and genome complexity." Nat Genet **30**(1): 29-30.

Buchan, J. R. and R. Parker (2009). "Eukaryotic stress granules: the ins and outs of translation." Mol Cell **36**(6): 932-941.

Calcaterra, N. B., P. Armas, A. M. Weiner and M. Borgognone (2010). "CNBP: a multifunctional nucleic acid chaperone involved in cell death and proliferation control." IUBMB Life **62**(10): 707-714.

Carballo, E., W. S. Lai and P. J. Blackshear (1998). "Feedback inhibition of macrophage tumor necrosis factor-alpha production by tristetraprolin." Science **281**(5379): 1001-1005.

Castello, A., B. Fischer, K. Eichelbaum, R. Horos, B. M. Beckmann, C. Strein, N. E. Davey, D. T. Humphreys, T. Preiss, L. M. Steinmetz, J. Krijgsveld and M. W. Hentze (2012). "Insights into RNA biology from an atlas of mammalian mRNA-binding proteins." Cell **149**(6): 1393-1406.

Chelly, J. and J. L. Mandel (2001). "Monogenic causes of X-linked mental retardation." Nat Rev Genet **2**(9): 669-680.

Cook, K. B., T. R. Hughes and Q. D. Morris (2015). "High-throughput characterization of protein-RNA interactions." Brief Funct Genomics **14**(1): 74-89.

Datu, A. K. and J. Bag (2013). "Enhanced translation of mRNAs encoding proteins involved in mRNA translation during recovery from heat shock." PLoS One **8**(5): e64171.

De Boulle, K., A. J. Verkerk, E. Reyniers, L. Vits, J. Hendrickx, B. Van Roy, F. Van den Bos, E. de Graaff, B. A. Oostra and P. J. Willems (1993). "A point mutation in the FMR-1 gene associated with fragile X mental retardation." Nat Genet **3**(1): 31-35.

De Dominicis, A., F. Lotti, P. Pierandrei-Amaldi and B. Cardinali (2000). "cDNA cloning and developmental expression of cellular nucleic acid-binding protein (CNBP) gene in Xenopus laevis." Gene **241**(1): 35-43.

Draper, D. E. (1999). "Themes in RNA-protein recognition." J Mol Biol **293**(2): 255-270.

Dreyfuss, G., Y. D. Choi and S. A. Adam (1984). "Characterization of heterogeneous nuclear RNA-protein complexes in vivo with monoclonal antibodies." Mol Cell Biol **4**(6): 1104-1114.

Eis-Hubinger, A. M., J. P. Kleim, K. Mohr and K. E. Schneweis (1991). "A related epitope is consistently present on glycoprotein C of herpes simplex virus type 1 and 2." Acta Virol **35**(3): 276-281.

Fairman-Williams, M. E., U. P. Guenther and E. Jankowsky (2010). "SF1 and SF2 helicases: family matters." Curr Opin Struct Biol **20**(3): 313-324.

Finerty, P. J., Jr. and B. L. Bass (1997). "A Xenopus zinc finger protein that specifically binds dsRNA and RNA-DNA hybrids." J Mol Biol **271**(2): 195-208.

Furney, S. J., D. G. Higgins, C. A. Ouzounis and N. Lopez-Bigas (2006). "Structural and functional properties of genes involved in human cancer." BMC Genomics **7**: 3.

Gerbasi, V. R. and A. J. Link (2007). "The myotonic dystrophy type 2 protein ZNF9 is part of an ITAF complex that promotes cap-independent translation." Mol Cell Proteomics **6**(6): 1049-1058.

Gerstberger, S., M. Hafner and T. Tuschl (2013). "Learning the language of post-transcriptional gene regulation." Genome Biol **14**(8): 130.

Gerstberger, S., M. Hafner and T. Tuschl (2014). "A census of human RNA-binding proteins." Nat Rev Genet **15**(12): 829-845.

Graifer, D. and G. Karpova (2015). "Roles of ribosomal proteins in the functioning of translational machinery of eukaryotes." Biochimie **109**: 1-17.

Griffiths-Jones, S., H. K. Saini, S. van Dongen and A. J. Enright (2008). "miRBase: tools for microRNA genomics." Nucleic Acids Res **36**(Database issue): D154-158.

Hachet, O. and A. Ephrussi (2004). "Splicing of oskar RNA in the nucleus is coupled to its cytoplasmic localization." Nature **428**(6986): 959-963.

Hafner, M., M. Landthaler, L. Burger, M. Khorshid, J. Hausser, P. Berninger, A. Rothballer, M. Ascano, Jr., A. C. Jungkamp, M. Munschauer, A. Ulrich, G. S. Wardle, S. Dewell, M. Zavolan and T. Tuschl (2010). "Transcriptome-wide identification of RNA-binding protein and microRNA target sites by PAR-CLIP." Cell **141**(1): 129-141.

Huichalaf, C., B. Schoser, C. Schneider-Gold, B. Jin, P. Sarkar and L. Timchenko (2009). "Reduction of the rate of protein translation in patients with myotonic dystrophy 2." J Neurosci **29**(28): 9042-9049.

Iadevaia, V. and A. P. Gerber (2015). "Combinatorial Control of mRNA Fates by RNA-Binding Proteins and Non-Coding RNAs." Biomolecules **5**(4): 2207-2222.

Imig, J., A. Kanitz and A. P. Gerber (2012). "RNA regulons and the RNA-protein interaction network." Biomol Concepts **3**(5): 403-414.

Ingolia, N. T., S. Ghaemmaghami, J. R. Newman and J. S. Weissman (2009). "Genome-wide analysis in vivo of translation with nucleotide resolution using ribosome profiling." Science **324**(5924): 218-223.

Keene, J. D. (2007). "RNA regulons: coordination of post-transcriptional events." Nat Rev Genet **8**(7): 533-543.

Klug, A. (2010). "The discovery of zinc fingers and their applications in gene regulation and genome manipulation." Annu Rev Biochem **79**: 213-231.

Klug, A. and D. Rhodes (1987). "Zinc fingers: a novel protein fold for nucleic acid recognition." Cold Spring Harb Symp Quant Biol **52**: 473-482.

Laity, J. H., B. M. Lee and P. E. Wright (2001). "Zinc finger proteins: new insights into structural and functional diversity." Curr Opin Struct Biol **11**(1): 39-46.

Le Hir, H., D. Gatfield, E. Izaurralde and M. J. Moore (2001). "The exon-exon junction complex provides a binding platform for factors involved in mRNA export and nonsense-mediated mRNA decay." EMBO J **20**(17): 4987-4997.

Lin, S. and R. I. Gregory (2015). "MicroRNA biogenesis pathways in cancer." Nat Rev Cancer **15**(6): 321-333.

Linder, P. (2006). "Dead-box proteins: a family affair--active and passive players in RNP-remodeling." Nucleic Acids Res **34**(15): 4168-4180.

Linder, P. and E. Jankowsky (2011). "From unwinding to clamping - the DEAD box RNA helicase family." Nat Rev Mol Cell Biol **12**(8): 505-516.

Lukong, K. E., K. W. Chang, E. W. Khandjian and S. Richard (2008). "RNA-binding proteins in human genetic disease." Trends Genet **24**(8): 416-425.

Maquat, L. E., W. Y. Tarn and O. Isken (2010). "The pioneer round of translation: features and functions." Cell **142**(3): 368-374.

Marchese, D., N. S. de Groot, N. Lorenzo Gotor, C. M. Livi and G. G. Tartaglia (2016). "Advances in the characterization of RNA-binding proteins." Wiley Interdiscip Rev RNA.

Mazza, C., A. Segref, I. W. Mattaj and S. Cusack (2002). "Large-scale induced fit recognition of an m(7)GpppG cap analogue by the human nuclear cap-binding complex." EMBO J **21**(20): 5548-5557.

Meola, G. (2000). "Clinical and genetic heterogeneity in myotonic dystrophies." Muscle Nerve **23**(12): 1789-1799.

Miller, J., A. D. McLachlan and A. Klug (1985). "Repetitive zinc-binding domains in the protein transcription factor IIIA from Xenopus oocytes." EMBO J **4**(6): 1609-1614.

Muto, Y. and S. Yokoyama (2012). "Structural insight into RNA recognition motifs: versatile molecular Lego building blocks for biological systems." Wiley Interdiscip Rev RNA **3**(2): 229-246.

Nagai, K., Y. Muto, D. A. Pomeranz Krummel, C. Kambach, T. Ignjatovic, S. Walke and A. Kuglstatter (2001). "Structure and assembly of the spliceosomal snRNPs. Novartis Medal Lecture." Biochem Soc Trans **29**(Pt 2): 15-26.

Nam, Y., C. Chen, R. I. Gregory, J. J. Chou and P. Sliz (2011). "Molecular basis for interaction of let-7 microRNAs with Lin28." Cell **147**(5): 1080-1091.

Nott, A., H. Le Hir and M. J. Moore (2004). "Splicing enhances translation in mammalian cells: an additional function of the exon junction complex." Genes Dev **18**(2): 210-222.

Pais, H., S. Moxon, T. Dalmay and V. Moulton (2011). "Small RNA discovery and characterisation in eukaryotes using high-throughput approaches." Adv Exp Med Biol **722**: 239-254.

Parraga, G., S. J. Horvath, A. Eisen, W. E. Taylor, L. Hood, E. T. Young and R. E. Klevit (1988). "Zinc-dependent structure of a single-finger domain of yeast ADR1." Science **241**(4872): 1489-1492.

Pavletich, N. P. and C. O. Pabo (1991). "Zinc finger-DNA recognition: crystal structure of a Zif268-DNA complex at 2.1 A." Science **252**(5007): 809-817.

Picard, B. and M. Wegnez (1979). "Isolation of a 7S particle from Xenopus laevis oocytes: a 5S RNA-protein complex." Proc Natl Acad Sci U S A **76**(1): 241-245.

Pinol-Roma, S., Y. D. Choi, M. J. Matunis and G. Dreyfuss (1988). "Immunopurification of heterogeneous nuclear ribonucleoprotein particles reveals an assortment of RNA-binding proteins." Genes Dev **2**(2): 215-227.

Price, S. R., P. R. Evans and K. Nagai (1998). "Crystal structure of the spliceosomal U2B"-U2A' protein complex bound to a fragment of U2 small nuclear RNA." Nature **394**(6694): 645-650.

Rajavashisth, T. B., A. K. Taylor, A. Andalibi, K. L. Svenson and A. J. Lusis (1989). "Identification of a zinc finger protein that binds to the sterol regulatory element." Science **245**(4918): 640-643.

Ray, D., H. Kazan, K. B. Cook, M. T. Weirauch, H. S. Najafabadi, X. Li, S. Gueroussov, M. Albu, H. Zheng, A. Yang, H. Na, M. Irimia, L. H. Matzat, R. K. Dale, S. A. Smith, C. A. Yarosh, S. M. Kelly, B. Nabet, D. Mecenas, W. Li, R. S. Laishram, M. Qiao, H. D. Lipshitz, F. Piano, A. H. Corbett, R. P. Carstens, B. J. Frey, R. A. Anderson, K. W. Lynch, L. O. Penalva, E. P. Lei, A. G. Fraser, B. J. Blencowe, Q. D. Morris and T. R. Hughes (2013). "A compendium of RNA-binding motifs for decoding gene regulation." Nature **499**(7457): 172-177.

Remenyi, A., H. R. Scholer and M. Wilmanns (2004). "Combinatorial control of gene expression." Nat Struct Mol Biol **11**(9): 812-815.

Riggi, N., L. Cironi, M. L. Suva and I. Stamenkovic (2007). "Sarcomas: genetics, signalling, and cellular origins. Part 1: The fellowship of TET." J Pathol **213**(1): 4-20.

Rockman, M. V. and L. Kruglyak (2006). "Genetics of global gene expression." Nat Rev Genet **7**(11): 862-872.

Rojas, M., G. W. Farr, C. F. Fernandez, L. Lauden, J. C. McCormack and S. L. Wolin (2012). "Yeast Gis2 and its human ortholog CNBP are novel components of stress-induced RNP granules." PLoS One **7**(12): e52824.

Rothman, S. (2010). "How is the balance between protein synthesis and degradation achieved?" Theor Biol Med Model **7**: 25.

Sammons, M. A., A. K. Antons, M. Bendjennat, B. Udd, R. Krahe and A. J. Link (2010). "ZNF9 activation of IRES-mediated translation of the human ODC mRNA is decreased in myotonic dystrophy type 2." PLoS One **5**(2): e9301.

Sammons, M. A., P. Samir and A. J. Link (2011). "Saccharomyces cerevisiae Gis2 interacts with the translation machinery and is orthogonal to myotonic dystrophy type 2 protein ZNF9." Biochem Biophys Res Commun **406**(1): 13-19.

Schneider, C., A. Ziegler, K. Ricker, T. Grimm, W. Kress, C. D. Reimers, H. Meinck, K. Reiners and K. V. Toyka (2000). "Proximal myotonic myopathy: evidence for anticipation in families with linkage to chromosome 3q." Neurology **55**(3): 383-388.

Searles, M. A., D. Lu and A. Klug (2000). "The role of the central zinc fingers of transcription factor IIIA in binding to 5 S RNA." J Mol Biol **301**(1): 47-60.

Semrad, K. (2011). "Proteins with RNA chaperone activity: a world of diverse proteins with a common task-impediment of RNA misfolding." Biochem Res Int **2011**: 532908.

Shimizu, K., W. Chen, A. M. Ashique, R. Moroi and Y. P. Li (2003). "Molecular cloning, developmental expression, promoter analysis and functional characterization of the mouse CNBP gene." Gene **307**: 51-62.

Skelly, M. J., L. Frungillo and S. H. Spoel (2016). "Transcriptional regulation by complex interplay between post-translational modifications." Curr Opin Plant Biol **33**: 126-132.

Stefl, R., L. Skrisovska and F. H. Allain (2005). "RNA sequence- and shape-dependent recognition by proteins in the ribonucleoprotein particle." EMBO Rep **6**(1): 33-38.

Tenenbaum, S. A., C. C. Carson, P. J. Lager and J. D. Keene (2000). "Identifying mRNA subsets in messenger ribonucleoprotein complexes by using cDNA arrays." Proc Natl Acad Sci U S A **97**(26): 14085-14090.

Thandapani, P., T. R. O'Connor, T. L. Bailey and S. Richard (2013). "Defining the RGG/RG motif." Mol Cell **50**(5): 613-623.

Valverde, R., L. Edwards and L. Regan (2008). "Structure and function of KH domains." FEBS J **275**(11): 2712-2726.

Vaquerizas, J. M., S. K. Kummerfeld, S. A. Teichmann and N. M. Luscombe (2009). "A census of human transcription factors: function, expression and evolution." Nat Rev Genet **10**(4): 252-263.

Wachtel, C. and J. L. Manley (2009). "Splicing of mRNA precursors: the role of RNAs and proteins in catalysis." Mol Biosyst **5**(4): 311-316.

Walsh, G. and R. Jefferis (2006). "Post-translational modifications in the context of therapeutic proteins." Nat Biotechnol **24**(10): 1241-1252.

Wang, G. S. and T. A. Cooper (2007). "Splicing in disease: disruption of the splicing code and the decoding machinery." Nat Rev Genet **8**(10): 749-761.

Warden, C. H., S. K. Krisans, D. Purcell-Huynh, L. M. Leete, A. Daluiski, A. Diep, B. A. Taylor and A. J. Lusis (1994). "Mouse cellular nucleic acid binding proteins: a highly conserved family identified by genetic mapping and sequencing." Genomics **24**(1): 14-19.

Wei, H. M., H. H. Hu, G. Y. Chang, Y. J. Lee, Y. C. Li, H. H. Chang and C. Li (2014). "Arginine methylation of the cellular nucleic acid binding protein does not affect its subcellular localization but impedes RNA binding." FEBS Lett **588**(9): 1542-1548.

Wilkinson, K. A., E. J. Merino and K. M. Weeks (2006). "Selective 2'-hydroxyl acylation analyzed by primer extension (SHAPE): quantitative RNA structure analysis at single nucleotide resolution." Nat Protoc **1**(3): 1610-1616.

Wolfe, S. A., L. Nekludova and C. O. Pabo (2000). "DNA recognition by Cys2His2 zinc finger proteins." Annu Rev Biophys Biomol Struct **29**: 183-212.

Wong, C. H. (2005). "Protein glycosylation: new challenges and opportunities." J Org Chem **70**(11): 4219-4225.

Yoon, J. H., S. De, S. Srikantan, K. Abdelmohsen, I. Grammatikakis, J. Kim, K. M. Kim, J. H. Noh, E. J. White, J. L. Martindale, X. Yang, M. J. Kang, W. H. Wood, 3rd, N. Noren Hooten, M. K. Evans, K. G. Becker, V. Tripathi, K. V. Prasanth, G. M. Wilson, T. Tuschl, N. T. Ingolia, M. Hafner and M. Gorospe (2014). "PAR-CLIP analysis uncovers AUF1 impact on target RNA fate and genome integrity." Nat Commun **5**: 5248.

7 Acknowledgements

I would like to sincerely thank all the people who helped me in this project and thus contributed to successfully finish this thesis.

First and foremost, I would like to thank my primary supervisor Dr Stefan Juranek, who gave me an opportunity to work under his supervsion. Without his constant support and guidance this journey would have not been possible.

My sincere thanks to our collaborator Dr Markus Hafner and his lab members (Charles, Daniel, Aishe, Xintao) who were directly or indirectly involved in this project. Dr Hafner not only provided this project with his bioinformatic expertise and in house sequencing platforms but also helped me to get detailed insights into the project. His moral guidence and support during my stay in NIH, USA and thoughout the project helped me in a great deal to bring this project to successful completion.

I am highly thankful to Prof Dr Utz Fischer (secondary supervisor), Dr Markus Landthaler (third supervisor), Dr Katrin Paeschke and Prof Dr Alexander Buchberger for their contant inputs and ideas in lab meetings, annual reports and outside work.

This work wouldnot have been possible without the constant support and help of all the people of the biochemistry department.

Thomas, Eike, Nadine, Markus and Jürgen for scientific and unscientific discussions and ofcourse the amazing kicker and tabletennis matches.

Clemens E, Georg, Lissy, Raji, Conni, Jyotish and all the technical and not technical staff for helping in one way or the other.

I would also like to thank all my friends Anindya, David, Dharmesh, KKya, Paddy, Aniket, Pratik and specially Katrin.

Last but not least, this journey would not have been possible without the constant moral support of my parents my brothers and my sister in law (and little Aura).

8 Publication

The part of this work is submitted in „Cell reports“ for publication and is under revision.

Sanjay K Gupta, Daniel Benhalevy, Charles H Danan, Markus Hafner# & Stefan A Juranek# (2016). The human CCHC-type Zinc Finger, Nucleic Acid Binding Protein binds G-rich elements close to translation initiation sites and promotes translation. Cell Reports, (*under revision*).

Book Chapter:
Kai Papenfort, Colin P. Corcoran, **Sanjay K. Gupta**., et. al. (2013) Regulatory Mechanism of Special Significance: Role of small RNAs in Virulence regulation**.** American Society of Microbiology (ASM).

9 Curriculum vitae

Sanjay Gupta

Address	Peterplatz 6A, Würzburg
	Germany, 97070
Email	sanjaygupta.de@gmail.com
Date of birth	27.10.1987

EDUCATION

May 2012- till date	**Department of Biochemistry, Biozentrum**
	University of Wuerzburg, Germany
	PhD Student (RNA biology group)
	Thesis title: Biochemistry of human RNA binding protein, CNBP.
	Supervisors: Dr. Stefan Juranek, Prof. Utz Fischer, Dr. Markus Landthaler
Oct 2008- Oct 2009	**School of Biological Sciences**
	University of East Anglia, Norwich, UK
	MSc Biotechnology for a Sustainable Future
	Thesis title: Role of small Nucleoid Associated Proteins (NAPs) in the virulence of *S.* Typhimurium.
	Supervisors: Dr. Gary Rowley, Dr. Mark Coleman
July 2005- June 2008	**Rajiv Gandhi Institute of IT and Biotechnology**
	Bharati Vidyapeeth University, Pune, India
	BSc Biotechnology

RESEARCH EXPERIENCE

Oct 2010- April 2012	**Institute of Molecular Infection Biology (IMIB)**
	University of Wuerzburg, Germany
	Research Associate
	Project title: Identification and characterization of small RNAs in *Shigella flexineri.*
	Supervisor: Prof. Jörg Vogel
Oct 2009-July 2010	**School of Biological Sciences**
	University of East Anglia, Norwich, UK
	Research Associate
	Project title: Defining the role of Tat pathway in the virulence of *S.* Typhimurium.
	Supervisor: Dr. Gary Rowley

PUBLICATION AND BOOK CHAPTER

- **Gupta S**., et. al. (2016) The human CCHC-type Zinc Finger, Nucleic Acid Binding Protein binds G-rich elements close to translation initiation sites and promotes translation. Cell Reports, (*under revision*).
- Kai Papenfort, Colin P. Corcoran, **Sanjay K. Gupta**., et. al. (2013) Regulatory Mechanism of Special Significance: Role of small RNAs in Virulence regulation**.** American Society of Microbiology (ASM).

SKILLS & EXPERTISE

Wet laboratory skills	Cross-linking and immunoprecipitation (PAR-CLIP, iCLIP), Protein purification, Cell culture, Northern blot, Western blot, Sequencing gels, RNAseq, CRISPR-cas gene knockout and basic molecular biology and biochemistry lab practices.
Computer skills	Well skilled with Adobe photoshop, CS Coreldraw, MS office, Basic knowledge of PAR-CLIP Paralyzer, Cummer-Bund, R,
Teaching skills	Mentored junior PhD, master and bachelor students during PhD. Worked as teaching assistant in "Student Associate Scheme" by University of East Anglia.

AWARDS & FELLOWSHIPS

- **"DAAD STIBET"** fellowship from the Graduate School of Life Sciences, Wuerzburg, Mar'2016.
- **"Travel fellowship"** to visit collaboration lab for research stay, Mar' 2015.
- **"Student scholarship"** for academic excellence by the University of East Anglia, Sept'2008.

WORKSHOPS & RESEARCH VISITS

Mar 2015	**National Institute of Health (NIH), Bethesda, USA**
	Bioinformatics of next generation sequencing
Sept 2014	**University of Regensburg, Germany**
	Current methods in RNP analysis
Aug 2015	**University of Wuerzburg, Germany**
	Statistical analysis by R
Dec 2015	**University of Wuerzburg, Germany**
	Poster design and presentations

POSTER PRESENATION

- **Gupta S,** Hafner M, Juranek S. Cellular nucleic acid binding protein (CNBP) binds G-rich elements in target mRNA CDS promotes translation. **RNA workshop**, Regensburg, Germany, 2014.

- **Gupta S**, Hafner M, Juranek S. Characterization of Human RNA binding proteins; its RNA binding partners and biochemistry. **Eureka/EPOS**, by GSLS university of Wuerzburg, 2015/2013.
- **Gupta S**, Papenfort K, Vogel K. The role of Hfq in virulence of *Shigella flexneri.* **62 Mosbacher Kolloquium**, Machenisms of RNA mediated regulation, 2011.

Date, Place **Signature**

10 Affidavit

I hereby confirm that my thesis entitled **„The human CCHC-type Zinc Finger Nucleic Acid Binding Protein (CNBP) binds to the G-rich elements in target mRNA coding sequences and promotes translation“** is the result of my own work . I didnot recieve any help or support from commercial consultants. All sources and/ or mateirals applied are listed dnd sepcified in the thesis.

Furthermore I confirm that this thesis has not yet been submitted as part of another examination process neither in identical nor in similar form.

Place, Date Signature

Eidesstattliche Erklärung

Hiermit erkläre ich an Eides statt, die Dissertation **“Das humane CCHC-Typ-Zinkfinger-Nukleinsäure-bindende-Protein (CNBP) bindet an G-reiche Elemente in der kodierenden Sequenz seiner Ziel-mRNAs und fördert deren Translation”** eigenständig, d.h. insbesondere selbständig und ohne Hilfe eines kommerziellen Promotionsberaters, angefertigt und keine anderen als die von mir angegebenen Quellen und Hilfsmittel verwendet zu haben.

Ich erkläre außerdem, dass die Dissertation weder in gleicher noch in ähnlicher Form bereits in einem anderen Prüfungsverfahren vorgelegen hat.

Ort, Datum Unterschrift